CERN-LHCC-2004-031 and LHCC-RD-005

CERN, January 2005

RD50 Status Report 2004

Radiation hard semiconductor devices for very high luminosity colliders

Centro Nacional de Microelectrónica (IMB-CNM, CSIC)
Francesca Campabadal, Celeste Fleta, Manuel Lozano, Giulio Pellegrini, Joan Marc Rafí, Miguel Ullán

Dipartimento Interateneo di Fisica & INFN - Bari, Italy
Donato Creanza, Mauro De Palma, Norman Manna, Valeria Radicci, Luigi Schiavulli

Institut für Kristallzüchtung, Berlin, Germany
Klaus Irmscher, Günter Wagner

Brookhaven National Laboratory, Upton, NY, USA
Jim Kierstead, Zheng Li

Department of Physics, University of Bologna, Bologna, Italy
Anna Cavallini

National Institute for Materials Physics, Bucharest - Magurele, Romania
Manuela Buda, Sorina Lazanu, Lucian Pintilie, Ioana Pintilie, Andreia-Ioana Popa

University of Bucharest, Faculty of Physics
Ionel Lazanu

CERN, Geneva, Switzerland
Paula Collins, Karl Aaron Gill, Maurice Glaser, Christian Joram, Michael Moll[§]

Universitaet Dortmund, Lehrstuhl Experimentelle Physik IV, Dortmund, Germany
Claus Goessling, Jonas Klaiber-Lodewigs, Reiner Klingenberg, Olaf Krasel, Renate Wunstorf

CiS Institut für Mikrosensorik gGmbH, Erfurt, Germany
Ralf Roeder, Dieter Stolze, Hartmut Uebersee

University of Exeter, Department of Physics, Exeter, EX4 4QL, United Kingdom
James Adey, A. Blumenau, J. Coutinho, T. Eberlein, C. Fall, J. Goss, B. Hourahine, Robert Jones, N. Pinho

[§] *Deputy Spokesperson*

Fermilab, USA
Rita Coluccia, Simon Kwan, Greg Sellberg

INFN Florence – Department of Energetics, University of Florence, Italy
Emilio Borchi, Mara Bruzzi[♦], Ettore Focardi, Stefano Lagomarsino, Anna Macchiolo, David Menichelli, Stefania Miglio, Monica Scaringella, Silvio Sciortino

Dept. of Physics & Astronomy, Glasgow University, Glasgow, UK
Adwan Al-Ajili, Richard Bates, Andrew Blue, Craig Buttar, Liam Cunningham, Alison Gouldwell Bates, Lina Haddad, Meg Horn, Keith Mathieson, J. Melone, Val OShea, Chris Parkes, Victoria Wright

Institute for Experimental Physics, University of Hamburg, Germany
Peter Buhmann, Devis Contarato, Eckhart Fretwurst, Frank Hönniger, Gunnar Lindström, Uwe Pein, Jörg Stahl

Helsinki Institute of Physics, Helsinki, Finland
Jaakko Härkönen, Katri Lassila-Perini, Panja Luukka, Jukka Nysten, Eija Tuominen, Esa Tuovinen

Ioffe Phisico-Technical Institute of Russian Academy of Sciences, St. Petersburg, Russia
Vladimir Eremin, Igor Ilyashenko, Alexandr Ivanov, Evgenia Kalinina, Alexander Lebedev, Nikita Strokan, Elena Verbitskaya

Institute of Electronic Materials Technology, Warszawa, Poland
Andrzej Brzozowski, Pawel Kaminski, Roman Kozlowski, Zygmunt Luczynski, Elzbieta Nossarzewska-Orlowska, Barbara Surma, Piotr Zabierowski

Institute of Physics PAS and Institute of Electronics Technology, Warsaw, Poland
Adam Barcz

University of Karlsruhe, Institut fuer Experimentelle Kernphysik, Karlsruhe, Germany
Wim de Boer, Florian Hauler, Levin Jungermann, Valery Zhukov

Institute for Nuclear Research of the Academy of Sciences of Ukraine, Radiation PhysicDepartments
L. Barabash, A. Dolgolenko, A. Groza, A. Karpenko, V. Khivrich, V. Lastovetsky, P. Litovchenko, L. Polivtsev

Department of Physics, Lancaster University, Lancaster, United Kingdom
Timothy John Brodbeck, Duncan Campbell, Alexandre Chilingarov, Gareth Hughes, Brian Keith Jones, Terence Sloan

Lappeenranta University of Technology, Department of Electrical Engineering, Lappeenranta, Finland
Miia Koski, Kari Leinonen, Tanja Palviainen, Tuure Tuuva

Department of Physics, University of Liverpool, United Kingdom
Phillip Allport, Stephen Biagi, Themis Bowcock, Gianluigi Casse, Jaap Velthuis

♦ *Spokesperson*

Jožef Stefan Institute and Department of Physics, University of Ljubljana, Ljubljana, Slovenia
Vladimir Cindro, Gregor Kramberger, Igor Mandic, Marko Mikuž, Marko Zavrtanik

Université catholique de Louvain, Institut de Physique Nucléaire, Louvain-la-Neuve, Belgium
Samia Assouak, Eric Forton, Ghislain Grégoire

Belarusian State University, Minsk
Leonid Makarenko

Groupe de la Physique des Particules, Université de Montreal, Canada
Sébastien Charron, Marie-Helene Genest, Alain Houdayer, Celine Lebel, Claude Leroy

State Scientific Center of Russian Federation, Institute for Theoretical and Experimental Physics, Moscow, Russia
Gleb Bondarenko, Victor Golovine, Eugene Grigoriev, Aleksey Karpov, Mikhail Kozodaev, Pavel Polozov, Alexandre Suvorov, Alexandre Zaluzhny

University of New Mexico
Igor Gorelov, Martin Hoeferkamp, Giuseppe Latino, Dmitri Naoumov, Sally Seidel

University of Oslo, Physics Department/Physical Electronics, Oslo, Norway
Giovanni Alfieri, Klaus M H Johansen, Andrej Kuznetsov, Edouard Monakhov, Bengt G. Svensson

Dipartimento di Fisica and INFN Sezione di Padova, Via Marzolo 8, I-35131, Padova, Italy
Dario Bisello, Andrea Candelori, Vladimir Khomenkov, Alexei Litovchenko, Riccardo Rando

I.N.F.N. and Università di Perugia - Italy
Gian Mario Bilei, Francesco Moscatelli, Daniele Passeri, Marco Petasecca, Giorgio Umberto Pignatel, Andrea Scorzoni

Universita` di Pisa and INFN sez. di Pisa, Italy
Laura Borrello, Alberto Messineo, Gabriele Segneri, Daniel Sentenac

Institute of Physics, Academy of Sciences of the Czech Republic, Praha, Czech Republic
Jiri Popule, Petr Sicho, Michal Tomasek, Vaclav Vrba

Czech Technical University in Prague, Czech Republic
Dominik Chren, Tomas Horazdovsky, Zdenek Kohout, Vladimir Linhart, Stanislav Pospisil, Michael Solar, Vít Sopko, Bruno Sopko, Josef Uher

Charles University Prague, Czech Republic
Jan Broz, Zdenek Dolezal, Peter Kodys, Alexej Tsvetkov, Ivan Wilhelm

Paul Scherrer Institut, Laboratory for Particle Physics, Villigen, Switzerland
Roland Horisberger, Tilman Rohe

Purdue University, USA
Gino Bolla, Daniela Bortoletto, Kim Giolo, Jun Miyamoto, Carsten Rott, Amitava Roy, Ian Shipsey, SeungHee Son

University of Rochester
Veronique Boisvert, Regina Demina, Thomas Ferbel, sergey korjenevski, Paul Tipton

Rutgers University, Piscataway, New Jersey, USA
L. Perera, S. Schnetzer, R. Stone, Steven Worm

Santa Cruz Institute for Particle Physics
Alexander Grillo, Jessica Metcalfe, Hartmut Sadrozinski, Bruce Schumm, Abraham Seiden, Ned Spencer

Dept of Physics and Astronomy, University of Sheffield, Sheffield, U.K.
Ian Dawson, Paul Dervan

SINTEF ICT P.O.Box 124 Blindern N-0314 Oslo, Norway
Berit Sundby Avset

Department of Physics, University of Surrey, Guildford, United Kingdom
Paul Sellin

Experimental Particle Physics Group, Syracuse University, Syracuse, USA
Marina Artuso

Tel Aviv University, Israel
J. Guskov, Sergey Marunko, Arie Ruzin, Tamir Tylchin

Experimental Physics Department, University of Torino, Italy
Floriana Fasolo, Franco Fizzotti, Alessandro Lo Giudice, Claudio Manfredotti, Paolo Olivero, Chiara Paolini, Garino Yiuri

ITC-IRST, Microsystems Division, Povo, Trento, Italy
Maurizio Boscardin, Gian - Franco Dalla Betta, Paolo Gregori, Claudio Piemonte, Alberto Pozza, Sabina Ronchin, Mario Zen, Nicola Zorzi

Universita di Trieste & I.N.F.N.-Sezione di Trieste, Italy
Luciano Bosisio, Selenia Dittongo

IFIC Valencia, Apartado 22085, 46071 Valencia, Spain
Carmen Garcia, Jose Enrique Garcia-Navarro, Sergio González Sevilla, Salvador Marti i Garcia

Institute of Materials Science and Applied Research, Vilnius University, Vilnius, Lithuania
Eugenijus Gaubas, Kestutis Jarasiunas, Vida Kazlauskiene, Vaidotas Kazukauskas, Stanislavas Sakalauskas, Jurgis Storasta, Markas Sudzius, Juozas Vidmantis Vaitkus

Contents

1. Introduction

The objective of the CERN RD50 Collaboration is the development of radiation hard semiconductor detectors for very high luminosity colliders, particularly to face the requirements of a possible upgrade scenario of the LHC to a luminosity of $10^{35}cm^{-2}s^{-1}$, corresponding to expected total fluences of fast hadrons above $10^{16}cm^{-2}$ and reduced bunch-crossing interval of ~10 ns [1]. This document reports the status of research and main results obtained after the second year of activity of the collaboration.

Presently, RD50 counts a total of 252 members with 50 participating institutes, from 16 different countries in West and East Europe, 9 from North America (USA, Canada), one from middle east (Israel). During the second year of activity two workshops and collaboration board meetings have been held to discuss the recent results and co-ordinate the research activities of RD50: May 5-7 at CERN and Oct. 14-16, 2004 in Florence, Italy. Each workshop has registered a quite high rate of participation, counting an average of 80 participants with about 30 talks. More details can be found at the collaboration web-site [2].

Some papers describing the common research activities of the RD50 collaboration have been published recently [3-5]. During this second year of work, the research activity of RD50 has been presented in form of invited oral contributions at several international conferences [6]:

- IWORID Conference, Glasgow, UK, July 2004. Invited Talk, paper submitted to Nucl. Instr. and Meth. A [7].
- 13th International Workshop on Vertex Detectors, VERTEX 2004, Como, Italy, September 2004. Invited Talk, paper submitted to Nucl.Instr.and Meth.A [8].
- 5th International Conference on Semiconductor Tracker Detectors, Hiroshima, June 2004. Invited Talk, paper in press on Nucl. Instr. and Meth. A [9].
- 5th International Conference on Radiation Effects on Semiconductor Materials detectors and Devices, October 10-13, 2004, Firenze, Italy. Invited Talk, paper submitted on Nucl. Instrum. Meth. A.[10].
- IEEE NSS-MIC , October 2004, Rome, Italy: Invited Talk [11]

The scientific organization of RD50 is organised in two major lines, Material Engineering and Device Engineering, each of the two lines are subdivided into three projects as shown in Table 1-1. The management of the projects is assigned to members of RD50 of proven relevant experience (conveners). In the framework of the research activity of each project, working groups are active with specific tasks. Each working group is composed of few institutes, which are directly involved in the research program and co-ordinated by an RD50 member. During this year one additional working group has been assessed in the FDS project, focussed on the development of radiation-hard pixels detectors. The coordinators of this research group are Daniela Bortoletto from Purdue and Tilman Rohe of PSI. Table 1-1 lists working groups and common activities within each project, with the corresponding co-ordinator.
Besides working groups, common activities have been started on subjects of common interest. Some of these activities are partially supported with the RD50 common fund.
In the next section our scientific work is reviewed in an executive summary. This section is followed by six sections describing the status of the research activities of each individual research line. Finally a work plan, milestones and an overview about the needed resources for 2005 are given.

	Line	Project Convener	Main Research Activity	Working groups and common acitivities
Spokesperson / Deputy Mara Bruzzi (INFN and Uni. of Florence) / Michael Moll (CERN)	Material Engineering	Defect/Material Characterisation Bengt G. Svensson Univ. Oslo, Norway	Characterisation of the microscopic properties of standard-, defect engineered and new materials, pre- and post-irradiation.	
		Defect Engineering Eckhart Fretwurst Univ. of Hamburg, Germany	Development and testing of defect engineered silicon: Oxygen enriched FZ (DOFZ), High res. Cz, Epitaxial, Si enriched with Oxygen dimers	(1) Oxygen Dimer (M. Moll)
		New Materials Juozas Vaitkus Univ. of Vilnius, Lithuania	Development of new materials with promising radiation hard properties: bulk and epitaxial SiC, GaN	(1) SiC (I. Pintilie) (2) GaN (J. Vaitkus) (3) Other Materials
	Device Engineering	Pad Detector Characterisation Jaakko Harkonen Helsinki Inst. Physics, Finland	Characterisation of macroscopic properties of heavily irradiated single pad detectors in different operational conditions.	(1) Standardisation of macroscopic measurements (A.Chilingarov) (2) Technotest (V.Eremin)
		New Structures Richard Bates Univ. of Glasgow, UK	Development of 3D, semi-3D and thin detectors and study of their pre- and post-irradiation performance.	(1) 3D (M.Boscardin) (2) Semi-3D (Z.Li)
		Full Detector Systems Gianluigi Casse Univ. of Liverpool, UK	- Systematic characterisation of segmented (microstrips, pixels) LHC-like detectors. - Links with LHC epxeriments	(1) Pixel detectors (D.Bortoletto- T.Rohe)

Table 1-1.: Organisation structure of the research activity in RD50.

References for Chapter 1

[1] R&D Proposal - DEVELOPMENT OF RADIATION HARD SEMICONDUCTORDEVICES FOR VERY HIGH LUMINOSITY COLLIDERS, LHCC 2002-003 / P6, 15.2.2002.
[2] RD50 collaboration web site: http://www.cern.ch/rd50/.
[3] Michael Moll on behalf of the CERN RD50 collaboration, “Development of radiation hard sensors for very high luminosity colliders - CERN - RD50 project – “Nucl. Instr. & Meth. in Phys. Res. A 511 (2003) 97-105.
[4] Mara Bruzzi on behalf of the CERN RD50 Collaboration, “Material Engineering for the Development of Ultra-Radiation Hard Semiconductor Detectors”, Nucl. Instrum. & Meth. A 518, 1-2, 2004, 336-337.
[5] Panja Luukka on behalf of the CERN RD50 Collaboratin “Status of Defect Engineering Activity of the RD50 Collaboration” Nucl. Instrum. & Meth. A 530, 1-2, 2004, 152-157.
[6] Electronic versions of the talks are available on the RD50 www-page under http://www.cern.ch/rd50/doc/

[7] Michael Moll on behalf of the RD50 Collaboration.
[8] Andrea Candelori on behalf of the CERN RD50 Collaboration.
[9] Mara Bruzzi on behalf of the CERN RD50 Collaboration.
[10] Eckhart Fretwurst on behalf of the CERN RD50 Collaboration.
[11] Mara Bruzzi on behalf of the CERN RD50 Collaboration.

2 Executive summary

2.1 Defect and Material Characterization (DMC)

1. *Defects with strong impact on the performance of Si detectors using high resistivity silicon wafers of different types*, Standard Float Zone (STFZ), Diffusion oxygenated Float Zone (DOFZ), Czochralski-grown (CZ) and epitaxial material (Epi). Irradiations have been performed using 23 GeV protons, Co^{60} – gamma and MeV electrons. A particular focus, both experimentally and theoretically, has been on the oxygen dimer and its influence on the defect evolution and thermal donor formation during irradiation and thermal treatment. The controversy about the identity of the so-called I- and X-levels is still not resolved but strong evidence is presented showing that both levels originated from defects involving multivacancies. A specific important result is that a donor state of the X-center has been detected.
2. *Detailed comparison between CZ- and DOFZ-Si materials at low irradiation doses;* during annealing at temperatures in excess of ~325 °C substantial differences between the two materials are revealed. Especially, DOFZ-Si is found to contain a high concentration of hydrogen which is shown, in a separate study, to have a strong impact on the thermal stability of prominent irradiation-induced defects like the divacancy (provided that the hydrogen content is sufficiently high).
3. *Modeling of the defect reaction kinetics for different irradiation scenarios*; in particular, the role of a new 'fourfolded coordinated silicon defect" is investigated with respect to leakage current and effective carrier concentration after hadron irradiation (an old but still very central topic). The preliminary results look promising but further work is needed to obtain a solid verification.

2.2 Defect Engineering (DE)

1. *Standard and Oxygen enriched FZ silicon (DOFZ).* Both material types have been studied mainly for comparison with the other type of materials under investigation of the RD50 collaboration.

2. *High resistivity Cz silicon*: The radiation hardness of Cz silicon grown by Sumitomo and MCz silicon grown by Okmetic has been investigated by several irradiation campaigns. Due to the high oxygen concentration of this material the radiation induced change of the effective space charge concentration or the depletion voltage is considerably smaller compared to DOFZ material. Microscopic studies have proven that in the Cz material the formation of shallow oxygen related donors (early thermal donors) by irradiation play a major role in the macroscopic behavior of the devices. As a special variant p-type MCz material was converted to n-type by thermal treatments at 430°C and 450°C introducing thermal double donors. Detailed microscopic studies on this TD doped material are in progress.

3. *Epitaxial silicon*: A different approach for increasing the radiation tolerance of silicon detectors is the use of thin epitaxial silicon layers. The superior radiation tolerance of these devices with respect to the radiation induced change of the depletion voltage has been demonstrated for irradiation with 23 GeV protons, 58 MeV Li ions and reactor neutrons up to fluences of $F_{eq} \approx 10^{16}$ cm^{-2}. For all particles no type inversion is observed which can be explained by a generation of shallow donors which overcompensates the creation of deep acceptor like defects at high fluences. The creation of shallow donors by proton irradiation and the presence of oxygen dimers was proven by TSC measurements. In continuation of the work in 2003 new epitaxial layers with a thickness of 25 µm and 75 µm were grown by ITME and the production of detectors was performed by CiS. First studies on their radiation tolerance have been performed and so far no evident differences to 50 µm thick devices could bee observed.

4. *Hydrogen in silicon*: First studies on hydrogen in FZ silicon have shown that already in non-hydrogenated FZ devices the hydrogen related defect VOH could be detected after electron irradiation and isochronal annealing up to 350°C. From measurements of the donor depth profile on the same sample it could be demonstrated that the hydrogen in the device is concentrated at the p^+- and the n^+-surface and diffuses at 350 °C up to about 80 µm into the bulk. A hydrogenation of FZ samples from the n^+-side was performed. Defect reactions with hydrogen after irradiation with 3.5 MeV electrons and isochronal annealing up to 350 °C have been studied by DLTS in correlation with measurements of doping depth profiles. The results indicate that during annealing hydrogen diffuses strongly throughout the whole bulk material and promotes the formation of thermal donors.

5. *Defect engineering by pre-irradiation treatments:* Various pre-irradiation processes with fast reactor neutrons followed by subsequent annealing of high resistivity float zone (FZ) and Magnetic Czochralski (MCz) silicon were performed. Detectors of different type and design were processed at ITC-IRST in Trento. From electrical characterizations of all wafers it was found that the required quality was not achieved for many devices. The reason for this reduced success rate was due to a not sufficient surface quality after polishing. Nevertheless, first irradiation experiments with 23 GeV protons at CERN and fast reactor neutrons at research reactor in Kiev were undertaken and the study and analysis of macroscopic and microscopic measurements is in progress. Because of the polishing problems a new set of FZ wafers with guarantied surface quality is in the phase of processing.

2.3 Pad Detector Characterization (PDC)

1. *Radiation hardness* of different detector materials was studied in more than 10 irradiation campaigns. The silicon materials under investigation were standard Float Zone silicon n-type (nFz), standard Float Zone silicon p-type (pFz), oxygenated Float Zone silicon n-type (nDOFz), oxygenated Float Zone silicon p-type (pDOFz), Czochralski silicon n-type (nCz), magnetic Czochralski silicon n-type (nMCz), magnetic Czochralski silicon p-type (pMCz) and pad detectors with epitaxial silicon layer (Epi). More than 400 pad detectors were irradiated and characterized by IV, CV, CCE and TCT methods.

2. *Technotest sub-project.* The objective of this project is to find correlations between the properties of initial high resistivity silicon, processing and design of detectors, detector electrical characteristics and radiation hardness with respect to different types of radiation. The sub-project will continue in 2005 and the participating institutes are Ioffe Physico-Technical Institute (PTI), Research Institute of Material Science and Technology (RIMST), Brookhaven National Laboratory (BNL), Helsinki Institute of Physics (HIP), Iosef Stefan Institute, and Glasgow University.

3. *Epi-detectors* radiation hardness in terms of full depletion voltage deterioration was established. The main difference between n-type epi-Si and FZ materials is generation of positive space charge in epi-Si, which doesn't anneal out (stable damage). Although epitaxial silicon is normally essentially free of oxygen (precursor for TD formation), there are clues of oxygen diffusion from the substrate during the epitaxy and device processing. This is believed to allow the generation of thermal donors in thin active epi-layer and thus the compensation of radiation induced defects.

4. *Type inversion in MCz* detectors was studied by Transient Current Technique (TCT) method. A TCT setup was constructed within the premises of the CERN Solid State Detectors Section in 2004. The results demonstrate that MCz silicon still is not type inverted after a fluence of 5×10^{14} p/cm^2 (24 GeV/c protons).

2.4 New Materials (NM)

1. *SiC:* Growth of thick, low-doped epitaxial layers (2" wafers, up to 50μm thick, down to $1x10^{14}cm^{-3}$ p-type or n-type shallow dopants) and processing of Schottky barriers and p^+n junctions have been significantly progressed in 2004. The material shows high and uniform crystalline quality. Before irradiation the electrical and charge collection properties of diodes manufactured within RD50 are of the quality needed to use these devices as detectors for ionising irradiation. Average electron-hole pair creation energy in 4H-SiC was determined to be 7.7eV. The spectrometry properties of 4*H*-SiC based detectors as measured by the Ioffe group is commensurable with precision Si-detectors. Preliminary radiation damage tests have been performed in 2004 with different particles, energies and fluences up to fast hadron fluences of $10^{16}cm^{-2}$. The results show that N_{eff} decreases with increasing fluences. Maximum fast hadron fluences investigated ($7x10^{15}cm^{-2}$ reactor neutrons at Ljubljana, $1.4x10^{16}cm^{-2}$ 23GeV/c p at CERN) resulted in capacitance values independent of reverse bias, indicating a semiconductor material in which the shallow dopants are almost compensated by radiation-induced traps. The charge collection efficiency was studied in Florence at room temperature with mips from a ^{90}Sr source and a low noise electronic read-out with 2μs shaping time. A charge collection efficiency of the order of 30% was found at 800V for a 20μm thick diode after irradiation with $1.4x10^{16}cm^{-2}$ 24eV/c p. Various samples with thickness 40-50μm have been irradiated with neutrons up to $7\times10^{15}/cm^2$ in Ljubljana: the charge collection efficiency was studied with α-particles at room temperatures before and after irradiation at the University of Modena. Up to $1x10^{14}n/cm^2$ a 90% charge collection was measured, however at $7x10^{15}n/cm^2$ only a 20% was attained (at 700V). More radiation damage studies will be carried out in the course of 2005 to consolidate these preliminary results.

2. *GaN:* More materials, thicker and with high morphological quality, were available in 2004 within RD50. The material (epitaxial and bulk crystals) was supplied by Tokushima University&Nitride Ltd. (Japan) and Lumilog, Ltd. (France). Samples presently available to RD50 are: one 2" wafer 12μm thick (Lumilog); 3 wafers 2μm thick (Tokushima University & Nitride Ltd.). According to preliminary agreements with Lumilog, Ltd. one 50μm-thick epilayer wafer (substrate: sapphire) and one 50μm-thick semi-insulating GaN epilayer grown on a highly conductive substrate should be available in near future. The material grown by Tokushima University & Nitride Ltd showed the best charge collection efficiency (90% for a 12μm-thick diode before irradiation). Radiation damage tests have up to now been carried out only on thin samples. The CCE was measured with α-particles at room temperature after irradiation with reactor neutrons at Ljubljana. The neutron irradiated samples suffer of a dramatic decrease in CCE for fluences in the range 10^{15}-$10^{16}cm^{-2}$. More radiation damage studies will be carried out in the course of 2005 to consolidate these preliminary results.

3. *a-Si(H):* Recently, 10-50 μm-thick a-SiC(H) samples have been made available to RD50. They have been tested by Glasgow and Vilnius groups before and after $10^{15}cm^{-2}$ to $10^{16}cm^{-2}$ neutron fluence irradiation in Ljubljana. After irradiation to $10^{15}cm^{-2}$ the α-particle charge collection efficiency decreased to few percents of the value before irradiation. No charge collection was observed in the sample irradiated to 10^{16} cm^{-2}.

2.5 New Structures (NS)

1. *3D detectors:*
   Columnar electrodes allow in principle to obtain a full depletion voltage and a collection time significantly lower than those of standard planar detectors, while maintaining the same active detector thickness. The standard designs of 3D detectors, as firstly proposed by Parker et al., have electrodes of both doping types arranged in adjacent cells. The fabrication process of such structure is rather long and requires several steps that are not commonly used in standard detector

technology. One aim of this subproject in 2004 has been to develop alternative architectures and simplified geometries from the original design of 3D detectors. ITC-irst, Trento, in conjunction with CNM Barcelona, has developed a new 3D detector architecture to simplify the manufacturing process. Electrodes of one doping type only, (n+) are embedded in a p-type substrate. Main advantages are that column etching and doping are performed only once. Moreover, the columns may extend deep into the bulk, which is a further process simplification as the initial wafer bonding and the final mechanical lapping of the support wafer are not required. A layout, containing various detectors based on vertical electrodes has been designed. The fabrication of a first batch is starting, and it is expected to be completed in the beginning of 2005. A drawback of the proposed structure could be a larger extension of the low-field regions, which could slow down collection times. Nevertheless, simulation carried out at IRST showed that the time to collect signal even in worst cases is within 10ns. Devices will be tested by CV, IV, and CCE in 2005 before and after irradiation.
Glasgow has also pursued the fabrication of 3D detectors. By electrical chemical etching produced very parallel pores with aspect ratio of 30:1 (10μm hole diameter's). Boron diffusion has been performed in order to form p-n junctions in n-type silicon pore walls. A second set of holes has been then etched into the wafer, due to the fact that phosphorous could not be used at Glasgow the second set of holes was filled with metal to form a metal-semiconductor contact.

2. *Pixel and strip detector masks* have been designed. A first Pixel mask compatible with the Medipix-1 chip has been designed and fabricated. A square unit cell has been fabricated with a cell pitch of 57 μm repeated three times to give a unit cell of 170 μm which is consistent with the 170 μm Medipix-1 pixel size. The p-pores were fabricated from boron diffusion into the pore. The n-pores were fabricated with metal deposition into the pores using atomic layer deposition at Metorex. CV showed full depletion at 1.5V with a capacitance for a given Medipix-1 pixel of 500 fF (50 times higher than for a standard planar device). Leakage current was of a few pA per pixel.

3. *Semi-3D detectors:* A semi-3D detector has both p^+ and n^+ strips implanted on the top side of an n-type substrate while the backside has a uniform n^+ implant. All n^+ strips are connected to a positive bias or left floating while each p^+ strip is connected to an electronics channel for signal readout. Before space charge sign inversion, the depletion develops both vertically from the p^+ strips to the back n^+ plane and laterally from the p^+ strips to the neighbouring n^+ strips. During 2004 BNL, Syracuse and Purdue simulated the performance of these detectors with ISE-TCAD. The simulation shows that after the sensors are irradiated beyond type inversion a reduction in the full depletion voltage of about a factor 2 is expected compared to standard planar strip detectors. A few wafers containing semi-3D detectors and standard pad diodes were fabricated by BNL in 2004. The Purdue group measured several devices before and after irradiation. Samples were irradiated at CERN with a 24 GeV/c proton beam to two fluences of 5×10^{14} n_{eq}/cm^2 and 1×10^{15} n_{eq}/cm^2. Several diodes were also irradiated at the Indiana University Cyclotron Facility (IUCF) with a 200 MeV proton beam to a total fluence of 5×10^{14} n_{eq}/cm^2. To date, only the samples irradiated to 5×10^{14} n_{eq}/cm^2 have been measured. The expected depletion voltage of a standard planar diode exposed to this fluence is about 370 V. The depletion voltages of the semi-3D detectors were measured to be 125 V and 150 V for the samples irradiated at CERN and at IUCF respectively, as expected from simulation. A study of the detectors charge collection efficiency is planned for 2005.

4. *Thin Silicon:* Purdue group has received several 150, 200 and 300 μm thick silicon strip detectors manufactured by Micron Semiconductor. The depletion voltage decreases from ~100 V for the 300 μm device to ~15 V for the 150 μm thick sensors. The SVX4 chip developed for Run IIb of the Tevatron will be used for S/N studies of the thin strip detectors in 2005. Purdue has also received thin pixel wafers manufactured by Micron but these have not so far been measured. After the measurement of their DC characteristics the Purdue group plans to conduct studies of the detectors coupled to the CMS .25 μm readout chip S/N performance using the laser system that has been set up for the CMS pixels. Trento, Padova and Firenze groups in 2004 have

characterized thin devices fabricated at IRST in 2003. Radiation damage tests have been performed with 58 MeV Li ions at the INFN National Laboratory of Legnaro, Italy. Diodes fabricated on 50 μm and 100 μm thick high resistivity Si have been irradiated up to 1×10^{14} Li/cm^2. Devices made from thinned substrates exhibit a very low depletion voltage even after the maximum fluence. In particular, V_{fd} does not exceed 60 V for the 50 μm thick detectors even at the highest fluence, confirming the expected higher radiation hardness with respect to 300 μm thick sensors, for which V_{fd} = 230 V at only 10^{13} Li/cm^2. Charge collection efficiency was tested with a ^{90}Sr β-particle source, using a low-noise electronic read-out with 2.4μs shaping time. After irradiation, the CCE was studied for devices irradiated up to $1.8\text{x}10^{13}\text{Li}^{+}\text{cm}^{-2}$. A 100% CCE can always be measured if a sufficiently high voltage is applied to the thin detectors. E.g., to achieve a 90% CCE ~75V is needed in 50μm-thick diodes irradiated up to $1.8\text{x}10^{13}\text{Li}^{+}\text{cm}^{-2}$. Devices irradiated with higher Li ion fluences and with 24GeV/c protons up to 10^{16}cm^{-2} are presently under study.

2.6 Full detector Systems (FDS)

1. *Radiation hardness of oxygen enriched Si microstrip detectors* A few oxygenated and standard p-type microstrip Si detectors produced by CNM Barcelona have been irradiated to 1.1, 3 and 7.5 $10^{15}\text{p}\cdot\text{cm}^{-2}$ in the CERN-PS IRRAD facility at room temperature and unbiased. After irradiation they were kept at low temperature (<-10^{o}C). The irradiated devices have been measured by the Liverpool group using a 1060 nm laser and fast electrons from a ^{106}Ru source (with an energy deposition comparable to minimum ionising, m.i.p., particles). The source measurements allowed the evaluation of the absolute CCE(V) (relative to the pre-irradiation value of identical detectors) and the laser measurements allowed the study of the relative CCE(V) at low biases. The detectors were read-out with a SCT128A LHC speed (40MHz) chip. The CCE(V) and the noise measurements have been performed at –20/25 ^{o}C. The noise does not show a clear dependence on the bias or on the irradiation level, though a substantial increase of the reverse current is measured after the different radiation doses. This is expected because the noise, with LHC speed electronics, is dominated by the input capacitance, with reduced dependence on the shot noise induced by the increased reverse current. The charge collection efficiency is strongly dependent on the irradiation dose, being further reduced with fluence as a result of charge trapping. After the highest fluence of $7.5\text{x}10^{15}\text{p}\cdot\text{cm}^{-2}$, the charge collected at the maximum applied bias (900 V) by these n-in-p mini-strip detectors is > 6500 electrons. This corresponds to a signal over noise value of ~7.5, which is still sufficient for efficient tracking. This is presently the only measurements made with segmented detector at such a high fluence and it is used to inform the extrapolation of collected charge for the highest doses expected in the innermost layers of sLHC. The collected charge at the highest dose corresponds to the signal deposited in ~90μm thick non-irradiated silicon detector. It should also be noted that the charge collection is still not saturated at 900V. These results already show that with the choice of the appropriate geometry (cell size) and with low noise electronics, silicon detectors able to survive doses anticipated for the SLHC trackers can be fabricated.

3 Defect and Material Characterization (DMC)

3.1 Defects with strong impact on the Si detector performance

3.1.1 Motivation

Experiments after irradiation of diodes processed on different silicon material (STFZ, DOFZ, Czochralski (Cz)) with high fluences of 23 GeV protons have shown that the "type inversion" effect as seen in STFZ and at larger fluences in DOFZ does not occur in Cz-Si. Comparing the oxygen concentration in these materials determined by SIMS measurements ($< 5x10^{15}cm^{-3}$ in STFZ, $1.2x10^{17}cm^{-3}$ in DOFZ and $8x10^{17}cm^{-3}$ in Cz) the beneficial effect of oxygen seems to be a straightforward conclusion. However, recent irradiation experiments on Epi-diodes (epitaxial silicon grown on low resistivity Cz substrate) have shown that, despite the low oxygen concentration ($\approx 10^{17}$ cm^{-3}), these devices are highly superior to any standard or oxygenated float zone silicon devices and that contrary to those and similar to Cz material the Epi diodes do not get "type inverted" [1, 2]. The effect has been explained on the basis of an enhanced generation of the bistable donors BD which can even overcompensate the negative space charge introduced by deep acceptors [3, 4]. These latter investigations led us to consider that the beneficial effect of oxygen may not only be connected with the concentration of oxygen interstitial O_i, which influence the generation of deep acceptors (the I defect), but also with the concentration of oxygen dimers O_{2i}, which may determine the generation of shallow donors (BDs) in the material.

3.1.2 Results after 23 GeV proton irradiations [5]

a) ***Evaluation of O_{2i} concentration in different types of Si via the IO_{2i} defect***

The oxygen dimer is electrically inactive (cannot be detected by DLTS or TSC techniques), but it gives rise to local vibration modes and can hence be detected by IR-absorption measurements if their concentration is larger than $10^{15}cm^{-3}$ – the detection limit of the technique. The O_{2i} was detected in as grown silicon only in Cz material, where it exists in a concentration of a few 10^{15} cm^{-3} (i.e. about 3 orders of magnitude lower than the O_i concentration). Although its concentration in FZ type silicon is below the detection limit, O_{2i} can nevertheless act as a sink for radiation induced migrating interstitials I by forming the IO_{2i} defect which is electrically active and can be detected by more sensitive techniques like DLTS and TSC. A relative estimation of the dimer concentration in different types of silicon (FZ, Cz and Epi) was done via the detection of the IO_2 defect after 23 GeV proton irradiation.

The introduction rates of all defects detected after low proton fluences in different type of silicon (STFZ, DOFZ, Cz and Epi) were determined via DLTS measurements and they are given in Fig. 3-1. The IO_{2i} complex was detected only in Cz and Epi material. The introduction rate of IO_{2i} was evaluated to be 1.9 cm^{-1} and 0.7 cm^{-1} in Cz and Epi materials respectively. In our opinion, as long as there is no evidence of more interstitials trapped in other types of defects in Cz material (electrically active or inactive), the factor of about 2.7 higher concentration of IO_{2i} in Cz compared with the Epi material, indicates a 2.7 higher dimer concentration in Cz compared with Epi diodes. It is worth mentioning here that the IO_{2i} defect was not detected after low fluences of 23GeV proton irradiation in any float zone silicon based structures (STFZ or DOFZ) indicating a much lower concentration of oxygen dimers in these materials.

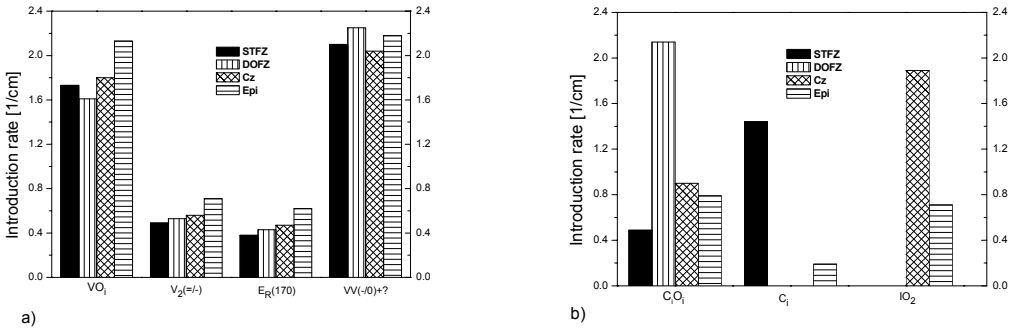

Fig. 3-1 The introduction rates of the defects detected after low proton fluences in different type of silicon (STFZ, DOFZ, Cz and Epi): a) vacancy related defects; b) interstitial related defects

b) Radiation induced donor generation in Cz and Epi silicon

Defects like BDs or the I center start to be generated after high irradiation fluences where the DLTS method cannot longer be applied. As described in previous work [3], the BDs are detectable in two configurations, via two energy levels - BD tail$^{+/++}$ shallower than BD$^{0/++}$, from which only the BD$^{0/++}$ level can be used for quantitative evaluations with our experimental setup (the lowest reachable temperature is 15 K). However, it should be mentioned that, independent of their configuration, the BDs are positively charged in the space charge region at room temperature (RT). The characteristics of BDs (donor activity, energy level position, bistability) are very similar to that of the earlier thermal donors TDD2, facts which sustain an identification of BDs with these TDDs. Exposing the material to daylight can easily change the configuration corresponding to the BD$^{0/++}$ energy level to that associated with the BD tail$^{+/++}$ level. The reverse process may take place during long time storage in the dark at RT, without any bias applied on the sample. As well as in the case of earlier TDDs the BDs cannot always be detected in their full concentration via only one of the configurations. The existence of the defect in one or the other configuration depends on the Fermi level position with respect to the defect energy levels [6,7]. An example in this respect is given in Fig. 3-2a where the TSC spectra recorded on a Cz diode after exposure to day light or after keeping it in the dark for 5 days are represented. In this figure the curve recorded after daylight exposure shows no BDs in the configuration BD$^{0/++}$ (the full concentration of BDs exists in the configuration corresponding to BD tail$^{+/++}$) while the curve after the sample was kept in the dark for 5 days shows a partial change of the configuration from BDs tail$^{+/++}$ to BDs$^{0/++}$. In contrast, the measurements performed on Epi material (see Fig. 3-2b) had shown that the BDs can be fully converted in the configuration corresponding to the BD$^{0/++}$ energy level. This fact allows an accurate evaluation of the BD introduction rates in Epi material. The differences seen in the TSC spectra of the Cz and Epi materials (Fig. 3-2b) regarding the V_2 and VO concentration are mainly due to the differences in the free electrons concentration (15 times higher in Epi compared with Cz). The filling of these electron traps starts already during the cooling process under zero bias. As higher the concentration of free electrons as better is the filling of electron traps during the cooling process under zero bias. During the cooling the existing free carriers will first be trapped on the deepest levels (like the I defect). By forward injection performed at low temperature additional free electrons are generated but also free holes and the VO and V_2 defects can only be partly filled with electrons at this temperature. Thus, the concentration of deeper levels can be evaluated more accurately from these TSC experiments. However, despite this fact, the BDs concentration can be accurate determined via BD$^{0/++}$ level since

the BD conversion in this charge state takes place already at room temperature. Once the change of the configuration is successful this cannot be changed at temperature lower than 200 K no matter the filling procedure [7].

In our measurements the forward injection was performed at 15 K. In addition, the missing of the BD tail$^{+/++}$ from the TSC spectrum corresponding to Epi material represents a good argument for an accurate evaluation of the BD concentration via the BD$^{0/++}$ state. *The BDs introduction rate in Epi material after proton irradiation is determined to be 0.7x10^{-2}cm^{-1}*. Unfortunately, in the case of Cz material the BD concentration couldn't be evaluated in a direct way as in the case of Epi material. However, a rough estimation can be done starting from the hypothesis, suggested by the previous experiments, that the dimers are the origin for the generation of BDs. As argued above, the dimers are in a 2.7 times higher concentration in Cz material compared with the Epi one. Thus, the BDs introduction rate in Cz diodes is estimated to be 1.9x10^{-2}cm^{-1}.

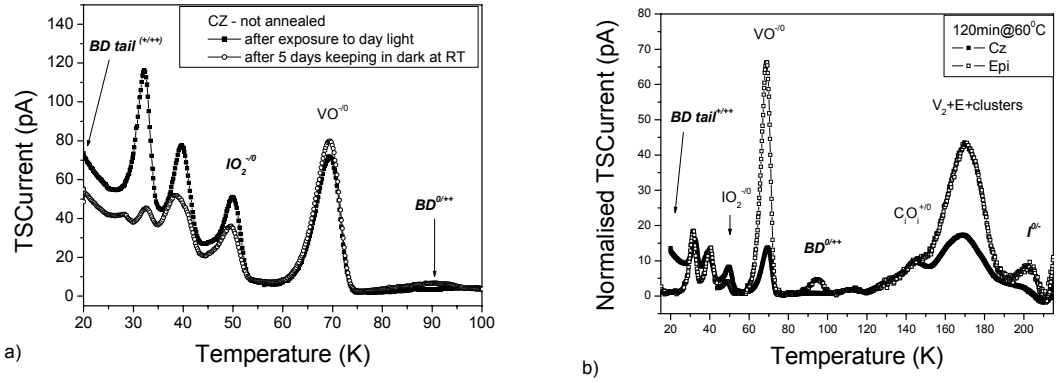

Fig. 3-2 TSC spectra after irradiation with 23 GeV protons with an equivalent fluence of 1.84x10^{14} cm^{-2} recorded on: a) Cz diode after exposure to day light or after keeping it in the dark for 5 days; b) Cz and Epi material after an annealing treatment at 60^{0}C for 120 min. The diodes were kept 2 days in dark at RT prior to TSC measurement.

c) The I defect in Cz and Epi silicon

For a better evaluation of the I defect concentration we have chosen the spectra after 120 min annealing at 60^{0}C where the contribution of the clusters is reduced as well as the value of the leakage current which both reduce the resolution of TSCurrent in the I defect corresponding TSC peak temperature range (see Fig. 3-2b). The I defect is partly negatively charged at room temperature (RT) and its contribution to the effective doping concentration N_{eff}, after an equivalent fluence of 1.8 x 10^{14} cm^{-2}, is evaluated to be 6.8 x 10^{12}cm^{-3} and 1.8 x 10^{12} cm^{-3} for Epi and Cz materials respectively.

d) Contribution of radiation induced defects on the N_{eff} measured at room temperature

The change in N_{eff} due to proton irradiation can be partly explained by the TSC evaluations presented above – the negative charge introduced by the I defect and the positive charge introduced by the BDs in the space charge region of the investigated Epi diode. Thus, due to the proton irradiation of 1.8 x 10^{14} cm^{-2} equivalent fluence, the effective doping concentration at RT changes from 7.2 x 10^{13} cm^{-3} to 5.7 x 10^{13} cm^{-3}. The positive space charge introduced by BDs in Epi material at RT was evaluated to be 1.3x10^{12} cm^{-3} for this equivalent fluence. By taking into account also the donor removal (the formation of E center in a concentration of 7.4x10^{12} cm^{-3}) our evaluations predict the change of the initial N_{eff} to a value of 6.0 x 10^{13} cm^{-3}. The missing part represents a concentration of negative charge of 2.5 x 10^{12} cm^{-3} which may be due to clusters (expected to be the same in both

Epi and Cz materials) or other deep defects not detected in our experiments for an equivalent fluence of 1.8 x 10^{14}cm^{-2}. In the case of Cz material it was not possible to determine the full concentration of BDs from TSC experiments. However, an estimation of the BDs concentration, considering a 2.7 higher concentration of oxygen dimers in Cz compared with the Epi material has led, as expected, to similar values for the introduction rate of the negative space charge introduced by clusters at RT (~1.4x10^{-2}cm^{-1}). We mention here that error margins of 5% apply to both the estimations of N_{eff} from C-V measurements and for the space charge concentration introduced by defects as I and BDs at RT determined from TSC experiments.

3.1.3 Results after Co60 – gamma irradiation [5, 8]

a) ***TDDs - electron capture cross section*** **[5]**

Until now the capture cross section of TDDs has not been measured, because most of the Cz materials used for material investigations have a maximum resistivity of 50 Ωcm and the TDDs electron capture cross section is above 10^{-13} cm^2. On such a low resistivity material the calculated capture time constant is 30 ns for a capture cross section of 10^{-13} cm^2 which cannot be measured with most standard DLTS equipments. The Cz material used in this work has a higher resistivity (1.2 kΩcm) allowing the detection of capture cross sections lower than 5x10^{-12} cm^2. The direct measurement of the TDDs electron capture cross section could thus be performed an resulted at 60 K in a value of σ_n^{TDD}= 2.7x10^{-12} cm^2.

b) The I center - annealing at high temperatures **[8]**

Annealing experiments performed on STFZ material, irradiated with 360 and 400 Mrad respectively, have shown that the I defect (the main cause for the changes in silicon diodes characteristics after high levels of gamma-irradiation) is stable up to 325-350 ^{0}C (see Fig. 3-3). The change in the concentration of I center with the annealing time at 300 ^{0}C is shown in Fig. 3-3a. As can be seen the I center starts to anneal out after 460 min at 300 ºC**.** Thus, the I center does not dissociate or migrate and does not react with any of the impurities or defects existing during the first 460 min of annealing. The annealing-out of I center is due to reaction with migrating defects resulting from the dissociation of some very abundant defects (e.g. VO). Once such reaction became possible the annealing-out of I center can be described by a time constant of 950 minutes in our oxygen lean material, if fitted with an exponential decay. The filling of V_2, H(172K) and VO traps depend on the temperature where the carrier injection is performed. The strongest dependence is observed for the VO center (a 10 times higher concentration after filling at 50K compared with 20K).

The V_2 anneals out in two steps: drastically (80%) during the first 7.5 min, then almost constant up to 40 minutes when a decrease is observed again. Such behaviour is an indication that at this temperature V_2 does not dissociate but rather reacts with other migrating defects. During the first 7.5 minutes no significant increase of new TSC signals are detected indicating that V_2 mainly reacts with some impurities forming complexes which are not electrically active. We have to mention here that due its temperature dependent capture cross section the real V_2 concentration is higher than detected by performing electron injection at 20 K with at least a factor of 5.

By accounting the I defect characteristics - detected as a direct result of irradiation in oxygen lean material, formed via a second order process (up to 500 Mrad dose), thermally stable up to 325-350 ^{0}C in STFZ - it is very likely that the I center is generated via $V+VO \rightarrow V_2O$. The formation of V_2O from V_2 and O is by 0.9 eV less favorable than from V and VO [9]. Other possible complexes formed via a second order process are: divacancy-oxygen dimer ($V+O_2 \rightarrow VO_2$, $VO_2+V \rightarrow V_2O_2$) or

trivacancy ($V+V_2 \rightarrow V_3$) as was suggested in [10]. However, an identification of the I center with V_2O_2 can be excluded since this center should be more stable than was observed for the I center (to appear during the annealing out of VO) and its formation as a direct result of irradiation should be enhanced in materials with high concentrations of oxygen dimers (e.g. in Cz)- not experimentally observed. An identification with V_3 would imply that single vacancies would rather react with V_2 than with VO although the concentration of the VO is at least one order of magnitude higher than of V_2. In addition, according to EPR results, V_3 should anneal out prior to the V_2 (see [11]) – not seen in the case of the I center. The arguments given here are the reasons for the identification of the I center with the V_2O complex.

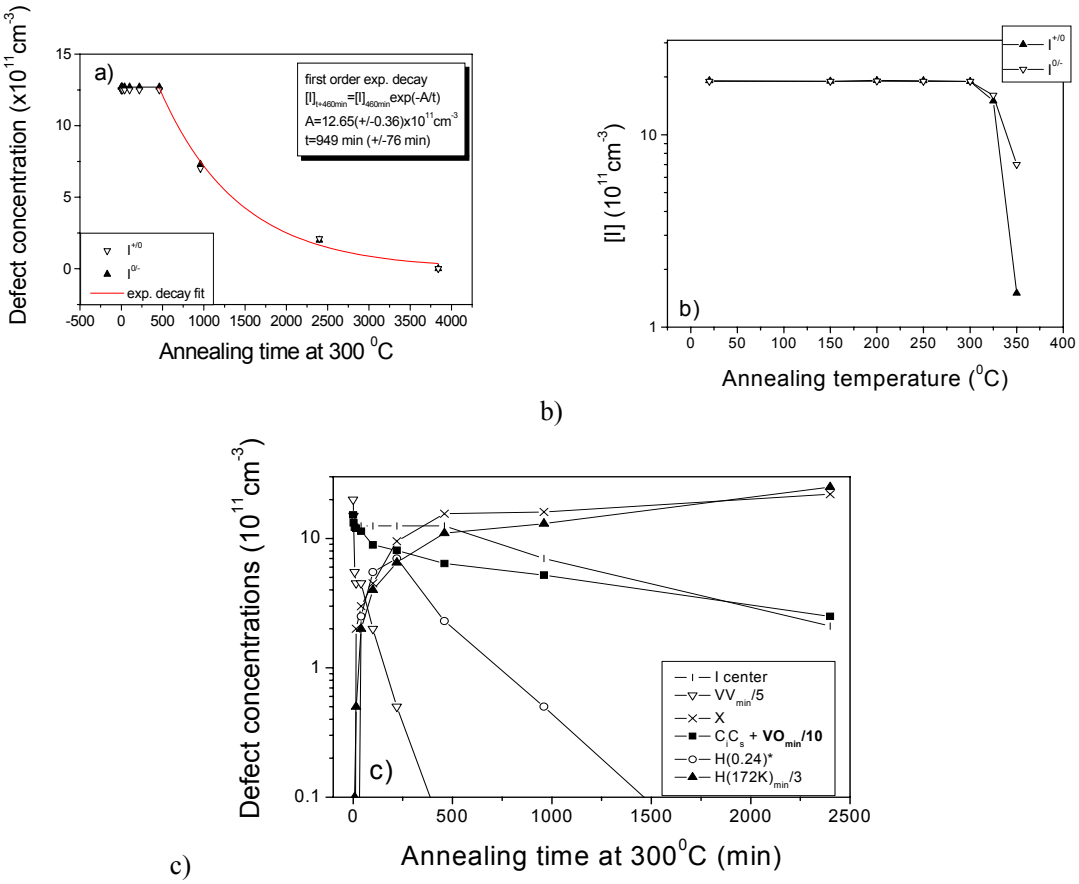

Fig. 3-3 Defect concentration after 400 Mrad irradiation dose as evaluated from TSC spectra after filling at 20K: a) annealing of I center and fit assuming an exponential decay, b) 30 min. isochronal annealing - Concentration of I center (both the donor and acceptor state) versus annealing temperature. c) all defects which may be connected with the annealing behaviour of the I center.

c) The X defect - after high irradiation doses [8, 12, 13]

The X center is one of the two candidates presently associated with the V_2O complex. This identification is connected with (a) the quantitative annealing kinetics of V_2 in electron irradiated DOFZ-Si and high purity/resistivity Cz-Si, (b) the dependence on oxygen concentration for the transformation rate between V_2 and X, and (c) theoretical predications based on local density calculations.

i) STFZ material – 400 Mrad dose

The X center (same trapping parameters as reported in [10]) appears in very small concentration during the annealing of V_2 but its generation is enhanced when VO starts to anneal out (after ~ 40 min at 300^0C).

ii) Epi material – doses between 105 and 520 Mrad

DLTFS and TSC experiments performed on Epi material for irradiation doses higher than 100 Mrad have shown that the X center is generated not only during annealing at high temperatures but also during irradiation. In Fig. 3-4a the TSC spectra recorded after an irradiation dose of 520 Mrad are represented. The X center generation rate is not linear (see Fig. 3-4b) suggesting that it is formed via a second order process. The evaluations of X defect concentrations as given in Fig. 3-4b were determined to be the same by using both DLTFS (a high resolution technique [14]) and TSC methods.

The DLTFS and TSC spectra recorded in the case of diodes irradiated with 105 Mrad and 520 Mrad, respectively, for the annealing at temperatures higher than 200°C, are represented in Fig. 3-5. In the temperature range between 200 and 280°C no change in the spectra are observable. After the annealing step at 300°C the X centers start to be formed and after the annealing at 320°C min. their concentration exceed the initial concentration of the divacancy.

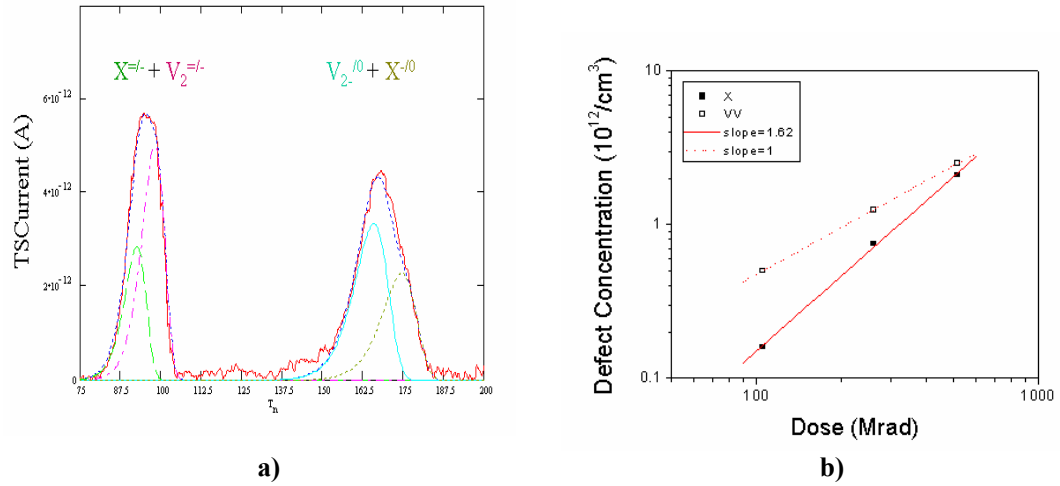

Fig. 3-4 The X center as a direct result of irradiation. a) Experimental TSC spectrum and the fit according to the trapping parameters of V_2 and X center

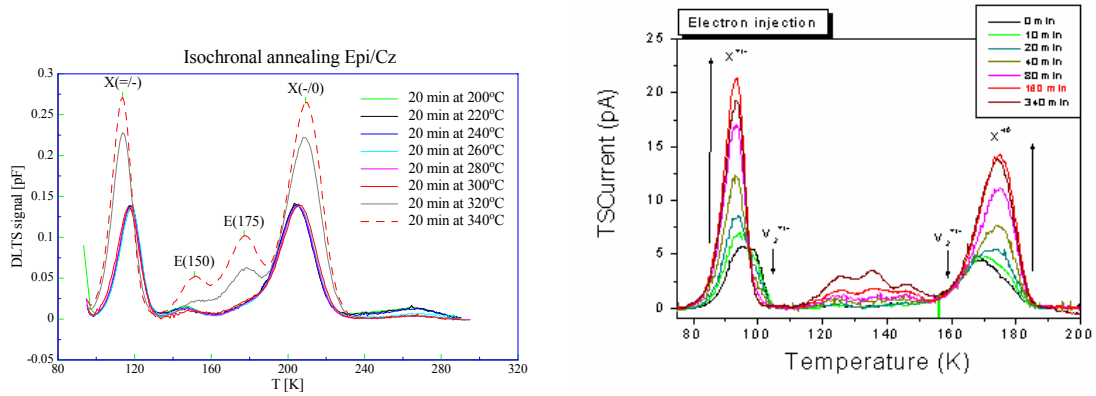

Fig. 3-5 Annealing of X center at 320^0C; a) after 105 Mrad dose [X]~2[V_2]; b) after 520 Mrad dose [X]~ 5[V_2]

After last step of annealing (20 min. at 350^{0}C) the concentration of X defects is more than double compared with of the divacancy for 105 Mrad dose and about 5 times higher for 520 Mrad dose. Thus, this increase in the concentration of X-center cannot be explained anymore only with the decrease of the divacancy clearly showing that independent of the annealing out of V_2 there is another path for forming X centers. Considering also that during irradiation the X center is formed via a second order process and that the aforementioned second path is detected after quite high irradiation levels the most plausible defect which can determine the generation of X center in much higher concentration than V_2 is the VO center. Considering the diffusion coefficients of V_2 and VO as they were reported in literature so far the formation of the X center during annealing at high temperatures can be nicely explained for both low and high doses. For low doses the formation of X center via the annealing of V_2 at 320 °C can be explained if the impurity concentration with which V_2 reacts is lower than 10^{15} cm^{-3} (see [12]). As the oxygen concentration is higher in any of the investigated materials (STFZ, DOFZ, Cz, Epi) the identification of the X center with V_2O is doubtful. However, a reaction between V_2 and oxygen dimers can easy explain the experimental results after low doses (see Fig. 3-6a). After high dose the second path for generating X centers starts to count. A reaction like $VO+VO \rightarrow V_2O_2$ can best describe the formation of X centers during the annealing at high temperatures (see Fig. 3-6b). The diffusion coefficients for V_2 and VO used in the simulations shown in Fig. 3-6 are given below:

$$DVV(y) := 1 \cdot 10^{-5} \cdot \exp\left(\frac{-1.3 \cdot q}{k \cdot y}\right) \qquad DVO(y) := 6 \cdot 10^{-4} \cdot \exp\left(\frac{-1.8 \cdot q}{k \cdot y}\right) \tag{1}$$

No further reactions regarding the annealing out of the X center were taken into account in these simulations. The formation of V_2O_2 complex during irradiation can be described via a second order process via the reactions $V+O_2 \rightarrow VO_2$ (not electrically active) and $VO_2+V \rightarrow V_2O_2$. Following this idea, the fact that, for the same irradiation dose range (100 to 500 Mrad dose), the X center was not detected directly after irradiation in STFZ and DOFZ materials indicates that the concentration of oxygen dimers in these materials is lower compared with Cz and Epi material which is in accordance with the results from Fig. 3-1 regarding the IO_2 defect as a measure of oxygen dimers concentration in different materials.

Another important result of the study of X center in Epi material is the detection of its donor state $X^{+/0}$ at ΔH ~0.22 eV with σ_p~ 7x10^{-16}cm^2.

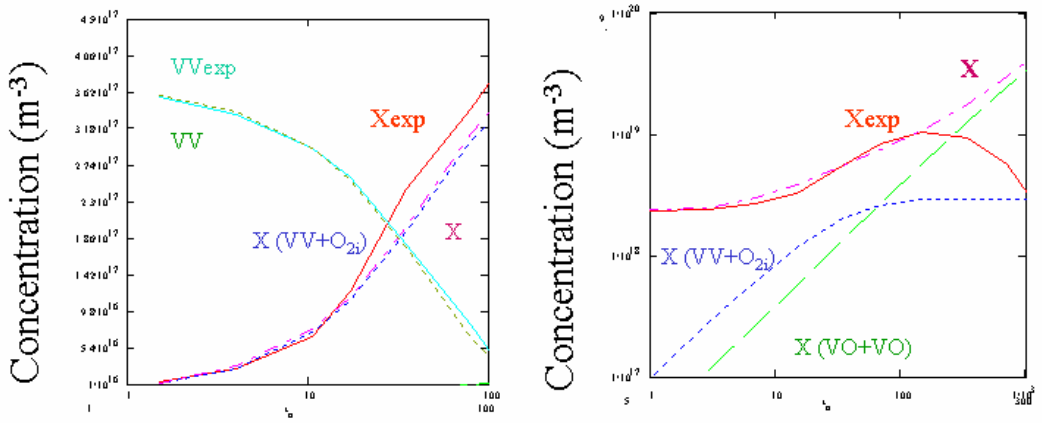

a) low dose (25Mrad) *b) high dose (520Mrad)*

Fig. 3-6 Formation of V_2O_2 during annealing at 320^{0}C via the reactions V_2+O_{2i} and VO+VO.

3.1.4 Results after 1 MeV electron irradiation of epi-Si detectors [15]

The samples used in this study are p^{+}-n-n^{+} structures where the n-type layer is a 25 μm (± 15%) epitaxially grown silicon with a resistivity of 20-25 Ωcm (doping of ~$2x10^{14}$ cm^{-3}). The p^{+}-layer is formed with boron implantation and the active area of the detectors is 0.085 x 0.25 cm^2. The detectors were irradiated with 1 MeV electrons with doses of $4.5x10^{14}$ cm^{-2} (sample A) and $3.0x10^{15}$ cm^{-2} (sample B). The samples were irradiated and stored at room temperature (RT).

The DLTS spectra of the as-irradiated samples A and B presented in Fig. 3-7 indicate presence of at least four defects. Three of the defect levels are identified as the vacancy-oxygen pair (VO) and the singly and doubly negative charge states of the divacancy ($V_2^{(0/-)}$ and $V_2^{(-/--)}$). Due to the high irradiation dose sample B demonstrates considerable carrier compensation at temperatures ≤150 K. This affects the amplitude of the $V_2^{(-/--)}$ and VO levels in the spectra for sample B. Besides the VO and V_2 levels, a mid-gap level with an activation energy of 0.52 eV can be observed in the DLTS spectra.

Because of the similarity of the activation energies, the 0.52-eV trap may be assigned to the previously reported I center in gamma-irradiated Si located at E_c-0.545 eV [16]. This identification, however, contradicts the observation of second-order generation for the I center, since the amplitude of the 0.52-eV peak is found to depend linearly on the irradiation dose. This contradiction, nevertheless, can be attributed to the different nature of the radiations. Gamma radiation is known to produce mainly monovacancies and interstitials in Si, while 1-MeV electrons can induce directly multivacancy complexes such as V_2.

Isochronal annealing for 30 min at temperatures ≤200°C does not lead to considerable changes in the amplitudes of the observed DLTS peaks. After the heat treatments at 250°C, a significant decrease in the peak amplitudes occurs and a new dominant level with an activation energy of 0.36 eV emerges in the spectrum (Fig. 3-8). The origin of the 0.36-eV level is not presently established. On one hand, it has been claimed that a level at E_c-0.36 eV in hydrogen-enriched Si is the carbon interstitial – oxygen interstitial – hydrogen complex (C_iO_iH) [17]. On the other hand, the growth of the 0.36-eV level is correlated with the annealing of the vacancy related centers. It can be suggested, however, that the 0.36-eV peak is hydrogen related.

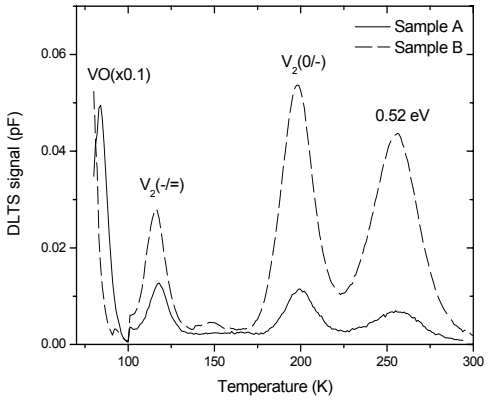

Fig. 3-7 DLTS spectra for samples A and B irradiated with electron doses of 4.5 10^{14} cm^{-2} and 3.0 10^{15} cm^{-2}, respectively. In the temperature range from 77 K to 100 K the signal has been scaled by 0.1.

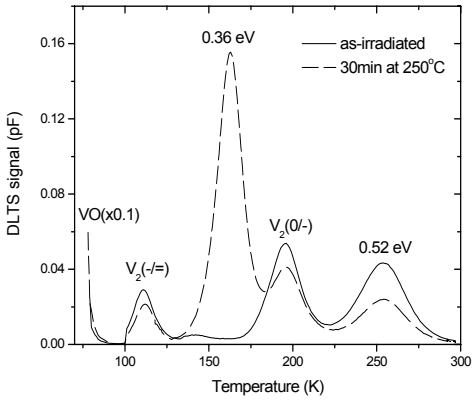

Fig. 3-8 DLTS spectra for sample B before and after annealing for 30 minutes at 250°C. In the temperature range from 77 K to 100 K the signal has been scaled by a factor of 0.1

3.2 Comparative studies of MCZ and DOFZ -Si [18]

High resistivity CZ-Si has recently become commercially available and in this study the defect evolution at low irradiation doses with subsequent annealing has been compared using CZ and DOFZ-samples. Two sets of samples were studied: the first set was prepared from MCZ-Si. The second set was prepared from DOFZ-Si. The manufacture of this material includes a step where high purity FZ-Si is O enriched: the FZ-wafers are dry-oxidized for 21 hours at 1200°C, and a subsequent anneal is then performed at 1200°C in a N_2 atmosphere where O-atoms from the pre-formed SiO_2 surface-layer diffuse into the bulk Si. For all samples boron and phosphorus implantations with post-implant annealing were performed to form $p^+n^-n^+$ diodes. As a final step aluminum contacts were deposited. Secondary ion mass spectrometry (SIMS) has been used to determine the oxygen and carbon concentrations, see Table 3-1 for a summary, where also the electron concentration in the n^- layer is given.. The samples were irradiated with 15 MeV electrons to a dose of of 4×10^{12} cm^{-2} for MCZ-Si and $2\times10^{12}cm^{-2}$ for DOFZ-Si.

Table 3-1 Survey of the samples used in the study.

Sample	Doping (P/cm^3)	Carbon (cm^{-3})	Oxygen (cm^{-3})
MCZ-Si	5.5×10^{12}	$\leq 10^{16}$	$(5–10)\times10^{17}$
DOFZ-Si	5.0×10^{12}	$(2–4)\times10^{16}$	$(2–3)\times10^{17}$

Fig. 3-1 shows DLTS spectra after annealing at temperatures in the range 250 to 350°C. Similarly to that reported in [10, 19], a gradual shift in the divacancy related peaks occurs, which has been interpreted as a transition form V_2 to V_2O, i.e., the X-center is assigned to V_2O. This behavior is observed in both DOFZ- and MCZ-Si**.** At 325°C the positions of the peaks stabilize suggesting that V_2 is annealed out. In refs. [10, 19] it is concluded that the E1 and E2 peaks are mainly X-related at 325°C. A difference in amplitude suggests, however, that other minor defects also may contribute to the single acceptor level (~200K). The activation enthalpies of X(0/-) and X(-/=) are 0.47eV and 0.23eV, respectively. We notice a minor peak at ~160K after annealing at 275°C present in both samples, and peak at ~170K after annealing at 300°C primarily pronounced in the DOFZ samples. The origins of these peaks have not been identified.

After annealing at the intermediate temperatures (250, 275 and 300°C), the E1 and E2 peaks are a mixture of V_2 and X. By using the obtained energy and capture cross-sections for the V_2 and X levels in the 200°C and 325°C annealed samples, respectively, the overlapping peaks are fitted to the sum of the two DLTS signals by varying only the amplitudes of V_2 and X. We thereby obtain the individual amplitudes for V_2 and X. Within experimental accuracy, the results of this fit agree with previous Laplace-DLTS studies [20].

The DLTS spectra for the MCZ- and DOFZ-Si are similar up to 325°C. After the annealing at 350°C, however, there are several differences (Fig. 3-10): In the MCZ-Si a decrease in the X-center concentration and a slight increase in the VO concentration takes place, while in DOFZ-Si the VO concentration decreases slightly. The E2 peak disappears while a fraction of E1 remains at 375°C. We interpret this as V_2O anneals out and a second level appears or remains at the E1 position. Another feature in DOFZ-Si is the appearance of a level labeled E4 (Fig. 3-10). This level is absent in the MCZ samples and occurs with an activation enthalpy of 0.32eV. Based on previous studies this level is identified as the vacancy-oxygen-hydrogen complex, VOH [21-25].

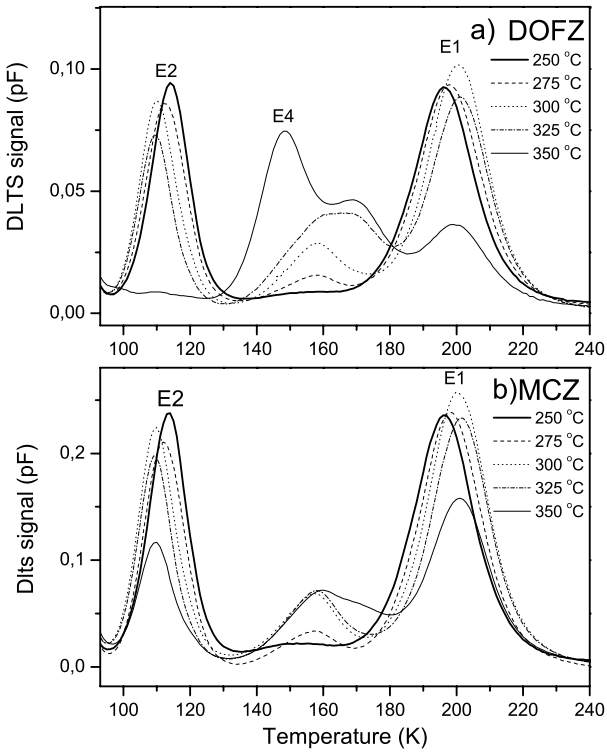

Fig. 3-9 DLTS spectra after annealing at temperatures between 250˚C and 350˚C, revealing a shift in the V_2 related peaks for both DOFZ- and MCZ-Si, and interpreted as a transition from V_2 to V_2O.

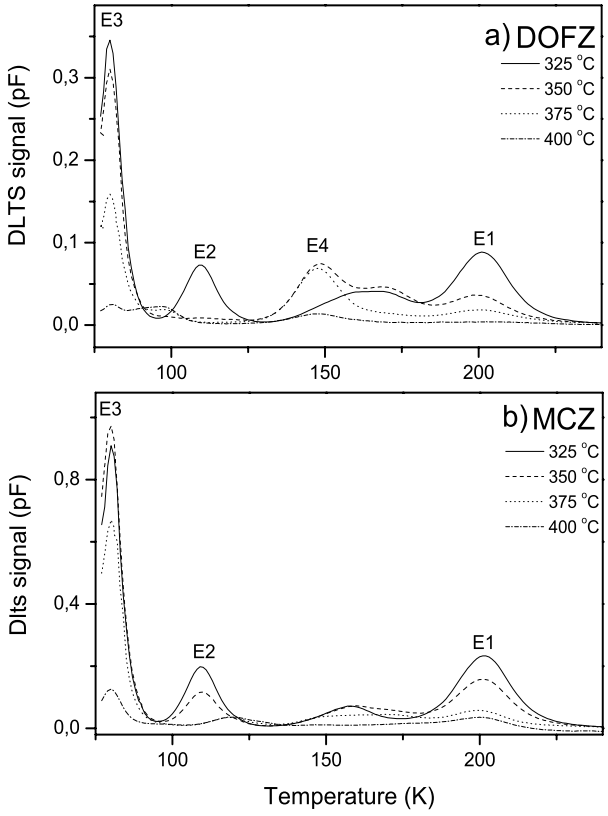

Fig. 3-10 DLTS spectra for samples annealed between 325˚C and 400˚C.

At 375°C, X has annealed out also in the MCZ-samples. There is also a decrease in the intensity the VO peak in both types of samples. It is interesting to note that this decrease is larger in the DOFZ-Si than in the MCZ-Si. VOH remains stable at 375°C, but after annealing at 400°C, it is hardly detectable. At 400°C both materials exhibit a strong decrease in the VO concentration. Fig. 3-11 shows the DLTS amplitudes for different defects after annealing steps between 200 and 400°C.

Finally, it can be reported that detailed investigations of the piezospectroscopic properties of VOH have been undertaken using stress Laplace DLTS, and they are compared with local density-functional calculations of (i) the acceptor level and its shift under stress, and (ii) the alignment of the neutral center under stress [26]. The theory is able to account for two acceptor levels observed for <100>, <111>, and <110> stress even though additional splitting is expected for a defect with static C_{1h} symmetry. This is related to (i) a rapid reorientation of the H atom within the defect at temperatures at which the DLTS experiments are carried out, and (ii) the small effect of stress on two orientations of the defect under <110> stress. The theory is also able to give a quantitative account of the alignment of the center. The effect of stress on the reorientation barrier of the defect is also investigated. The reorientation barrier of the defect in its positive charge state is found theoretically to be very small, consistent with the lack of any splitting in the donor level under stress.

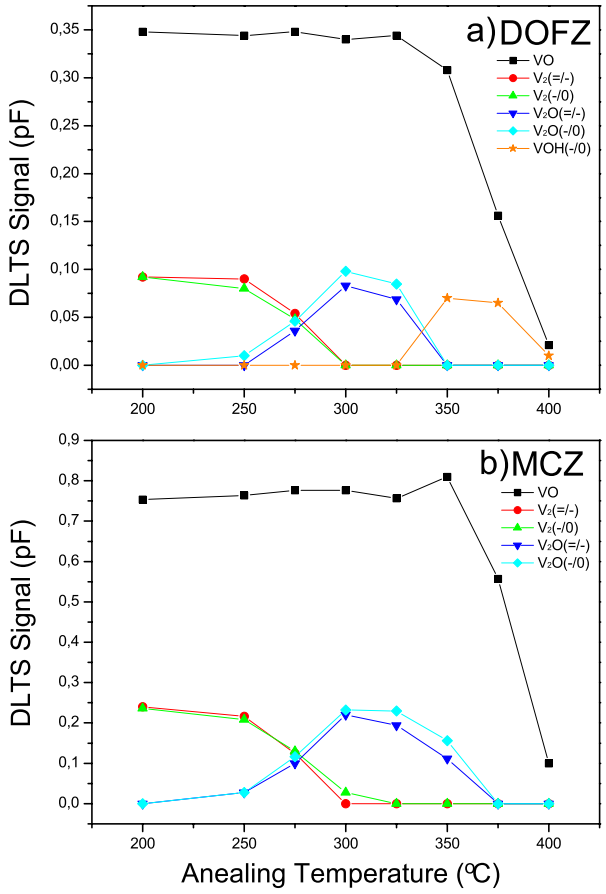

Fig. 3-11 Amplitudes of DLTS peaks corresponding to different defects. The amplitudes of the V_2 and X (interpreted as V_2O) levels in the overlapping region were obtained by fitting

3.3 Effect of hydrogen on annealing of radiation defects [27]

P^+-n^--n^+ diodes were made using high-resistivity and high purity FZ-Si wafers. As a part of the fabrication process, the wafers were oxidized in a dry oxygen atmosphere at 1200˚C for 21 hours. Subsequently, the wafers received a so-called oxygenation treatment. Oxygen was diffused into the wafer from the pre-formed silicon dioxide layer at the surface. The oxygenation was performed at 1150˚C in nitrogen atmosphere for 80 hours. An ordinary silicon diode process with boron and phosphorus implantation and post-annealing was then performed. The oxygen and carbon concentrations in the region of DLTS measurements, as determined by SIMS, are 2-3x10^{17} cm^{-3} and ≤10^{16} cm^{-3}, respectively.

Some of the samples were then hydrogenated. The hydrogenation was performed using an OXFORD Plasmalab microwave system, exposing the back n^+ side of the samples to hydrogen plasma at a pressure of 700 mTorr and a temperature of 300°C for 2 hours. This treatment results in formation of a hydrogen rich layer with a thickness of 0.5 μm and a hydrogen content of ~10^{20} cm^{-3} near the exposed surface[28]. However, the concentration of hydrogen near the front p^+ side of the diodes (~200-300 μm from the exposed surface), where the DLTS measurements take place, is expected to be substantially lower and not to exceed 10^{17} cm^{-3}. The diodes were irradiated at room temperature with 15-MeV electrons and doses of 2x10^{12} cm^{-2} and 4x10^{12} cm^{-2}. A survey of the samples used in the study is presented in Table 3-2.

Sample	Doping, P/cm^3	Oxidation	Oxygenation	Hydrogenation
A	5x10^{12}	21h dry at 1200°C	80h in N_2 at 1150°C	--
B	5x10^{12}	21h dry at 1200°C	80h in N_2 at 1150°C	2h in H plasma at 300°C

Table 3-2 Survey of the samples used in the study.

For both sample A and B, DLTS spectra of as-irradiated diodes show the presence of three major peaks with activation enthalpies of 0.43 eV, 0.23 eV and 0.18 eV that are primarily identified as the singly negative divacancy V_2(-/0), the doubly negative divacancy V_2 (=/-) and the vacancy-oxygen pair (VO), respectively. The concentration of VO and V_2, as determined by DLTS, is 1.2x10^{11} cm^{-3} and 3x10^{10} cm^{-3} for a dose of 2x10^{12} cm^{-2}, and 2.3x10^{11} cm^{-3} and 6x10^{10} cm^{-3} for a dose of 4x10^{12} cm^{-2}, respectively. The V_2(-/0) peak contains an overlapping minor contribution from other less stable centers that can be annealed out at 200°C.

The effect of hydrogenation on the annealing behaviour of V_2 is clearly seen at the annealing temperatures >200°C (Fig. 3-12). In the non-hydrogenated sample (Fig. 3-12a), heat treatments for 15 min. at 250°C and 275°C lead to transformation of V_2 to X almost without any loss in the peak intensity. The transformation is completed after 15 min at 300°C. The X peaks start to anneal out at 325°C and are considerably reduced after 15 min at 350°C. In contrast, the hydrogenated sample (Fig. 3-12b) reveals that the V_2 peaks start to disappear already at 250°C, and a significant loss of the amplitude occurs. After heat treatment at 275°C approximately 80% of the initial amount of V_2 is annealed out. It should be noted that a shift in the peak maxima is observed after the heat treatment at 275°C (Fig. 3-12b) indicating that some limited transformation of V_2 to X also takes place in the hydrogenated sample. After heat treatment at 300°C, no signals from V_2 and X can be observed in the

spectra for sample B. The amplitudes of the observed major peaks as a function of annealing temperature are presented in Fig. 3-13.

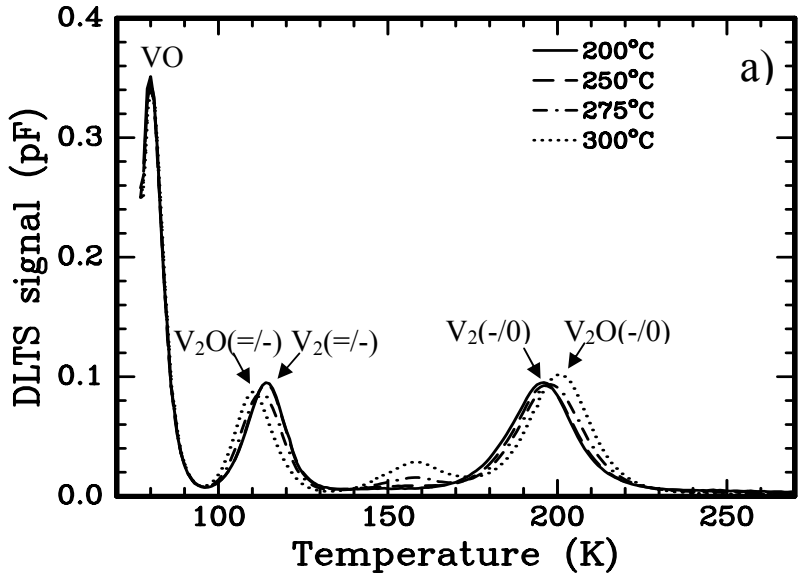

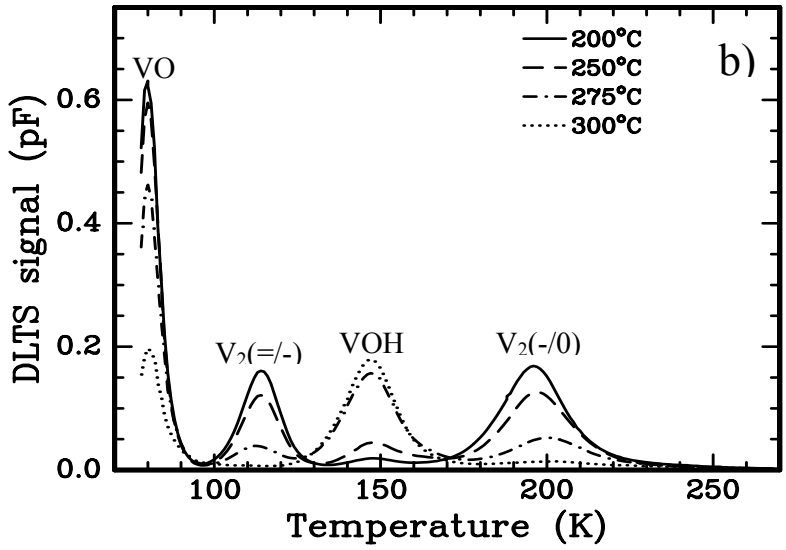

Fig. 3-12 DLTS spectra of sample A (a) and sample B (b) after annealing for 20 min at temperatures ≥200°C. The X-level is interpreted as V_2O.

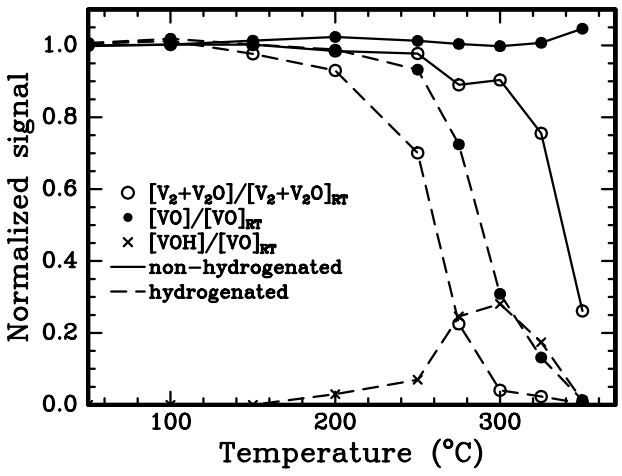

Fig. 3-13 Normalized amplitudes of the major DLTS peaks as a function of annealing temperature. The concentration $[V_2+V_2O]$ is deduced from the amplitudes of the $V_2(=/-)$ and $V_2O(=/-)$ peaks. The X-level is interpreted as V_2O.

3.4 Modeling of defect reactions in irradiated silicon

3.4.1 Irradiation scenarios at future colliders: LHC, SLHC, VLHC [29, 30]

At the present time the radiation fields are only estimated for the LHC experiments. In the case of the CMS experiment the simulated particle spectra at different positions inside the tracking volume have been published in [31]. The shape of the spectra depend strongly on the position inside the tracking volume. In the spectra, the main contribution is due to pions, followed by protons, other hadrons being irrelevant in the distributions. The two positions considered in this work are: a) r = 20 cm, z = 0÷60 cm, which corresponds to the maximum in flux, and b) r = 100 cm, z = 140÷280 cm; associated with the minimum hadron fluxes.

For LHC upgrades only rough estimates are possible. Following the ICFA Report, 9-10-2002, the following conditions for the SLHC and VLHC were assumed:

For SLHC environments:

a) the pion and proton spectra remain the same as in LHC conditions but with one order of magnitude increase in intensity, corresponding to the order of magnitude increase of luminosity,

b) the luminosity is increased as in a), but the beam energy is increased with a factor of two, the energetic distribution of pions and protons is the same as for LHC conditions, but the average energy of the spectra is shifted to higher energy with 50 MeV;

For the upgrade to VLHC:

c) the same geometrical configurations as for LHC, the same distributions of particles in the corresponding positions in the tracking cavity, but with the maximum in the spectra shifted to higher energies with about 150 MeV at the same luminosity,

d) one order of magnitude increase in the luminosity, in respect to c), respectively.

The generation rate of defects can be expressed by: $G_{irradiation} = \int CPD(E) \times Flux(E) dE$. The concentration of primary defects (CPD) has different values as a function of particle and energy. CPD is calculated considering an average energy threshold for displacements and consequently eliminating the influence of the anisotropy of the lattice on defect production.

In the LHC conditions the hadrons are the predominant particles in the tracker, especially low energy charged pions and protons. The maximum in the rates of primary defects generated by pions comes from the region around 200 MeV while for protons the major contribution comes from the lowest energy region. In our calculations, the energy dependence of CPD induced by pions is cut at 20 MeV. This cut represents only a contribution below 0.5% in the integrated defect spectra.

In Fig. 3-14 the differential energetic generation rates of primary defects, from left to right, for the LHC, SLHC and VLHC environment, for protons (triangles) and pions (asterisk and rhombus), for two positions in the tracking volume are represented. The SLHC and VLHC differential generation spectra have been obtained by increasing the average energy with 50 MeV and 150 MeV respectively. The increase in luminosity is not included.

In the two radiation fields considered in this work, the rates of generation of defects induced by pions and protons are: 6.8 x 10^8 VI/cm^3/s in the LHC conditions and SLHC condition hypothesis a), 7.2 x 10^9 VI/cm^3/s for the SLHC hypothesis b), 6.9 x 10^8 VI/cm^3/s for VLHC, hypothesis c) and 6.8 x 10^9 VI/cm^3/s, VLHC, hypothesis d) respectively.

In the considered scenarios, the maximum of the generation rate of primary defects is obtained in the hypothesis b) for the SLHC upgrade. However, normalized to the luminosity the introduction rates for the defects is very similar.

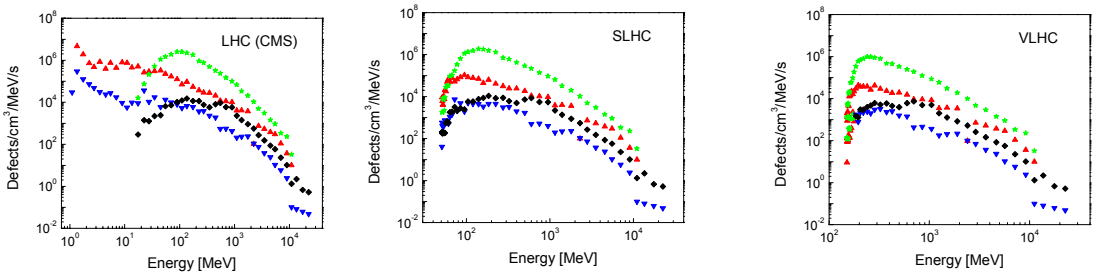

Fig. 3-14 Differential energetic generation rates of primary defects, from left to right, in LHC, SLHC and VLHC environment, for protons (triangles) and pions (asterisk and cross), for two positions in the tracking cavity, r=20 cm, z=60 ÷120 cm and r=100 cm, z=140÷280 cm respectively, in accord with hypotheses b) and c) – see text.

3.4.2. The role of initial impurities and irradiation rates in the formation and evolution of complex defects [29-32]

The concentrations of primary and complex defects have been estimated as well as their time evolution in the frame of a phenomenological model using the chemical rate theory for i) short time of irradiation; and ii) continuous irradiation, simulating the LHC, SLHC and VLHC conditions; starting from different possible silicon wafers: FZ, DOFZ, MCz, Cz, characterised only by their initial content of phosphorus, oxygen, carbon.

3.4.3 The role of oxygen dimers [29]

The study of oxygen dimers has been initiated in different laboratories in the hope to find new mechanisms by which the radiation hardness of silicon could be increased. In irradiated silicon, VO and V_2O are produced by the capture of moving vacancies by interstitial oxygen, by the VO centre respectively. While the VO centre is charged only at cryogenic temperatures, the V_2O defect is charged up to 90% at room temperature and therefore produces detrimental effects on the macroscopic detector parameters. A possible solution to diminish these uncalled effects is to produce dimers in silicon which could act as sinks for migrating interstitials by forming IO_{2i} and I_2O_{2i} defects. J. L. Lindström at al. [33] discussed the importance of the interactions between the oxygen dimers (O_{2i}) and silicon self-interstitials and vacancies. In Cz - Si, oxygen dimers are produced at least by two mechanisms: during the crystal growth, when their concentration is around 10^{15} cm^{-3} and/or during high temperature irradiation.

We discussed only the processes taking place at room temperature. The main reactions induced by dimers in these conditions are:

$$I + O_{2i} \rightarrow IO_{2i} \qquad \text{(a)}$$
$$I + IO_{2i} \rightarrow I_2O_{2i} \qquad \text{(b)}$$

Both reactions are initiated by self-interstitials. The IO_{2i} centre is electrically active with an acceptor level at E_C-0.11 eV. Both IO_{2i} and I_2O_{2i} are stable at room temperature and anneal out at about 400 K and 550 K, respectively.

If in the material there exist VO_2 centres (produced previously by irradiation at higher temperature, but which are stable at room temperature), they could also capture interstitials, producing oxygen dimers by the reaction:

$$I + VO_2 \rightarrow O_{2i} \qquad \text{(c)}$$

This reaction is also produced by the migration of interstitials, and has the same reaction constant as previous reactions. Model predictions have been compared with the experimental data published in [33], where the effect of electron irradiation at room temperature on a Cz-Si sample containing both VO_2 centres and oxygen dimers, in the concentration range $4 \div 5 \times 10^{16}$ cm^{-3}, is investigated.

In Fig. 3-15, the fluence dependence of the concentrations of O_{2i}, VO_2, IO_2 and I_2O_2 predicted by the present model are compared with experimental data after electron irradiation at room temperature of a dimer-rich Cz-Si sample.

Due to the incomplete information regarding irradiation and measurement conditions in the published paper, the comparison is only at the qualitative level. Nevertheless, a good agreement between model predictions and experimental data has been obtained.

Due to the fact that as-grown Cz-Si contains oxygen dimers on the order of 10^{15} cm^{-3}, mechanisms (a) and (b) have been introduced into the reaction scheme in the study of defect evolution of Cz and MCz-Si in LHC and SLHC conditions. Negligible contributions of these two mechanisms have been found in these conditions of irradiation and initial concentration of dimers.

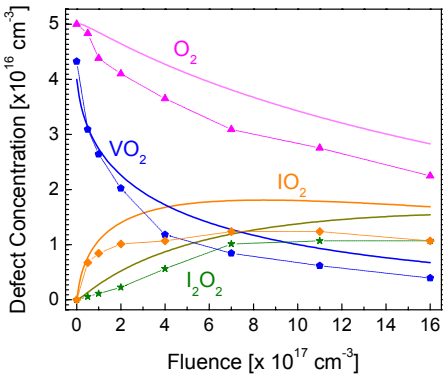

Fig. 3-15 The kinetics of complexes associated with dimers in Cz-Si at RT: model calculations – continuous line and normalised ; experimental data - points and dotted lines from Ref. [33].

3.4.4 The role of primary defects in the explanation of discrepancies between macroscopic effects in silicon detectors and model calculations [34]

An important observation is that there exists a good or reasonable agreement between model and data for the leakage current and effective carrier concentration after lepton or gamma irradiation, and discrepancies up to 2 orders of magnitude after hadron irradiation. We argue that the main discrepancies between model calculations and experimental data for leakage current after hadron irradiation could be explained considering for the contributions of primary defects in silicon: vacancy, interstitial and Si_{FFCD} defect to macroscopic effects. The source of discrepancies between data and previous modelling was tentatively attributed to the Si_{FFCD} (**Four**folded **C**oordinated Silicon **D**efect) defect. Vacancies and interstitials have a major contribution to the current short time after irradiation. If these hypotheses are correct, thus, in conditions of continuous long time irradiation, as e.g. LHC and its upgrades in energy and luminosity S-LHC and V-LHC respectively, these contributions could play a central role.

The reactions of production of primary defects considered in the present work are:

$$Si \begin{array}{l} \overset{G}{\rightarrow} \quad V + I \\ \overset{G}{\rightarrow} \quad Si_{FFCD} \end{array}$$

New experimental results [35] combined with some old data [36] permitted us to suggest the possible level position assignment for isolated vacancies and interstitials.

Goedecker and coworkers [37] predicted the existence of a new type of primary defect: Si_{FFCD} (**Four**folded **C**oordinated Silicon **D**efect). It is obtained by moving atoms from the initial positions,

but this displacement does not break the bonds with the neighbors. The defect has energy levels in the band gap (only calculated) and most probably it is very stable. We supposed that the Si_{FFCD} primary defect is uniformly introduced in the bulk during irradiation and the defect is stable in time. Also we supposed in accord with theoretical predictions that this defect has deep energy level(s) in the gap, probably in the proximity of free vacancy and interstitial.

In the calculation of the leakage current after irradiation, the SRH model is considered and some preliminary results are illustrated in Fig. 3-16.

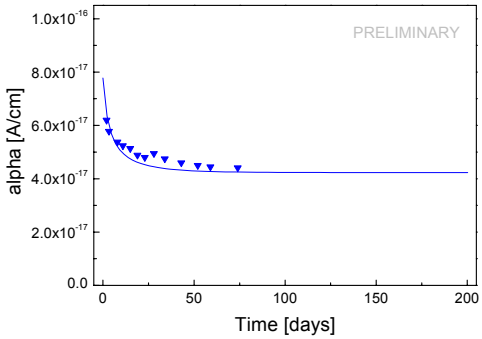

Fig. 3-16a Time dependence of degradation constant (α)after positive pion irradiation. Experimental data are from [38]

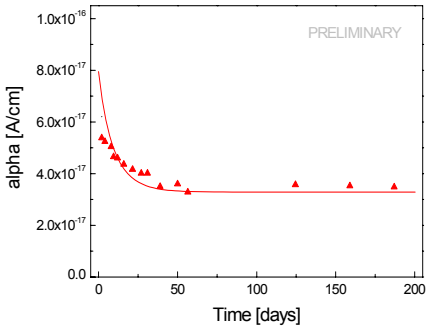

Fig. 3-16b Time dependence of degradation constant(α) after negative pion irradiation. Experimental data are from [38]

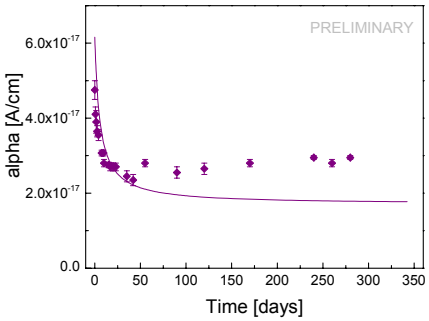

Fig. 3-16c Time dependence of degradation constant after proton irradiation. Experimental data are from[39].

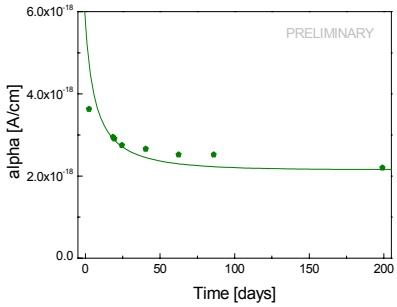

Fig. 3-16d Time dependence of degradation constant(α) after electron irradiation. Experimental data are from [40]

The existence of a "background" in the leakage current after irradiation, source of discrepancies between data and previous model calculations, was tentatively attributed to the Si_{FFCD} defect. This contribution has been found to be proportional to the concentration of primary defects at considered fluence. The contribution of value of this 'background' is around 10% of the leakage current produced by all primary defects immediately after the end of irradiation. If the Si_{FFCD} defect have a deep level in the band gap in the proximity of the intrinsic energy level, as the corresponding one for vacancy and interstitial, thus the concentration of the Si_{FFCD} could be around 10% from all primary defects contribution, but the existence of deep level needs confirmation.

In the frame of model, vacancies and interstitials have a major contribution to current short time after irradiation or during continuous irradiation. Primary defects and divacancies have the most important contributions to current. The Frenkel defect is described in the model as a bond defect. This is not a primary defect, it is obtained as a second step in interactions. The defect is rather stable at room temperature; where its lifetime is of the order of hours. In the present model calculations, the Frenkel defect, with a deep level supposed in the vicinity of intrinsic level and close to the free vacancy or interstitial levels, has a minor contribution to the leakage current, only short time after irradiation.

If these hypotheses and results are correct, thus, in the conditions of continuous irradiation (as for LHC and its upgrades) these contributions will play an important role. Further simulation work is in progress to enhance the comparison with experimental data..

3.5 References for Chapter 3

[1] G. Lindstroem, E. Fretwurst, G. Kramberger, I. Pintilie, Journal of Optoelectronic and Advanced Materials **6** (1) 23-38, (2004)
[2] G.Kramberger et al., Nucl. Instr. & Meth. in Phys. Res. A **515**, 655 (2003)
[3] I. Pintilie et al., Nucl. Instr. & Meth. A **514**, 18 (2003)
[4] J. Stahl, E. Fretwurst, G. Lindstroem and I. Pintilie, Physica B: Condensed Matter **340-342**, 705 (2003)
[5] I. Pintilie et al, "Radiation induced donor generation in epitaxial and Cz diodes" RESMDD 2004 (Italy))
[6] YA. I. Latushko et al., Phys. Stat. Sol. (a) 93, K181 (1986)
[7] A. Chantre, Appl. Phys. Lett. 50 (21), 1500 (1987)
[8] I. Pintilie, E. Fretwurst, G. Kramberger, G. Lindstroem, Z. Li and J. Stahl, Physica B: Condensed Matter, 340-342, 578 (2003)
[9] Pesola, J. von Boehm, T. Matila and R. M. Niemen, Phys. Rev. B60, 11449 (1999)
[10] G. Alfieri, E.V. Monakhov, B.S. Avset and B.G. Svensson, Phys. Rev. B68 (23), 233202 (2003)
[11] J. W. Corbett et al, Inst. Phys. Conf. Ser. No 31: Chapter 1, 1 (1977)
[12] I. Pintilie et al, "The X defect in Epi/Cz silicon diodes after high doses of Co60-γ irradiation", 5th RD50 workshop, 14-16 october 2004, Florence, Italy
[13] J. Stahl et al, 3rd RD50 workshop, Geneve, Switzerland
[14] J. Stahl et al, 2rd RD50 workshop, Geneve, Switzerland
[15] A. Ögmundsson, E.V. Monakhov, T.E. Hansen, J.K. Grepstad and B.G. Svensson, submitted to NIM A (2004)
[16] I. Pintilie, E. Fretwurst, G. Lindstroem and J. Stahl, Appl. Phys. Lett. 81, 165 (2002)
[17] O.V. Feklisova and N.A. Yarykin, Semicond. Sci. Technol. **12**, 742 (1997)
[18] M. Mikelsen, E. V. Monakhov, G. Alfieri, B. S. Avset, J. Härkönen, B. G. Svensson, submitted to Physica B (2004)
[19] E.V. Monakhov, B.S. Avset, A. Hallén and B.G. Svensson, Phys. Rev. B65, 233207 (2002)
[20] E.V. Monakhov, G. Alfieri, B.S. Avset, A. Hallén and B.G. Svensson , J. Phys.: Condens. Matter 15, S2771 (2003)
[21] P. Pellegrino, P. Lévêque, J. Lalita, A. Hallén, C. Jagadish, and B. G. Svensson, Phys. Rev. B64, 195211 (2001)
[22] K. Bonde Nielsen, L. D. Dobaczewski, K. Goscinski, R. Bendesen, O. Andersen, and B. Bech Nielsen, Physica B 273–274, 167 (1999)
[23] A. R. Peaker, J. H. Evans-Freeman, L. Rubaldo, I. D. Hawkins, K. Vernon-Parry, and L. Dobaczewski, Physica B 273–274, 243 (1999)
[24] Y. Tokuda and T. Seki, Semicond. Sci. Technol. 15, 126 (2000)
[25] P. Lévêque, P. Pellegrino, A. Hallén, B. G. Svensson, and V. Privitera, NIM. B174, 297 (2001)
[26] J. Coutinho, O. Andersen, L. Dobaczewski, K. Bonde Nielsen, A.R. Peaker, R. Jones. S. Öberg, P.R. Briddon, Phys. Rev. B**68**, 184106 (2003)
[27] E.V. Monakhov, A. Ulyashin, G. Alfieri, A.Yu. Kuznetsov, B.S. Avset and B.G. Svensson, Phys. Rev. B**69**, 153202 (2004)
[28] A. Ulyashin, R.Job, W.R. Fahrner, D. Grambole, and F. Herrmann, Diffusion and Defect Data B **82-84**, 315 (2002)
[29] S. Lazanu and I. Lazanu, Phys. Scripta, in press (2004)
[30] S. Lazanu and I. Lazanu, Rom. Rep. Phys., in press (2004)
[31] CMS Technical Report, CERN/LHCC/94-38
[32] S. Lazanu and I. Lazanu, Phys. Scripta **69**, 376 (2004)
[33] J. L. Lindström, et. al., Physica B 308-310 (2001) 264
[34] S. Lazanu and I. Lazanu, submitted to NIM A (2004)
[35] V. V. Lukianiza, FTP 33, (1999) 921, 37 (2003) 422
[36] P. M. Fahey, P. B. Griffin, J. D. Plummer, Rev. Mod. Phys. 61 (1989) 289
[37] S. Goedecker, Th. Deutsch, L. Billard, Phys. Rev. Lett. 88 (2002) 235501
[38] J. Bates et al, Nucl. Phys. B. (Proc. Suppl.) 44 (1995) 590.
[39] F. Lemeilleur et al., Nucl. Instr. Meth. Phys. Res. A 360 (1995) 438
[40] I. Rashevskaia et al., Nucl. Inst. Meth Phys. Res. A 485 (2002) 126

4 Defect Engineering

4.1 Standard and DOFZ silicon

Both standard and DOFZ silicon is mainly investigated for comparison with high resistivity Cz or Magnetic Czochralski silicon (MCz), epitaxial material (EPI), oxygen dimer enriched silicon or pre-irradiated FZ and MCz silicon. Investigations of a possible defect engineering by hydrogenation of silicon is until now concentrated on standard and oxygen enriched silicon only. The status of this subproject is reported separately.

4.2 High resistivity Czochralski silicon

Silicon crystals grown by the Czochralski (Cz) or the Magnetic Czochralski (MCz) method have a much higher oxygen concentration ([O] ≈ 4-20×10^{17} cm^{-3}) compared to any oxygen enriched DOFZ material ([O] ≈ 1-3×10^{17} cm^{-3}) due to the growth technology itself.

It has been demonstrated by recent studies that such high concentration of oxygen will strongly influence the radiation induced creation of oxygen related defects and the defect kinetics resulting in improved radiation hardness beyond the level observed so far in DOFZ silicon.

It had been shown by ^{60}Co gamma radiation damage studies of FZ silicon that the formation of two deep acceptors (I-defect, possibly V_2O; Γ-defect, structure not known) is strongly suppressed in oxygen enriched FZ material which leads to an essential lower introduction of negative space charge with increasing dose compared to standard FZ material. But in addition in DOFZ material also shallow donors (early TDD's) are created resulting in an introduction of positive space charge which over-compensates the negative space charge of the induced deep acceptors [1-5]. Both effects are more pronounced in Cz material not only in case of radiation damage by gamma radiation but also by exposures to charged hadrons [6]. In addition, it is known that in as grown Cz silicon oxygen is not only present as interstitial oxygen O_i but also in small concentration as oxygen dimers O_{2i} (see e.g. [7, 8]) which also has a strong impact on the defect formation. Furthermore, it is well known that in Cz material different thermal donors can be formed or annihilated by specific heat treatments. This also leads to a further possibility to influence the radiation tolerance of this material.

During the year 2004 test detectors had been processed by different manufacturer (Helsinki, CNM/Barcelona, ITC-IRST/Trento) on high resistivity n- and p-type MCz silicon substrates. On top of that a conversion of p-type to n-type material was performed by thermal treatments [9]. This conversion can be achieved by an introduction of thermal donors in the temperature range between 350°C and 600°C. This effect could be used to tailor the detector full depletion voltage before and after irradiation. To investigate this phenomenon a study has been carried out with six $p^+/p/n^+$ diodes, 300μm thick, manufactured on p-type Cz Si Okmetic wafers [9,10]. The six diodes belonged to the same wafer, manufactured at the Helsinki Institute of Physics and have been cut from two different regions: (P7, P8, P17) periphery, (P46, P57, P58) close to center, as indicated in Fig. 4-1.

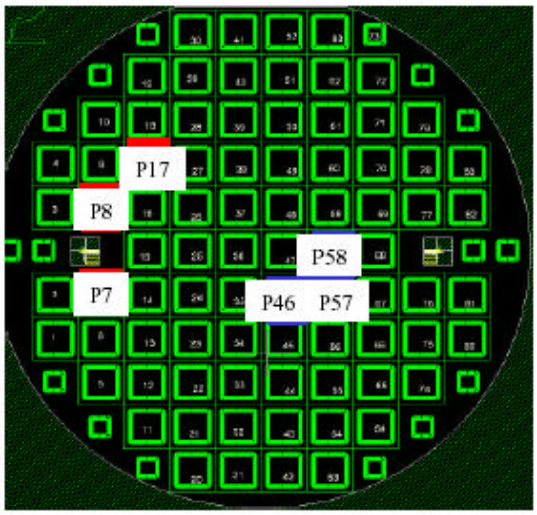

Fig. 4-1. p-type Cz silicon wafer and map of investigated diodes.

The devices have been investigated at BNL, Instr. Division, by Transient Current Technique (TCT) using a pulsed red (660nm) laser beam placed close either to the p^+ or the n^+ electrodes. The collected charge has been measured as a function of the reverse voltage in the range 0-400V, to determine the full depletion voltage and the sign of the space charge. As the devices are $p^+/p/n^+$, when the reverse bias is increased the space charge region develops from the n^+ electrode. Thus when TCT

is measured with the laser beam close to the p^+ electrode, the signal will appear only when the reverse voltage is similar or higher than the full depletion voltage, whereas by illumination of the n^+ electrode, a charge signal will be visible at any applied voltage. The effective doping of the 6 samples as measured by TCT is: $N_{eff} = -(3.44 \pm 0.23)\times10^{12}$ cm^{-3}, no correlation is observed between the N_{eff} values and the diode position in the wafer. The TCT measurements have been repeated for each diode after 5 different annealing steps (0, 45, 65, 90 and 120min) at 430°C. The results are shown in Fig. 4-2 for diode p46. The annealing process at 430°C activates shallow thermal donors (TD), which compensate the shallow acceptor dopant concentration (Boron) present in the starting material. Increasing the annealing time produces the progressive decrease of N_{eff} and eventually the inversion of the space charge sign from negative to positive: this shifts the space charge region from close to the n^+ electrode to the p^+ electrode side.

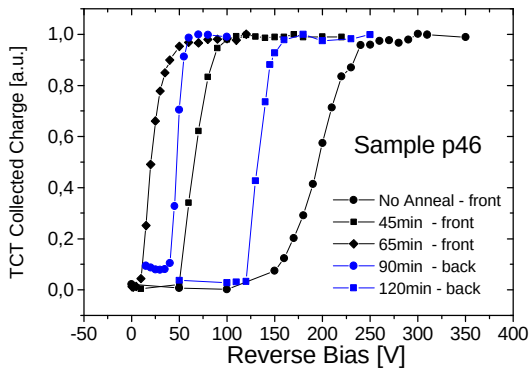

Fig. 4-2. Collected charge using laser front (black dots) or back (blue dots) before annealing and after four increasing annealing times at 430°C.

The sudden decrease in the collected charge at low reverse voltage is then observed when the laser is close to the opposite electrode, i.e. the n^+ one. Full depletion voltage and effective space charge concentration N_{eff} measured for the different annealing steps are shown in figs.3 and 4. From this study it is evident that the beneficial effect of the thermal procedure should be to produce Cz Si detectors made with high resistivity p- or n-type material, starting from wafers of lower resistivity (i.e. lower cost). Nonetheless, from data in Fig. 4-3 and Fig. 4-4 it is also evident that a correlation between the generation rates (slope of the linear fit of N_{eff} versus time) and the position of diodes in the wafer takes place. The process of activation of the shallow thermal donors in Si has been described in previous papers to be a function of $[Oi]^{\xi}$ where $[O_i]$ is the pre-existing interstitial oxygen concentration and ξ is between $2 < ? < 4$ [11]. Moreover, the role of H in the material should be also taken into account in the activation of TDs. Thus, non-homogeneities in O_i and H concentration, whereas not affecting the N_{eff} in the starting material, can give rise to a significant spread in the final values of N_{eff} after the annealing process. In our case, the spread in V_{fd} for the two groups is around 50-150V.

The same spread in V_{fd} an N_{eff} has been observed by ITC-IRST on single pad detectors made on p-type MCz Si Okmetic wafers [12]. During fabrication an annealing at 380°C was performed for sintering. We can conclude that p-type Cz Si detectors are feasible but presents, as a drawback, inhomogeneities in the concentration of native impurities (O_i, H) which, as a hidden parameter in the starting material, becomes important when annealing treatments at around 400°C or higher temperatures are undertaken.

In different irradiation experiments with different particles the radiation hardness of n-and p-type MCz silicon as well as TD doped material has been investigated and is presented in chapter 5 (PDC).

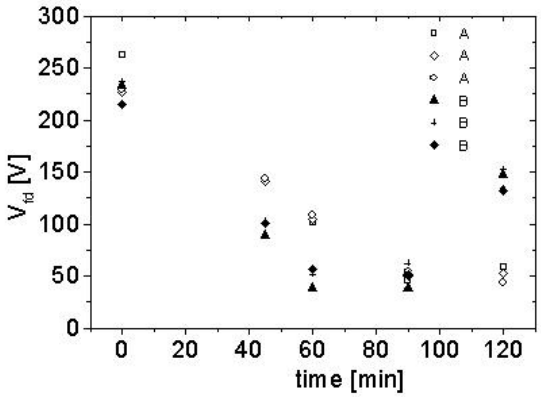

Fig. 4-3.. Full depletion voltage of the six diodes as a function of annealing time

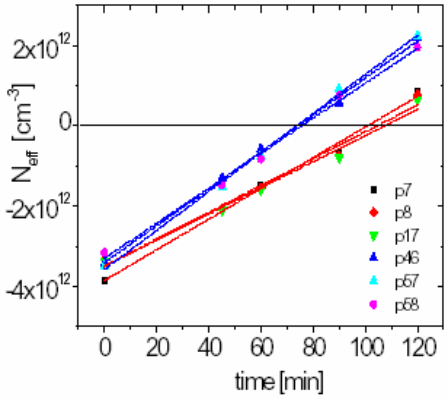

Fig. 4-4. Effective space charge concentration developing from negative to positive as a function of the annealing time.

4.3 Thin epitaxial silicon layers

The very promising first results on the radiation tolerance of 50 µm thick and highly doped n-type epitaxial silicon layers ([P] = 7 10^{13} cm^{-3}) up to a fluence of 2 10^{15} cm^{-2} of 24 GeV/c protons had been extended to 1.2 10^{16} cm^{-2} . It could be demonstrated that the devices do not undergo type inversion in the overall range, that the full depletion voltage after the maximal accumulated fluence of 1.2 10^{16} cm^{-2} increases to 250 V (two times the value before irradiation) and that a storage of these devices at room temperature for a prolonged period of 250 days (beam off period of LHC) will even reduce the full depletion voltage. More details are presented in section PDC (PDC).

According to the research plan for 2004 epitaxial layers with a thickness of 25 µm and 75 µm were grown by ITME and processed by CiS in order to investigate possible changes in the defect kinetics due to the different growth time needed for the different thicknesses and possible defect gettering effects at the interface between the epi-layer and the substrate. First results on the macroscopic properties of the devices are also reported in section PDC (PDC). From detailed defect characterization and defect kinetic studies on gamma and proton irradiated samples we can conclude that in these highly doped epi-layers the defect formation and kinetic is predominately influenced by the concentration of oxygen interstitials O_i, the presence of a relatively high concentration of oxygen dimers O_2 out-diffusing from the Cz substrate during the growth and the high phosphorus concentration. The presence of O_2 could be detected via the formation of the IO_2 complex by high energy proton irradiation and it was shown that the introduction rate is about 37% of that observed for high resistivity Cz material (see Fig. 4-5) which should reflect the corresponding ratio of the O_2 concentration in both materials [6,13,14]. A high O_i concentration reduces the formation of deep acceptors like V_2O, VP, V_2 and possibly higher order vacancy complexes. On the other hand a considerably high concentration of oxygen dimers promotes the formation of thermal donor like defects and might also reduce the formation of harmful vacancy related defects since the dominant reaction is $V + O_2 \rightarrow VO_2$ whereby the VO_2 defect complex is know to be electrically inactive (see also the next section).. Details of the microscopic studies are given in Chapter 3 (DMC).

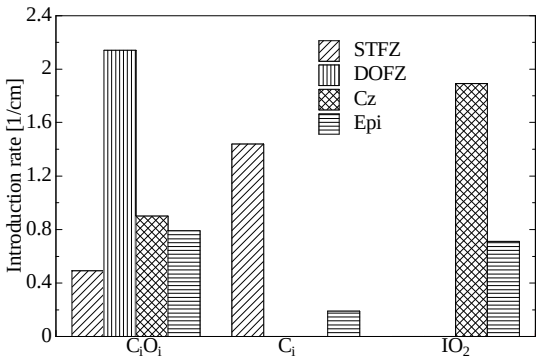

Fig. 4-5. Introduction rates of interstitial related defects in different silicon materials after irradiation

Several irradiation experiments with 23 GeV protons, reactor neutrons, Li-ions, high energy electrons and ^{60}Co gamma rays had been performed. The results derived from these experiments are partly published [15-17] and presented in Chapter 3 (DMC) and Chapter 5 (PDC).

4.4 Oxygen dimer enriched silicon detectors

4.4.1 Introduction

The improved radiation hardness properties of oxygen enriched silicon detectors have been discussed in the previous sections. Another defect engineering approach is the enrichment of silicon with oxygen dimers O_{2i}. Hence the aim of this defect engineering technique is to transform an as big part of the mono atomic oxygen concentration as possible into oxygen dimers (O_{2i}). Such a defect engineered material has completely different defect kinetics during irradiation. In standard silicon exposed to irradiation there is a production of *VO* (A center) defects and V_2O defects from the capture of moving vacancies (*V*) in the silicon lattice by mono atomic oxygen. While the *VO* center will only be charged at low temperatures (< 80 K) the V_2O defect, if assigned as proposed in [18], is known to be charged up to 90% at room temperature and therefore has detrimental influence on the macroscopic detector properties. On the other hand, the capture of vacancies by oxygen dimers O_{2i} leads to the

production of the VO_2 defect, proposed to be neutral and hence non damageable to detectors. The properties of the V_2O_2 defect, which is formed in oxygen dimer enriched silicon instead of the V_2O defect, are not known. It would however be very unfortunate if the electrical defect properties would have an as detrimental effect on the detector performance as the V_2O defect. Furthermore, O_{2i} can act as a sink for migrating interstitials I by forming the IO_{2i} defect with a relatively shallow ($\sim E_C - 0.1$ eV) acceptor level [19] and hence has also no influence on detector performance. On the other hand, it is widely accepted that O_{2i} are precursors for the formation of earlier stage thermal donors [20] which change the effective doping concentration of detectors and thus change the depletion voltage.

4.4.2 Description of samples

Pieces of silicon bulk material and silicon diodes were used for the "dimerization" experiment. The pieces of silicon with a few mm thickness were used for FTIR measurements while the diodes were used to investigate on the macroscopic properties of "dimerized" silicon detectors and for TCT measurements. Cz, MCz and Fz silicon pieces with different oxygen concentration (0.03 – 14 $x10^{17}cm^{-3}$) and different resistivity (30-3300 Ωcm) were investigated. The used p^+nn^+ diodes were produced by CIS, Erfurt from Cz, DOFZ and FZ material. Their thickness was 300μm, their electrode area 0.25 cm^2 and their resistivity was between 1.5 and 6 KΩcm.

4.4.3 Dimerization process

The oxygen dimer is always present in Cz silicon, but its concentration normally does not exceed 0.1% of the single interstitial oxygen concentration [8]. It has been demonstrated that the concentration of dimers can be strongly increased by irradiating Cz silicon crystals at elevated temperatures (300-400°C) with MeV electrons [21]. This process leads to specific reactions involving impurities in the original material that favor the formation of oxygen dimers. At this high temperature of 350°C the VO defect is mobile and can be captured by mono atomic oxygen ($VO_i + O_i \rightarrow VO_{2i}$). The production of dimers then follows from the capture of interstitials I by the formed VO_2 defect ($I + VO_{2i} \rightarrow O_{2i}$).

The dimerization process was performed at the KTH (Stockholm) facility using a 6 MeV electron beam and a setup described in [21]. The samples were irradiated up to a fluence of 1×10^{18} cm^{-2} while maintaining a temperature between 330°C and 340°C.

4.4.4 Macroscopic results after dimerization process

To study the effect of the dimerization process on the silicon diodes, we performed a macroscopic characterization by measuring the capacitance and current as a function of applied bias voltage (CV and IV). We observed that the dimerized diodes could not be fully depleted. Hence the dimerization process has lead to the formation of charged defects increasing the absolute effective donor concentration. Table 4-1 shows the depletion voltage before and after the dimerization process. For the dimerized samples the depletion voltage could not be reached. Therefore, the effective doping concentration N_{eff} and the depletion voltage V_{fd} were inferred from the slope of $1/C^2$ vs. V. This method is strictly valid only for unirradiated diodes when the effective doping concentration is dominated by the shallow doping. However, an assessment of the reliability of this method for the proton irradiated control diodes was performed and resulted in an uncertainty of 30% for V_{fd} as inferred by the above given relations.

Type	V_{fd} before dimerization (V)	V_{fd} after dimerization (V)
FZ	60	~ 550
DOFZ	50	~ 80000
Cz	200	~110000

Table 4-1.: Depletion voltage before and after dimerization process for the different diodes.

Despite the fact that the dimerized diodes could not be fully depleted after the dimerization process, we nonetheless proton irradiated them to study any change in their characteristics (see below).

4.4.5 Microscopic results after dimerization

FTIR characterization

Infrared absorption characterization of bulk silicon crystals was performed using a Fourier Transform Infra Red (FTIR) spectrometer. Fig. 4-6. shows the absorption spectra for the as-grown (1) and dimerized (2) Cz sample. The most prominent bands at 895 and 1012 cm^{-1} are due to oxygen vibrations in VO_2 and O_{2i} defects. A strong increase in the dimer band intensity is clearly seen. Estimated concentrations of the dimer are of about 1×10^{15} cm^{-3} and 4×10^{16} cm^{-3} before and after dimerization, respectively.

The weaker bands at 836 and 829 cm^{-1} are related to the VO and V_2O_2 defects [22]. There is also a pronounced shoulder at 834 cm^{-1} possibly arising from V_2O. Apparently, due to presence of defects the material is highly compensated. After the dimerization, the sample resistivity was increased up to about 3 kΩcm while in the as-grown state it was 30 Ωcm.

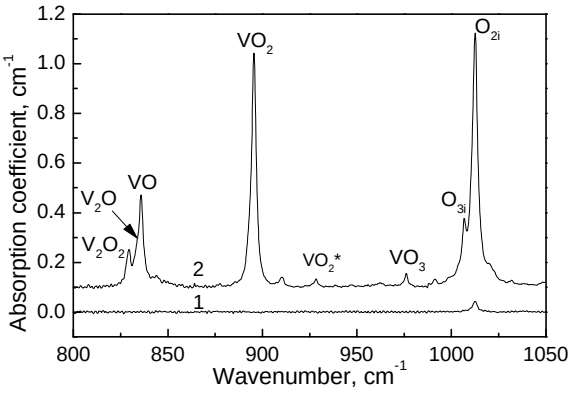

Fig. 4-6.: Absorption spectra measured at 20K for carbon-lean ($[C_S] \leq 10^{15}$ cm^{-3}) Cz sample: 1 – as-grown; 2 - after dimerization (6 MeV electron irradiation at 330-340 °C, $F=1\times10^{18}$ cm^{-2}).

The spectra of the FZ samples irradiated under the same conditions did not show any presence of the dimer defect (detection limit $\approx10^{15}$ cm^{-3}). Only a very weak band related to VO and V_2O was detected.

Several CZ samples with different oxygen content were investigated by FTIR to understand the influence of the oxygen concentration and the electron fluence on the oxygen dimer formation. The result is presented in and Fig. 4-8. In Fig. 4-7 the ratio between oxygen dimers and the oxygen concentration measured after the dimerization process is plotted versus the oxygen concentration before dimerization with an electron fluence of 1×10^{18} cm^{-2}. The data indicate that it is not possible to transform more than about 6-8% of the initial oxygen content into oxygen dimers by the applied dimerization process. In Fig. 4-8 the dependence of the oxygen dimer content on the electron irradiation fluence is presented. The data indicate that the concentration of dimers is saturating at high electron fluences.

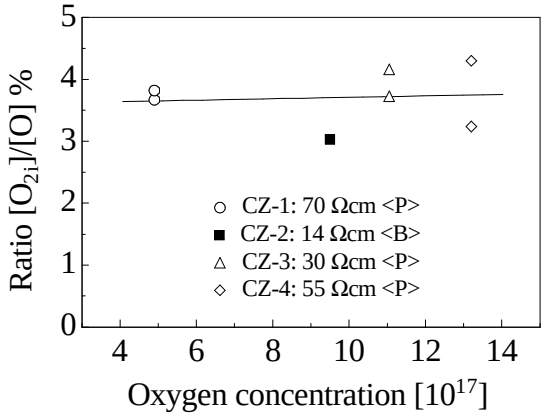

Fig. 4-7.: Ratio of oxygen dimers to oxygen after a dimerization process (T = 330-340ºC, $F=1\times10^{18}$ cm^{-2}) of CZ samples with different initial oxygen content.

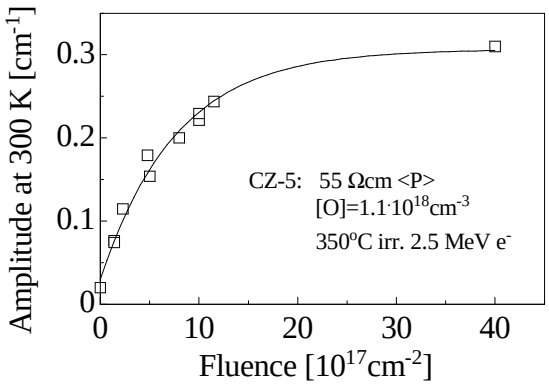

Fig. 4-8.: Oxygen dimer concentration (absorption at 1013 cm^{-1}) as function of the electron fluence used during the dimerization process.

TSC characterization

Deep Level Transient Spectroscopy (DLTS) measurements were not possible since the diodes were too saturated with defects. Thermally Stimulated Current (TSC) measurements however were possible and were performed on all dimerized diodes with a reverse bias of 100 V.

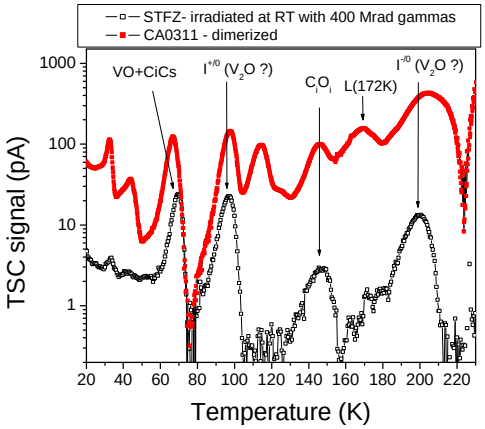

Fig. 4-9.: TSC spectra of dimerized float zone diode (lower curve) and of a float zone diode irradiated with 400 Mrad of gammas (upper curve).

In Fig. 4-9 the FZ diode TSC spectrum is compared with a FZ diode that has been irradiated at room temperature with 400 Mrad ^{60}Co-gammas. Many common defects are observed. They are those that require a very low formation energy and can be generated also by irradiation at room temperature. Among them are the well known *VO*, C_iO_i defects and the *I* center, generated through a second order process, associated with V_2O or V_3 [3, 18, 23]. In addition, we can see two peaks - L(115K) and L(172K) - present in the dimerized diode and not in the gamma irradiated diode. They can be correlated with multivacancies or interstitial related defects (due to the abundance of vacancies and interstitials during dimerization at high temperature). They require a high formation energy and have a high thermal stability. While there are no clear indication of what the L(115K) defect might be, the L(172K) level can be identified as the single acceptor state of the X center - associated with V_2O or V_2O_2 in [18, 23]. This center is known to be formed in different types of silicon (FZ, DOFZ and Cz) irradiated at room temperature but only after a thermal treatment at temperatures higher than 250°C is done to anneal out the V_2 defect [23, 24].

4.4.6 Macroscopic results after proton irradiation

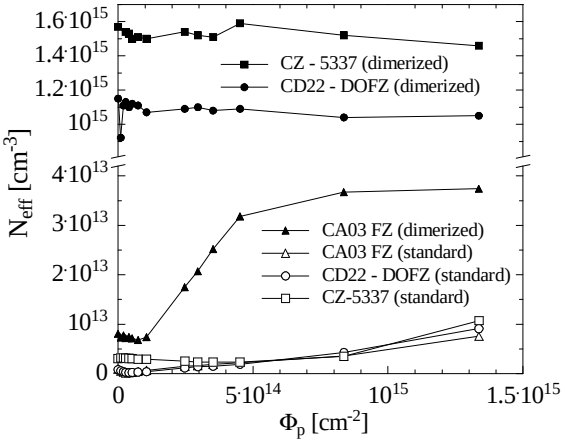

Fig. 4-10.: N_{eff} for non-dimerized (standard) and dimerized detectors as funciton of the 24 GeV/c proton fluence. Neff was deduced from the depletion voltage for the non-dimerized samples while for the dimerized ones Neff was inferred as described in section 4.4.4.

The dimerized as well as the control diodes described in section 4.4.2 were irradiated with 24GeV/c protons at the CERN PS facility [25]. The samples were irradiated in a so-called CERN scenario, meaning after each irradiation step the diodes were annealed at 80°C for 4 minutes before measuring the CV/IV characteristics. As a function of fluence the control diodes show the same behavior for the depletion voltage and leakage current, as shown in Fig. 4-10. The inferred V_{fd} of the dimerized FZ diode as a function of fluence shows a very different behavior from the other dimerized diodes. The standard FZ diode has an initial inferred V_{fd} of the order of 550V (corresponding to an N_{eff} of a few 10^{12} cm^{-3}) and varies with the fluence while for the DOFZ and the Cz diodes, the initial inferred V_{fd} is of the order of 100,000V (and a corresponding N_{eff} around 10^{15}cm^{-3}) and is constant as a function of fluence. These results are consistent with the fact that the FZ dimerized diode is the one that was least affected by the dimerization process.

4.4.7 Discussion and conclusion

The aim of the experiment was to transform as much oxygen into oxygen dimers as possible in order to test the radiation hardness of oxygen dimer enriched silicon detectors. Silicon detectors made from CZ, FZ and DOFZ silicon as well as pieces of FZ and CZ silicon underwent in parallel a dimerization process. FTIR measurements performed on the silicon bulk pieces demonstrated that independent of the oxygen content only a fraction of ≈ 6-8% of the oxygen could be transformed into

oxygen dimers in CZ silicon. Rising the electron fluence used for the dimerization (1×10^{18} cm^{-2}) to three times higher values did not significantly increase the dimer content indicating that the fraction of 6-8% dimer content might be a fundamental limit for the dimerization process as performed in this experiment. For the FZ samples the dimer concentration was below the FTIR detection limit of about 10^{15} cm^{-3}.

The results obtained on the dimerized diodes are very different from a dimerization experiment performed on FZ and DOFZ diodes with ^{60}Co-gammas [26]. The effective doping concentration respectively depletion voltage of the diodes in our experiment was changed to values which do not allow for proper detector operation. Due to the high defect concentration the DLTS method could not be applied to the dimerized diodes and the TSC method could only extract meaningful results from the dimerized standard FZ diode. Nonetheless it showed the presence of interesting defects, like the unknown L(115K) and the X center.

In summary, the material is radically changed by the dimerization process and constitutes a novel ground on which to perform macroscopic as well as microscopic characterization. It could be that the thermal donors that are created alongside the oxygen dimer, overwhelm the beneficial effects expected from the oxygen dimers.

Still, we are confident that there are more avenues to study the oxygen dimer as a defect engineering possibility leading to a radiation hard silicon detector. For example, performing the dimerization process at a temperature systematically at or above 350°C would anneal out the compensating defects, present in our dimerized Cz material.

Also, there might be a fluence lower than 1×10^{18} e/cm^2 which leads to a sufficient dimer concentration while still allowing for a full depletion of the diodes. This approach seems to be especially promising under the assumption that oxygen dimers are the defects that render oxygen rich silicon detectors more radiation hard than standard FZ silicon detectors. It might well be that oxygen dimers are transformed during irradiation into thermal donors that counter-balance a part of the negative space charge introduced by other radiation induced defects. If this is true, FZ detectors enriched even with a small concentration of oxygen dimers should be more radiation hard than FZ detectors without oxygen dimers.

4.5 Hydrogen in high resistivity FZ silicon

It is well-known that hydrogen can easily penetrate into silicon crystals at various stages of p-n structure processing [27,28]. Therefore, possibly all silicon particle detectors contain hydrogen which remain in these structures after fabrication. There are some indications on interaction of residual hydrogen with defects in irradiated Si detectors [29-31]. It is expected that an increase of the hydrogen content will lead to an increase of the radiation tolerance of devices. It may be due to hydrogen passivation of radiation induced defects [27, 28, 32], and the acceleration of oxygen diffusion by promoting the formation of oxygen dimers ? $_2$ [33-35].

Both high mobility and reaction ability of hydrogen result in its redistribution during subsequent technological processes occurring even at rather low temperatures 200-400 °? . Therefore, one expects that the concentration of hydrogen in various areas of the detector will depend substantially on the sequence of technological steps of the manufacturing process. Presently there is not enough information on hydrogen in fully processed detector structures.

First studies on residual hydrogen in p^+-n-n^+ structures processed on high resistivity FZ silicon and effects on hydrogenated FZ silicon devices have been undertaken. The hydrogenation was performed using a treatment in a hydrogen plasma at 300°C. The samples were arranged on the surface of a heater located in the discharge chamber in such a way that the structured p^+-side was in contact with the heater. This way the hydrogen could only penetrate into the device through the n^+-side. Irradiation with electrons (3.5 or 6 MeV) was done using the accelerator at the Institute of Solid State and Semiconductor Physics in Minsk. The irradiated samples were after irradiation subjected to a 30 minutes isochronal annealing in the temperature range 50°C - 350°C. The defect reactions have been investigated using DTLS and high frequency capacitance-voltage (C-V) measurements.

4.5.1 Results on a non-hydrogenated FZ diode

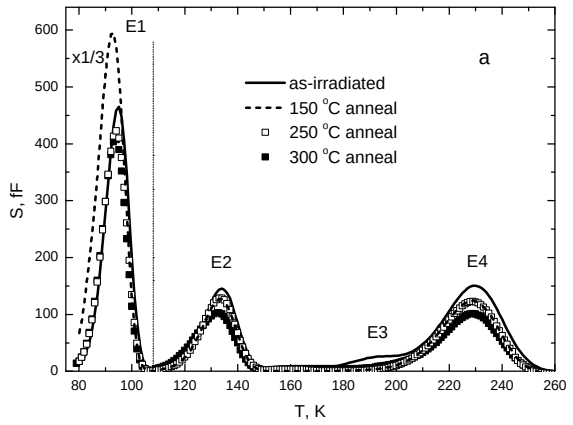

Fig. 4-11.: Development of DLTS spectra for standard FZ diodes (CA-sample – a) after electron irradiation at room temperature and 30-min isochronal annealing with temperature increments of 50 °C. Irradiation dose: 3×10^{12} cm^{-2} (E_e=3.5 MeV), measurement setting: rate window e_w = 190 s^{-1}, bias –5 → 0 V, pulse duration t_p=10 ms.

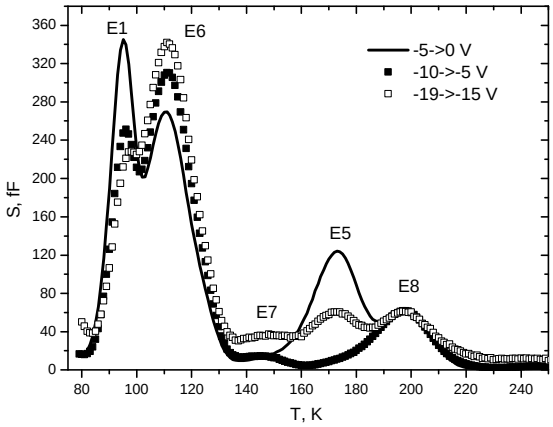

Fig. 4-12.: DLTS spectra after $3x10^{12}$ cm^{-2} 6 MeV electron irradiation and annealing at 350°. Measurement settings: rate window of 190 s^{-1}, pulse duration of 10 ms, bias: a) -5 → 0 V, b) −10→ −5 V and c) −19→ −15 V. The peak amplitudes are normalized assuming constant concentration of E8 trap.

Immediately after electron irradiation with a fluence of 3×10^{12} cm^{-2} 4 peaks in the DLTS spectrum are observed (see Fig. 4-11) for a non-hydrogenated FZ diode manufactured by CiS-Erfurt, Germany (CA-diode). These peaks are caused by the formation of 5 traps. The peak E1 is attributed to the VO and the C_iC_s complex, E2 to the $VV^{=/-}$ level and E4 to the $VV^{-/0}$ transition to which also another trap of unknown nature contributes. The peak E3 can also not be attributed to a know trap. With increasing temperature all peaks decrease with the exception of E1 which shows an increase after 150°C annealing due to an additional formation of C_iC_s complexes. For higher temperatures up to 300 °C also a decrease is observed.

After annealing at 350°C the DLTS spectrum changes dramatically (see Fig. 4-12). The peaks E2, E3 and E4 vanished and new trap peaks E5 , E6, E7 and E8 occurred. While the nature of the traps corresponding to the peaks E6, E7 and E8 is yet unclear, it is generally accepted that the trap E5 is the vacancy-oxygen-hydrogen complex VOH. Thus, E5 can be used as an indicator of the presence of hydrogen in this device introduced during processing. From measurements with different bias and pulse voltages (see Fig. 4-12) one observes a very strong non-uniformity of the peak amplitude for E5. At small inverse voltages its concentration is comparable to the concentration of other traps; increasing the voltage leads first to its disappearance and then to its reappearance. One can estimate a probing depth of DLTS measurements from C-V-measurements (Fig. 4-13).

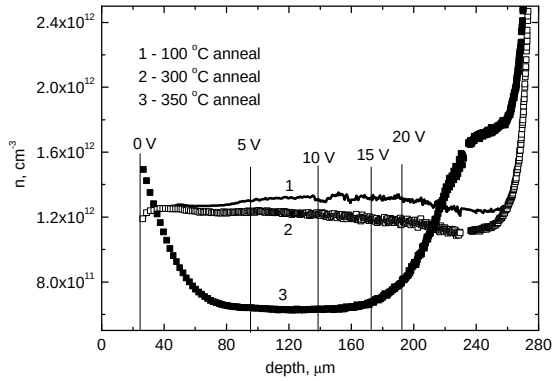

Fig. 4-13.: Carrier depth profile for a CA sample determined from C-V characteristics. Vertical lines mark the reverse bias voltage which correspond to the width of the depletion region for curve 3.

A correlation between the charge carrier concentration n(x) in the structure under study and the presence of VOH complex (trap ? 5) in the corresponding structure depth regions is clearly seen. In the middle region from ~80 up to ~170 microns a strong decrease of carrier concentration as compared to that one after $?_{ann}$=300 °C is observed. This can be explained by introduction of acceptors. Rising of *n(x)* dependence in the near surface regions (p^+ and n^+) can be related to a formation of thermal donors. Our DLTS-measurements have shown the absence of traps with activation energies $?_?$=0.14 - 0.15 eV related to oxygen thermal donors. Therefore, it is possible to draw the conclusion, that thermal donors are

formed due to hydrogen and their formation depth corresponds to the diffusion of hydrogen. In this structure hydrogen is present in significant concentrations only in near surface regions or at the Si-SiO_2 boundary.

4.5.2 Results on a hydrogenated FZ diode

It is of interest to study how radiation defects will be eliminated from ? ? -structures after their doping with hydrogen. We have carried out a plasma processing of a ? ? -diode in hydrogen plasma at a temperature of 300 °C for 1 hour. The hydrogen plasma was applied from the rear side of the diodes (from the n^+-contact).

The hydrogenated diode was irradiated with fast electrons of the same energy and fluence as the standard diode (Fig. 4-11). DLTS-spectra obtained after irradiation and subsequent annealing are shown in Fig. 4-14. As one can see the annealing behavior of radiation defects in the hydrogenated diode is totally different to the non-hydrogenated diode, that is, the formation of the VOH complex E5 is observed already at 150 °C and the divacancy (E2, E4) is completely eliminated after ? $_{ann}$=300 °C. Only a small amount of non-uniformly distributed VO complexes (trap E1) remained after 300 °C annealing. As seen from Fig. 4-15, this trap has remained only in the region adjacent to ?$^+$-contact, whereas E5 (VOH) seems to be homogeneously distributed throughout

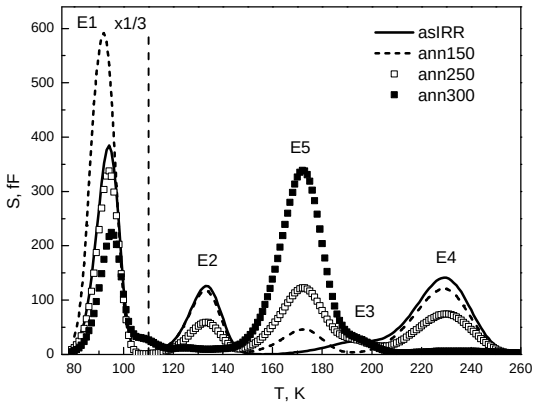

Fig. 4-14.: Development of DLTS spectra for hydrogenated standard FZ diode(CA-sample) after irradiation with 3.5 MeV electrons at room temperature and upon 30-min isochronal annealing with temperature increments of 50 °C. Dose of irradiation was 3×10^{12} cm^{-2}. Measurement settings were e_w = 190 s^{-1}, bias –5 → -0 V, and pulse duration 10 ms.

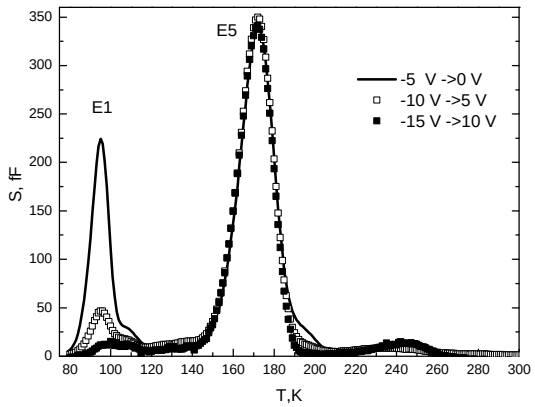

Fig. 4-15.: DLTS spectra for hydrogenated standard FZ diode(CA-sample) after irradiation with 3.5 MeV electrons at room temperature and upon 30-min annealing at 300 °C. Dose of irradiation was 3×10^{12} cm^{-2}. Measurement settings were e_n = 190 s^{-1}, pulse duration 10 ms bias: a) -5 → 0 V, b) −10→ −5 V, b) −15→ −10 V. All spectra normalized the E5 peak (VOH) amplitude.

the depth of the diode bulk. Using C-V measurements it is possible to estimate the depths at which VO complexes were retained (Fig. 4-16).

As seen in Fig. 4-16, the hydrogen plasma processing has led to some increase of charge carrier concentration in the base of the diode (Fig. 4-16, curve 2). After 250 °C annealing a maximum in the *n(x) curve appeared* (curve 3). After 300 °C annealing this maximum has increased and moved to the ?$^+$-contact. The analysis of Fig. 5 and 6 shows that these features can be explained by a hydrogen redistribution from n^+-to ?$^+$-regions under annealing. As a result of this redistribution there are both, the formation of donor centers and the passivation of different not hydrogen related electrically active centers. Due to the latter process VO complexes have been eliminated and remained only in regions where the concentration of hydrogen is insufficient for their full passivation.

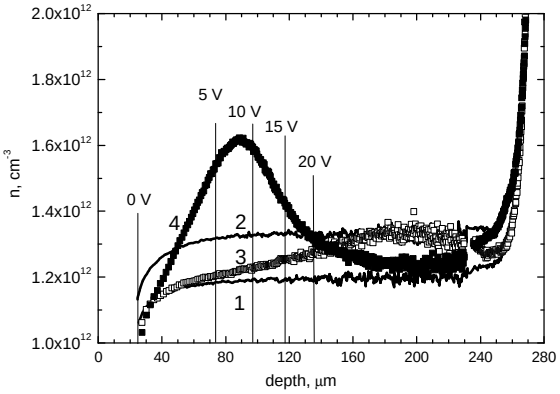

Fig. 4-16.: Carrier depth profile for a CA sample determined from C-V characteristics. Vertical lines mark the reverse bias voltage corresponding to the indicated width of depletion region for curve 4. Curve 1: as irradiated; curve 2: annealed at 150°C; curve 3: annealed at 250°C; curve 4: annealed at 300°C.

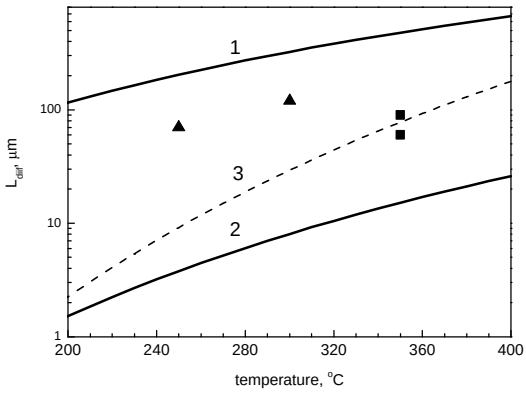

Fig. 4-17.: Diffusion length for different hydrogen forms (mono-atomic H curve 1, H dimmer curve 2) in silicon calculated for 30 min time period. Diffusion coefficients were taken from [36] for mono-atomic hydrogen and from [37, 38] for hydrogen dimer. Curve 3 represents data from obtained hydrogen enhancement of thermal donor formation [33]. Points show our estimations from the depth of donor formation in non-hydrogenated (squares) (seeFig. 4-13) and hydrogenated (triangles) (see Fig. 4-16) samples.

From the obtained data it is possible to estimate the hydrogen diffusivity. It is known, that hydrogen penetration into silicon crystals substantially depends on the presence of traps. Hydrogen atoms can be bounded in molecules which diffuse much more slowly than atomic hydrogen. Therefore there is some uncertainty in a prediction of hydrogen behavior in detector structures. As follows from Fig. 4-17, a mixed mechanism of diffusion of hydrogen takes place. Its penetration into the diode base under annealing occurs by both means (as molecules and atoms). We shall note that the depth of hydrogen penetration in detector structures measured here correlates well with the data obtained from studies of hydrogen acceleration of oxygen thermal donor formation [33,35].

More details and results on other non-hydrogenated standard high resistivity FZ devices manufactured by different companies are presented in [39].

4.6 Defect engineering by pre-irradiation treatments

The development of defect engineered silicon detectors by pre-irradiation treatments have been performed by the groups of Kiev, Padova, Trento and ICT-IRST-Trento. In 2004 five high purity n-type FZ wafer (4" in diameter) and two high resistivity n-type MCz wafer (4" in diameter) were pre-irradiated with fast neutrons up to a fluence of 1×10^{17} cm^{-2} at the research reactor WWR-M in Kiev and annealed at 800 °C. The detector processing using these pre-treated FZ and MCz wafers and non-treated reference FZ and MCz wafers was performed at ICT-IRST-Trento. The IRST mask-set includes several structures (strip-detectors, pad-detectors of different size and guard ring structures and other test structures).

The diodes were electrically characterized by C-V and I-V measurements. The quality of the main part of diodes processed on the pre-irradiated wafers was sufficient but in general not as good as expected from the results derived for the reference diodes. The main reason for the reduced quality and success rate was identified to be caused by the non-sufficient quality of the polishing procedure. The results of the wafer tests are summarized in Table 4-2.

The last column in table 1 presents the number of devices which were accepted for radiation hardness studies. In 2004 irradiation experiments have been performed with 23 GeV protons at CERN and reactor neutrons at Kiev. The irradiated devices are under investigation. In order to overcome the mentioned problem with the bad polishing a new set of pre-irradiated wafers which were polished according to the detector grade quality will be processed at IRST in 2005. Included in this new process run are also 7 NTD wafers supplied by Topsil and 7 high resistivity p-type FZ wafers.

Table 4-2: Results of wafer test measurements. FZ/MCz-ref: reference wafer, FZ/MCz-pre: pre-irradiated wafer.

Wafer No.	Type	d [µm]	V_{dep} [V]	N_{eff} [10^{11} cm^{-3}]	? [k·Ω·cm]	I_{rev}/V [µA/cm^3]	No. of devices
1	FZ-ref	360	60	6	7.7	5-15	19
2	FZ-pre	360	75-115	8-12	4-6	2-3	36
3	FZ-pre	360	70-110	7-11	4-7	0.5-4	40+strip
4	FZ-pre	360	65-110	6.5-11	4-7	0.4-0.9	40
5	FZ-pre	360	70-95	7-9.5	5-6.5	2-8	41+2 strips
6	FZ-pre	360	60-125	6-12.5	4-8	4-16	27
121	MCz-ref	260	450	85	0.55	0.07	12
112	MCz-pre	260	800	150	0.3	0.3	12
125	MCz-pre	260	490-730	90-140	0.33-0.5	0.6-6	12

4.7 References for Chapter 4

[1] E. Fretwurst et al., Nucl. Instr. and Meth. A 514 (2003) 1-8.
[2] I.Pintilie, E. Fretwurst, G. Lindström, J. Stahl, Appl. Phys. Letters 81, No. 1 (2002) 165.
[3] I.Pintilie et al., Appl. Phys. Letters 82 , No. 13 (2003) 2169& erratum in 83, (2003), 3216
[4] I.Pintilie et al., Nucl. Instr. and Meth. A 514 (2003) 18-24
[5] Z.Li et al., Nucl. Instr. and Meth. A 514 (2003) 25-37
[6] I. Pintilie et al., Radiation induced donor generation in epitaxial and Cz diodes, paper presented at RESMDD04, Florence, Oct. 10.-13. 2004
[7] J.L. Lindström, T. Hallberg, Phys. Rev. Lett. 72 (1994) 2729
[8] L.I. Murin, T. Hallberg, V.P. Markevich, J.L. Lindström, Phys. Rev. Lett. 80 (1998) 93
[9] J. Härkönen et al., Proton Irradiation Results of p+/n-/n+ Cz-Si Detectors Processed on p-type Boron Doped Substrates with Thermal Donor Induced Space Charge Sign Inversion, paper presented at RESMDD04, Florence, Oct. 10.-13. 2004
[10] M. Bruzzi et al., Neff tuning in MCz-Si detectors by isothermal annealing, 5-th RD50 Workshop, Florence, Italy, 14.-16. October 2004
[11] W. Wijaranakula, Appl. Phys. Lett. 59 (13) 1608 (1991).
[12] C. Piemonte, Electrical tests of the first n-on-p devices fabricated at ITC-irst, presented at the 5th RD50 Workshop, Florence, Italy, 14.-16. October 2004.
[13] J. Stahl, PhD-thesis, University Hamburg, DESY-THESIS-2004-028, July 2004, ISSN 1435-8085
[14] J. Stahl, E. Fretwurst, G. Lindstroem and I. Pintilie, Radiation hardness of silicon -a challenge for defect engineering, Physica B 340-342 (2003) 705-709
[15] A. Candelori et al., Lithium ion irradiation effects on epitaxial silicon detectors, IEEE Trans. Nucl. Sci., vol. 51, no. 4 (2004) 1766-1772
[16] S. Dittongo et al., Radiation hardness of different silicon materials after high-energy electron irradiation, Nucl. Instr. and Meth. A 530 (2004) 110-116
[17] G. Lindström, E. Fretwurst, G. Kramberger, I. Pintilie, Toward super radiation tolerant semiconductor detectors for future elementary particle research, Journal of Optoelectronics and Advanced Materials, Vol. 6, No. 1 (2004) 23-38
[18] I. Pintilie et al, Physica B, 340-342, (2003) 578-582.
[19] J.L. Lindstrom et al. , Physica B 308-310 (2001) 284.
[20] Y.L. Lee et al., Phys. Rev. B 65 (2002) 085205.
[21] J.L. Lindström et al., Materials Science Forum, 258-263 (1997) 367.
[22] J.L. Lindstrom et al., NIM B 186 (2002) 121.
[23] G. Alfieri et al, Phys. Rev. B, 68 (2003) 233202
[24] V.P. Markevich et al, J. Phys.: Condens. Matter. 15 (2003) S2779.
[25] M.Glaser et al., NIM A 426 (1999) 72-77; see also http://www.cern.ch/irradiation/.
[26] S.J. Watts et al., NIM A 485 (2002) 153
[27] S.J. Pearton, J.W. Corbett, T.S. Shi. Appl. Phys., A43, 153 (1987).

[28] S.J. Pearton, J.W. Corbett, and M. Stavola, Hydrogen in Crystalline Semiconductors. Springer-Verlag, Berlin, 1992
[29] M. Bruzzi, Nucl. Instr. and Methods Phys. Res. A 352, 618 (1995).
[30] C. Da Via and S. J. Watts, Nucl. Instr. and Methods Phys. Res. B 186, 111 (2002).
[31] L. F. Makarenko, F. P. Korshunov, S. B. Lastovski., N. I. Zamyatin, Semiconductors, Vol. 37, No. 5, 2003, pp. 611–615 (Translated from Fizika i Tekhnika Poluprovodnikov, Vol. 37, No. 5, 2003, pp. 629–633).
[32] O.V. Feklisova, N. Yarykin. Semicond. Sci. Techn., 12, 742 (1997).
[33] R. C. Newman, J. H. Tucker, A. R. Brown, and S. A. McQuaid. Hydrogen diffusion and the catalysis of enhanced oxygen diffusion in silicon at temperatures below 500 °C// J. Appl. Phys. 70(6), p. 3061, (1991)
[34] V. P. Markevich, L. I. Murin, J. L. Lindström and M. Suezawa. Early stages of oxygen precipitation in silicon: The effect of hydrogen. Semiconductors 34 (9) 998-1003, 2000.
[35] R C Newman, Oxygen diffusion and precipitation in Czochralski silicon // J. Phys.: Condens. Matter 12 (2000) R335–R365
[36] A. Van Wieningen and N. Warmoltz, Physica 22, 849 (1956)
[37] R. Rizk, P. de Mierry, D. Ballutaud, M. Aucouturier, and D. Mathiot, Phys. Rev. B 44, 6141 (1991)
[38] V. P. Markevich, M. Suezawa. J. Appl. Phys., Vol. 83, No. 6, 2990 (1998)
[39] L. Makarenko et al., Interaction of residual hydrogen with radiation defects in silicon particle detectors, paper presented at RESMDD04, Florence, Oct. 10-13, 2004

5 Pad Detector Characterization (PDC)

5.1 RD50 irradiations in 2004

Irradiation tests with different irradiation sources are mandatory in order to investigate the deterioration of bulk material properties caused by different kind of particles with different energies. In 2004 several irradiation campaigns were performed in the framework of the RD50 project. The used irradiation facilities as well as an overview of the irradiated materials are given in Table 5-1. During the irradiation tests, more than 500 pad and segmented detectors were irradiated.

Material \ **Facility**	**23 GeV protons** (CERN)	**10-50 MeV protons** (Univ. Of Jyvaskyla)	**Reactor neutrons (1MeV)** (JSI,Ljubljana)	γ ^{60}Co (Brookhaven)	900 MeV **e**lectrons (INFN Trieste)	15 MeV electrons (Univ. of Oslo)
Standard Float Zone silicon n-type (nFz)	x	x	x		x	
Standard Float Zone silicon p-type (pFz)	x	x	x		x	
Oxygenated Float Zone silicon n-type (nDOF)	x	x	x		x	x
Oxygenated Float Zone silicon p-type (pDOF)	x	x				
Czochralski silicon n-type (nCz)	x		x		x	
Magnetic Czochralski silicon n-type (nMCz)	x	x	x	x	x	x
Magnetic Czochralski silicon p-type (pMCz)	x	x	x	x	x	
Pad detectors with epitaxial silicon layer (Epi)	x		x		x	
Strip detectors	x	x				
Novel materials (SiC,GaN)	x		x			

Table 5-1.: Radiation facilities used for irradiation tests and materials irradiated by the RD50 collaboration in the year 2004.

The macroscopic effects, i.e. deterioration of full depletion voltage, leakage current and trapping time, in irradiated samples as well as their annealing behavior were characterized at RD50 member institutes. An overview of results obtained by IV, CV, CCE and TCT methods is given in the following chapters.

5.2 RD50 PDC subproject – ”Technotest”

The main objective of this subproject is to investigate the influence of the detector processing, performed at different processing facilities, on the radiation tolerance of detectors. Since the influence of the processing might depend on the type of the used high resistivity Si material as well as on the type of irradiation, several experiments on different Si materials and with different radiation sources have to be performed. This project actually deals with four research lines of the RD50 collaboration program: DMC, DE, PDC and FDS and is carried out as collaborative work of several institutions: Ioffe Physico-Technical Institute (PTI), Research Institute of Material Science and Technology (RIMST), Brookhaven

National Laboratory (BNL), Helsinki Institute of Physics (HIP), Josef Stefan Institute, and Glasgow University, ITEP (Moscow). The subproject is coordinated by V. Eremin (PTI) and the detector processing was carried out by PTI, BNL and HIP. The irradiations were performed at CERN (24 GeV/c protons) and Iosef Stefan Institute (reactor neutrons, 1 MeV). The silicon materials used in this study are n- and p-type Float Zone (Fz-Si, Wacker) and magnetic Czochralski (MCz-Si, Okmetic) wafers. The detectors were characterized by DLTS, IV and TCT methods.

5.2.1 Manufacturing procedures and material characteristics

The silicon materials used in this study are n- and p-type Float Zone (Fz-Si, Wacker) and magnetic Czochralski (MCz-Si, Okmetic) wafers. Resistivity of original wafers before detector processing was 4-6 kΩ·cm for n-FZ Wacker, 2-6 kΩ·cm for p-FZ Wacker and 1 kΩ·cm for n-CZ Okmetic. An overview of manufacturing procedures specific for each producer is presented in Table 5-1. The major features of processing used at BNL and PTI are very similar. Implantation was used for junction formation in all detectors. The main difference of HIP processing is that the implantation is the first step performed before the oxidation whereas BNL and PTI used the opposite sequence of these operations. The masks for device patterns were different, each producer used its own mask. The dimensions of p^+-n junction are: BNL: 12 mm^2, HIP and PTI: 25 mm^2.

During processing Thermally Induced Defects (TIDs) are introduced in the bulk of HIP and PTI detectors irrespective to the type of Si. These results are obtained using C-DLTS measurements of detectors irradiated by low neutron fluence of $F_n = 1 \cdot 10^{11}$ cm^{-2}. The parameters and concentrations of TIDs and radiation induced defects (RDs) as well as the DLTS spectra are presented in [1]. TIDs are so called Sah levels [2]: the midgap level at $E_C - 0.555$ eV and complementary level at $E_C - 0.27$ eV. The results on TID introduction are reproducible in all aspects:

a) no TIDs were ever detected earlier in detectors of BNL;
b) similar TIDs were observed earlier in PTI detectors [3] and in the recent study [4] of HIP detectors processed from CZ n-SI as well.

Since concentration of TIDs is lower than shallow donor concentration in the raw material they do not affect significantly on the resistivity. Before the measurements all detectors were annealed to reproduce the beneficial annealing stage and then they were kept in the fridge all together. Hence, the annealing state is the same for all detectors.

	BNL	**HIP**	**PTI**
Oxidation	1100ºC/6 h	done after implantation	1100ºC/6 h
p^+ - Implant	45 keV/$2 \cdot 10^{14}$ cm^{-2}	20 keV/$1 \cdot 10^{15}$ cm^{-2}	50 keV/$3 \cdot 10^{14}$ cm^{-2}
n^+ - Implant	80 keV/$6 \cdot 10^{14}$ cm^{-2}	70 keV/$1 \cdot 10^{15}$ cm^{-2}	80 keV/$9 \cdot 10^{14}$ cm^{-2}
Annealing	700ºC/30 min	1100ºC/4 h	700ºC/40 min
Al sintering	430ºC/5 min (low concentr. of TD)	370ºC/40 min (no TD)	430ºC/7 min

Table 5-2: Manufacturing procedures in TECHNOTEST

5.2.2 I-V characteristics of Si detectors irradiated by neutrons

I-V characteristics after irradiation with neutrons and an annealing of 4 minutes at 80ºC are shown in Fig. 5-1 for detectors processed at PTI and HIP on n-type FZ Si and in Fig. 5-2 for detectors processed by all the three institutes on n-type CZ Si. It can bee seen that all detectors irradiated to $5 \cdot 10^{13}$ cm^{-2} show

saturation of the current, which is the evidence of detector full depletion; for the PTI detector on FZ n-Si the current "bump" specific for SCSI is observed (shown in the figure by the arrow). Comparison of current density vs bias for detectors irradiated at the same fluence (Fig. 5-3) gave the following conclusions:

1) For n-type Si saturation occurs at lower voltages for detectors processed from FZ Si as compared to those processed from CZ Si;
2) In detectors processed from p-type FZ Si and irradiated to fluences $=5\cdot10^{13}$ cm^{-2} the saturated current density is achieved at higher voltage as compared to that for detectors processed from n-type FZ Si;
3) At very high fluence ($5\cdot10^{15}$ cm^{-2}) the current densities at same bias are close for all detectors irrespective to the type of Si and processing.

The results on I-V characteristics show that the difference related to the Si type and specific processing is observed in the range of low and medium neutron fluence and it becomes insignificant for detectors irradiated up to $5\cdot10^{15}$ cm^{-2}.

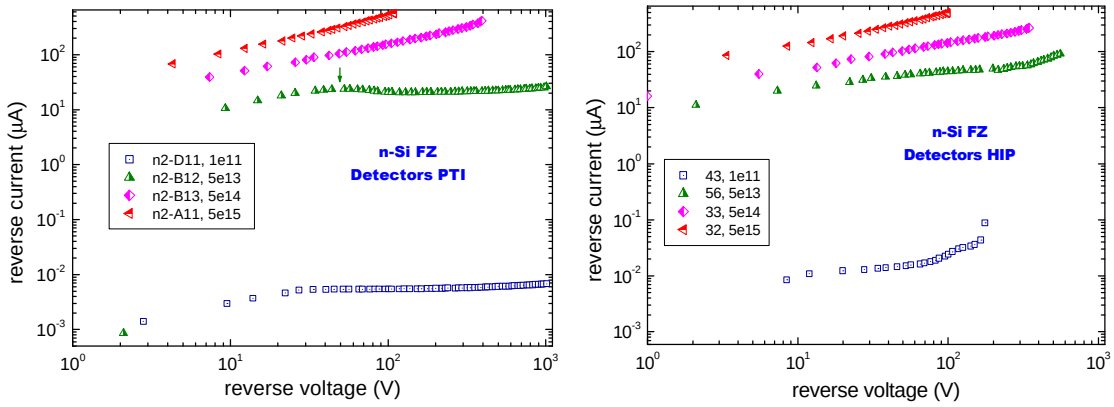

Fig. 5-1.: I-V characteristics of detectors processed at PTI and HIP on the wafers from n-type FZ Si and irradiated by 1 MeV neutrons.

In Fig. 5-4 the saturated current normalized to the detector volume V is shown as a function of the neutron fluence. The plot includes the data for all types of Si and can be approximated by a single linear dependence: $\Delta I/V = \alpha F_n$ with damage coefficient $\alpha = 5.9\cdot10^{-17}$ A/cm. The deviation from this dependence is observed only for HIP detectors processed from FZ Si and irradiated to $5\cdot10^{13}$ cm^{-2}.

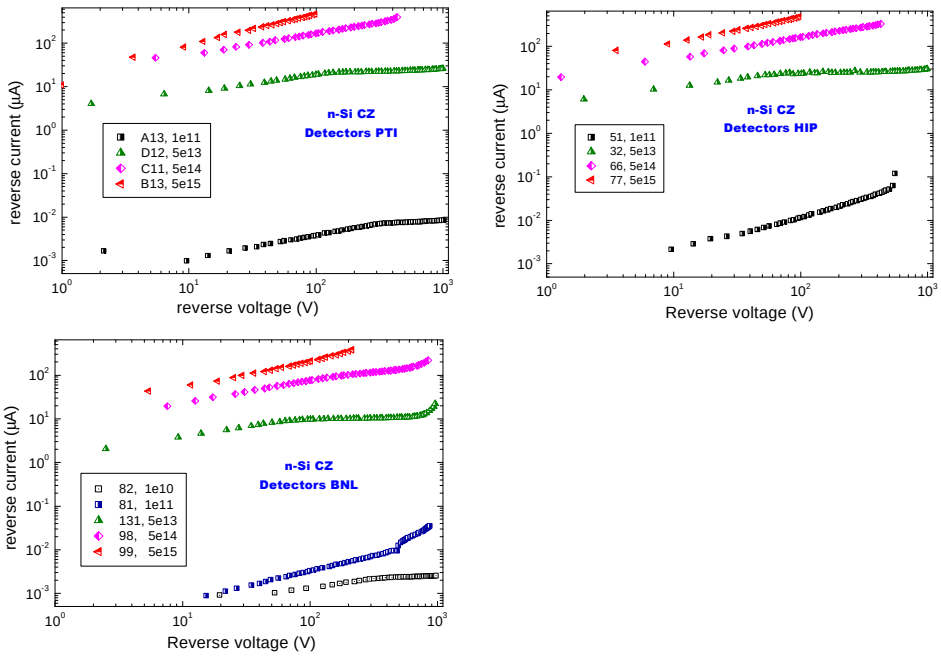

Fig. 5-2.: I-V characteristics of detectors processed by the three institutes on n-type CZ Si and irradiated by 1 MeV neutrons.

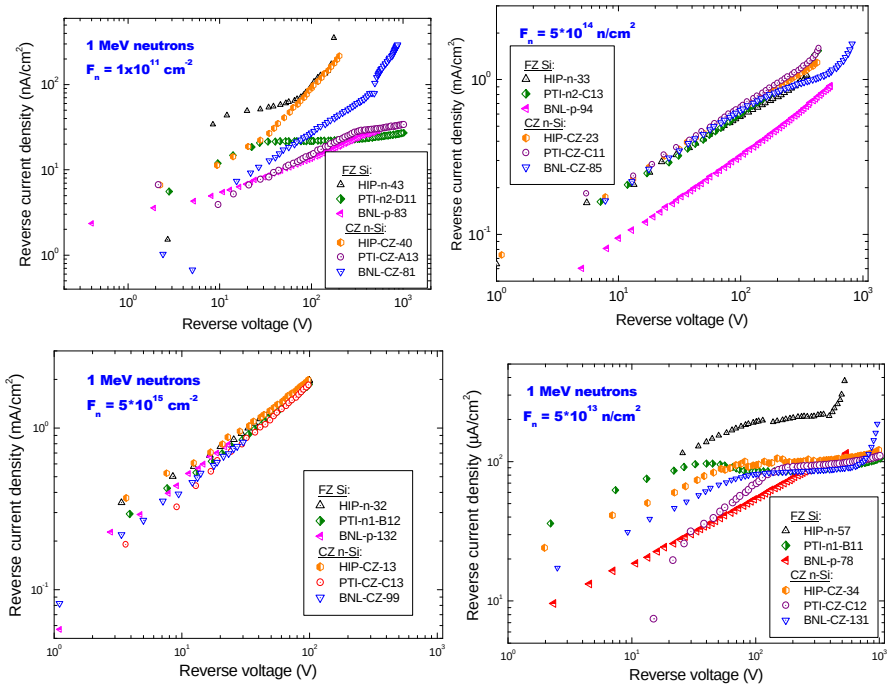

Fig. 5-3.: Comparison of reverse current density vs. bias voltage for the irradiated detectors

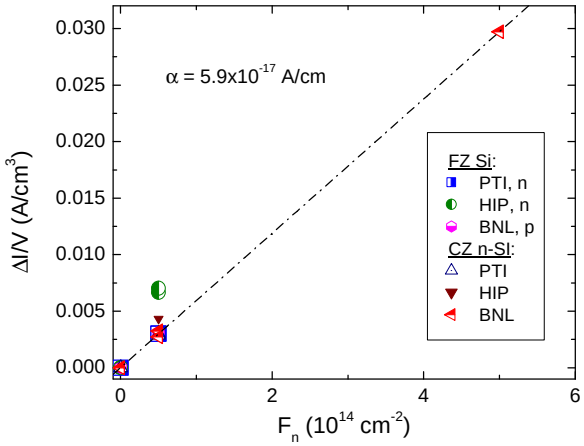

Fig. 5-4: Saturated current normalized to the detector volume vs. neutron fluence

5.2.3 Current pulse response

The measurements of current pulse response were performed with detectors processed from n-type Si irradiated up to $5 \cdot 10^{14}$ cm^{-2} using a TCT setup with laser pulse generation of non-equilibrium carriers. Due to the difference of detector design (hole in the Al contact was only at one side of the detector), in the measurements of detectors processed at PTI and HIP the pulse laser was at the p^+ side, and for BNL detector the laser was at the n^+ side. The shapes of the current pulse response of irradiated detectors obviously show the influence of different processing.

a) Low fluence, $F_n = (0.1\text{-}1) \times 10^{11}$ cm^{-2}

The TCT data for detectors irradiated at this fluence clearly demonstrate the difference of full depletion voltage V_{fd} for various types of Si and processing kind. The results on V_{fd} at neutron fluences of 10^{11} cm^{-2} and $5 \cdot 10^{13}$ cm^{-2} deduced from TCT data are presented in Fig. 5-5. For FZ n-Si detectors V_{fd} is about 30-40 V whereas for detectors from CZ n-Si this voltage is about 320 V for HIP and BNL samples and even more for PTI detectors. This implies introduction of donor-type defects into the bulk of CZ Si detectors processed at PTI.

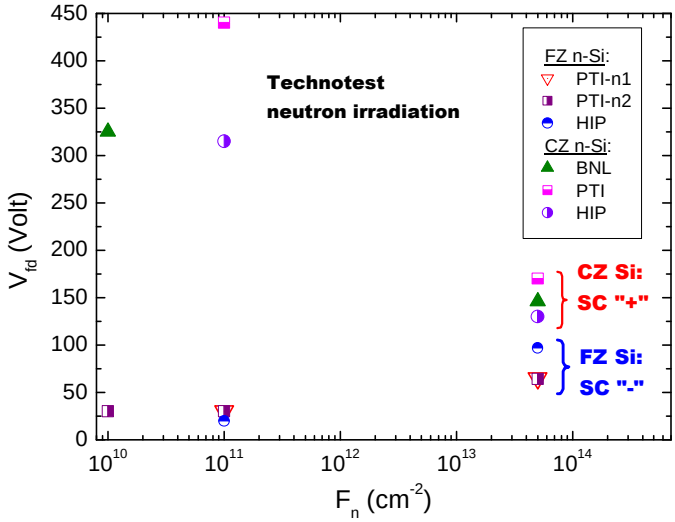

Fig. 5-5: Dependence of V_{fd} on neutron fluence deduced from TCT data

b) medium fluence, $F_n = 5 \cdot 10^{13}$ cm^{-2}

In Fig. 5-6 the shapes of current pulse response of detectors processed at PTI and HIP from n-type FZ Si and irradiated by 1 MeV neutrons at F_n of $5 \cdot 10^{13}$ cm^{-2} are shown. The range of the bias voltage is individual in each plot. It follows from the shapes of detector response that the space charge sign in PTI and HIP detectors is negative i.e. detectors are beyond SCSI. Since the signal from the p^+ side of PTI detector is observed at lower voltage than that in HIP detector, the effective space charge concentration N_{eff} is smaller for PTI detector. This is confirmed by a lower V_{fd} for PTI detectors (Fig. 5-5).

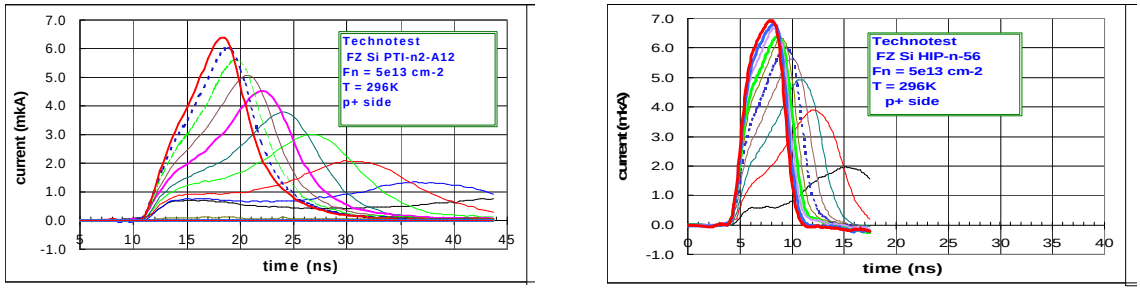

Fig. 5-6: Current pulse response of detectors processed from n-type FZ Si and irradiated by 1 MeV neutrons at F_n of $5 \cdot 10^{13}$ cm^{-2}. Laser is at the p^+ side. Range of applied bias: PTI – 40-84 V (left), HIP – 77-166 V (right).

Hence, the fluence corresponding to space charge sign inversion (SCSI) is larger for detector processed at PTI. The pulse width (collection time) for PTI detector was ~ 12 ns that is larger than that for HIP detector (~ 4 ns) since the measurements of PTI detector were carried out at lower bias, and the drift velocity was below its saturated value.

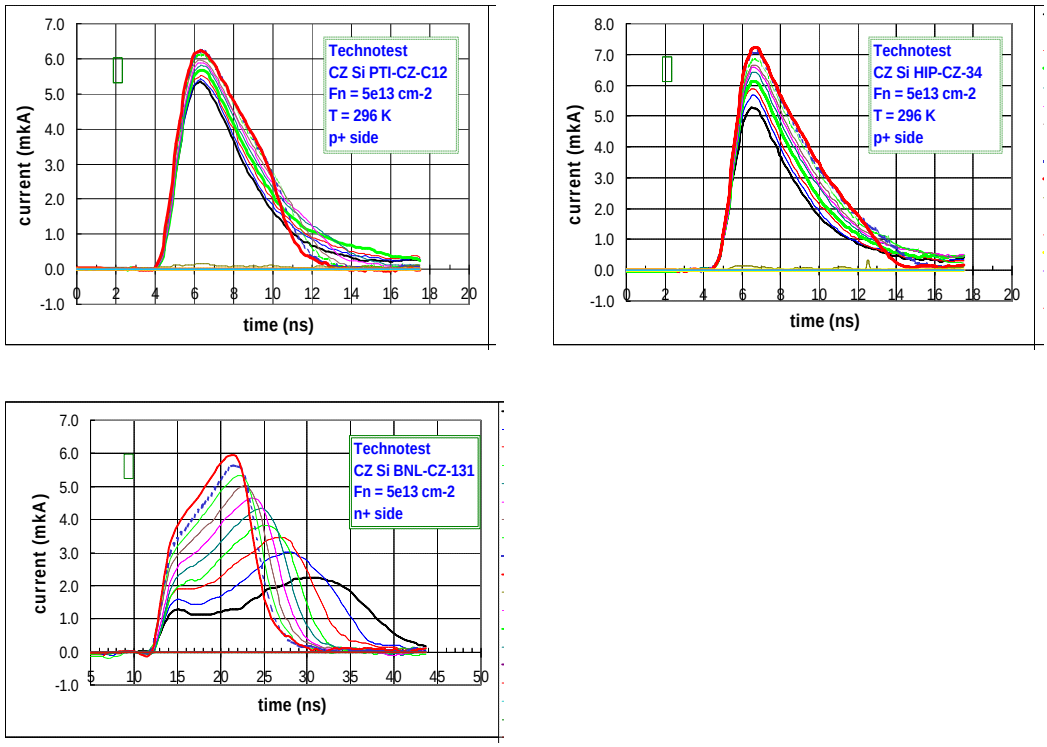

Fig. 5-7: Current pulse response of detectors processed from n-type CZ Si and irradiated by 1 MeV neutrons at F_n of $5 \cdot 10^{13}$ cm^{-2}. Laser is at the p^+ side for HIP and PTI detectors and at the n^+ side for BNL detector.

In the measurements of detectors processed from CZ Si for PTI and HIP samples the pulse laser was at the p^+ side, and for BNL detector the laser was at the n^+ side. The shape of response of all detectors processed from n-type CZ Si and irradiated by a fluence of $5 \cdot 10^{13}$ cm^{-2} (Fig. 5-7) unambiguously demonstrated the positive N_{eff} which was larger for PTI detector in accordance with higher V_{fd} (Fig. 5-5). The reasonable explanation of this behavior is that the introduction of donor-type defects (presumably of thermal donors) occurs in the bulk of PTI detectors irrespective to the type of Si and thus the results on V_{fd} after irradiation are also different. The response of BNL detector evidently shows full depletion. Since this response is due to hole collection, its width is rather large (~12 ns at V_{fd}) as compared to those of HIP and PTI detectors.

c) High fluence, $F_n = 5 \cdot 10^{14}$ cm^{-2}

The shapes of the current pulse response fater irradiation to $5 \cdot 10^{14}$ cm^{-2} and processed from FZ Si and CZ Si are presented in Figs. 5-8 and 5-9, respectively. The response of BNL detector is measured from the n^+ side whereas for the other detectors the response is from the p^+ side. The Double Peak (DP) shapes of the response from the p^+ side are observed for all detectors. The second peak of the response from the p^+ side increases with bias, which proves that detectors are beyond SCSI. The ratio of the peak amplitudes P_1/P_2 in the DP pulse shape is however different.
For HIP detectors processed from both types of Si the first peak of the DP shape stays dominating with increasing the bias. The same behavior is observed for PTI detector processed from FZ Si. These shapes with a dominating first peak do not show a direct evidence of detector full depletion. The difference of the response of PTI detector from CZ Si (Fig. 5-9a) is that the second peak of DP shape becomes dominating with bias and the ratio P_1/P_2 is <1. Thus the major difference of the pulse response is observed between HIP and PTI detectors processed from CZ Si that is discussed below.

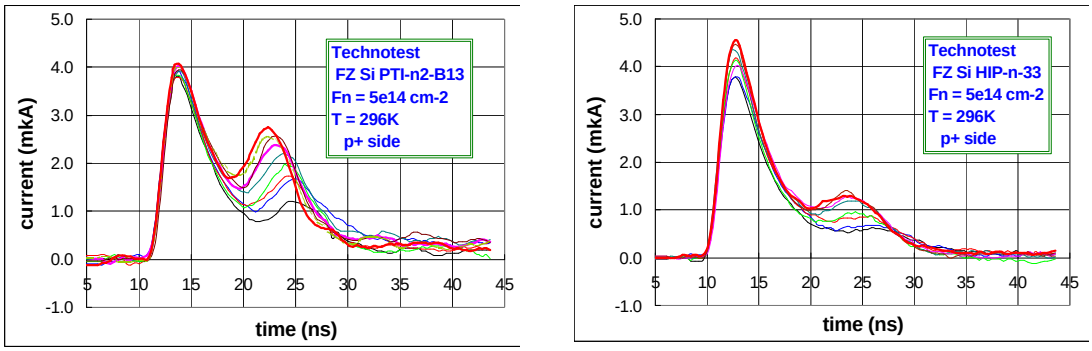

Fig. 5-8: Current pulse response of detectors processed from n-type FZ Si and irradiated by 1 MeV neutrons at F_n of $5 \cdot 10^{14}$ cm^{-2}. For PTI and HIP detectors laser is at the p^+ side, and for BNL detector laser is at the n^+ side. The range of the applied bias: PTI – 290-364 V, HIP – 267-410 V.

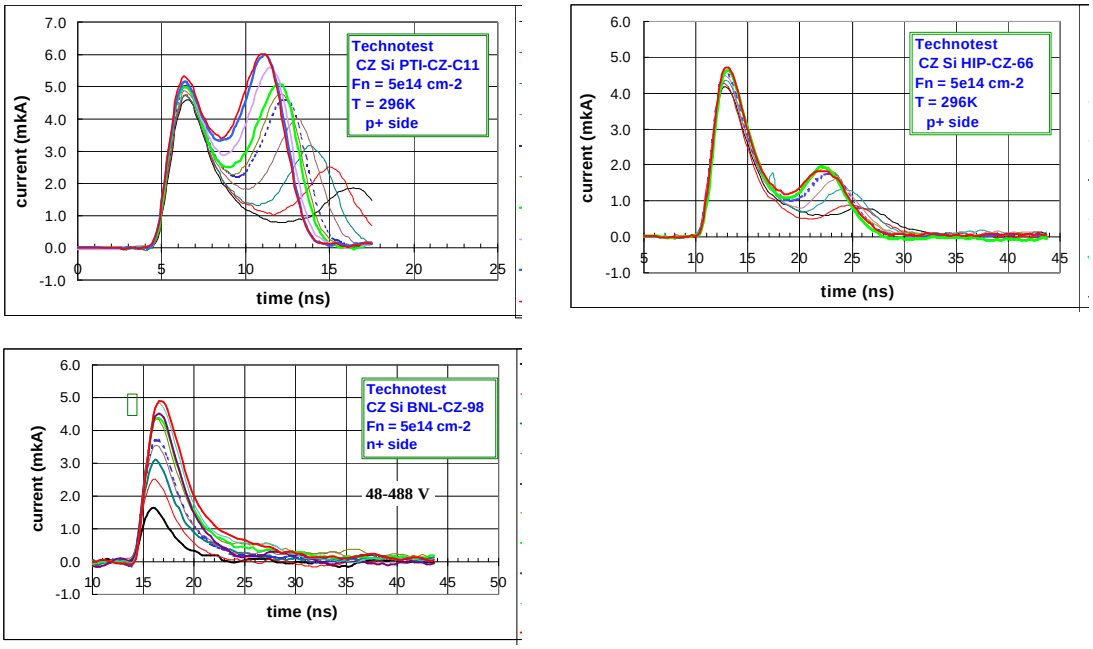

Fig. 5-9: Current pulse response detectors processed from n-type CZ Si and irradiated by 1 MeV neutrons at F_n of $5 \cdot 10^{14}$ cm^{-2}. The laser is at the p^+ side of PTI and HIP detectors and at the n^+ side of BNL detector. Range of the applied bias: PTI – 232-387 V, HIP – 271-410 V, BNL – 48-488 V.

5.2.4 Reconstruction of electric field distribution from DP pulse response

The double peak shape of the detectors response was observed for all detectors studied by the Technotest subproject irradiated to $5 \cdot 10^{14}$ cm^{-2}. This shape is specific for detectors with a high concentration of midgap energy levels (deep donors and deep acceptors) in which trapping of free carriers from bulk generation current leads to a double peaked (DP) electric field distribution E(x) [5,6]. Space charge concentration has also non-uniform distribution, in detectors based on n-type Si, N_{eff} is positive near the p^+ contact and negative near the n^+ contact.

Simulating the PD pulse response and the E(x) distribution was determined [7], to discuss and compare the response of PTI and HIP CZ Si detectors.

The approach used for simulation of the response of heavily irradiated detector and E(x) reconstruction considers three regions inside the detector structure (Fig. 5-10a): W_1 and W_2 – depleted regions near the p^+ and n^+ contacts, respectively, and W_b – the base region. In detectors irradiated beyond SCSI the region W_2 is the major depleted region, which extends towards the p^+ contact with increasing bias. The new consideration of the approach is that in heavily irradiated detectors the resistivity of the silicon bulk is close to intrinsic, therefore the high reverse current creates the potential drop (difference) over the bulk of the base region and the corresponding electric field E_b.

Application of this approach for the analysis of two detectors – PTI and HIP detectors processed from CZ Si and irradiated by a fluence of $5 \cdot 10^{14}$ cm^{-2} showed the difference in the electric field distribution (Fig. 5-10b). The electric field in the depleted region W_1 and base region in HIP detector are low enough (<1 kV/cm) whereas in PTI detector the maximal electric field near the p^+ contact and in the base region are higher and equal to 2.5 kV/cm and 1.5 kV/cm respectively. This difference is due to different effective space charge concentrations in the W_1 regions: $1.4 \cdot 10^{11}$ cm^{-3} and $1.1 \cdot 10^{12}$ cm^{-3} for HIP and PTI detectors

respectively. At the same time the electric field distribution in the major depleted region W_2 and the corresponding space charge concentration of $9.5 \cdot 10^{12}$ cm^{-3} are practically the same in both detectors. This result shows that the balance of deep donors and deep acceptors induced by radiation depends on the detector processing even in the same type of the initial Si.
The important practical consequence of the developed approach for the analysis of heavily irradiated detectors is that the studied detectors irradiated at F_n of $5 \cdot 10^{14}$ cm^{-2} can be divided into two groups. This distinction is based on the behavior of DP response with bias and the ratio of the two peaks P_1/P_2 in the experimental response curves:

1) the ratio P_1/P_2 is >1 at any bias – detectors processed at PTI from FZ n-Si and HIP detectors processed from FZ and CZ Si,
2) the ratio P_1/P_2 becomes close to 1 with increasing bias - detector processed at PTI from CZ Si.

Only in detectors from group 2 the shape of response shows the evidence of full depletion whereas the response of detectors from group 1 differs from standard shape specific for full depletion and is more typical for non-depleted mode. Meanwhile, reconstruction of E(x) distribution shows that in detectors from both groups the electric field extends over the entire detector bulk already in the range of medium bias of 200-300 V and the high electric field region (W_2) has similar dimensions. The difference between the electric field profile in the low field region may be significant that arises to the different doping profile dependent on explicit processing. The electric field profile specific for detectors with $P_1/P_2 \approx 1$ is favorable for reduction of the collection time that is an important operational characteristic for LHC upgrade. The results on collection time for detectors processed and studied within the Technotest project are described in the Section “FDS” of this report.

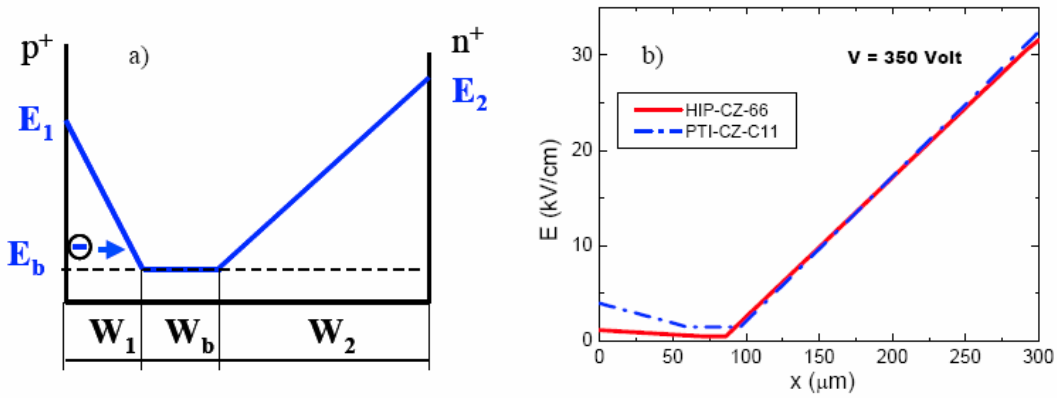

Fig. 5-10: Model of electric field distribution in heavily irradiated Si detectors (a) and electric field distribution at V = 350 V in HIP and PTI detectors processed from CZ Si and irradiated by neutrons to a fluence of $5 \cdot 10^{14}$ cm^{-2} (b)

5.2.5 Conclusions of Technotest project

1. A difference in the spectra of thermally induced defects is observed in detectors processed by different producers: two electron traps are induced in the silicon bulk in HIP and PTI detectors; no defects are detected in BNL detectors.
2. In irradiated detectors a difference was observed in the inversion fluence (corresponding to SCSI):
   FZ: inversion fluence higher for BNL detectors than HIP and PTI;
   CZ: inversion fluence higher for PTI detectors than HIP.
3. Double Peak shape response is observed for all detectors irradiated beyond SCSI.

4. Treatment of DP pulse response of detectors irradiated by $F_n = 5 \cdot 10^{14}$ cm^{-2} shows:
   - the same E(x) distribution in the depleted region extending from the n^+ contact;
   - higher E in the depleted region extending from the p^+ contact in PTI detectors.
5. Balance of DDs and DAs induced by radiation depends on the type of Si and detector processing.

Future plans for the Technotest subproject will be focussed on the evaluation of:

1. detectors irradiated at Fn = 10^{15} cm^{-2}
2. detectors processed from p-type Si
3. 24GeV/c proton irradiated detectors
4. Study of microstrip detectors. Detectors have been already processed in PTI and irradiated by 24 GeV/c protons.

5.3 Thin Epi-Si Pad-detectors

Epi-Si detectors grown on Cz substrate were found to exhibit the superior radiation hardness in terms of N_{eff}. Several wafers of different epitaxial layer thicknesses: 25, 50 and 75 μm were produced by ITME, Warsaw and processed by CiS, Erfurt. N-type epitaxial layer with homogenous resistivity of 50 Ωcm was grown on Cz substrate. The resistivity of the 300 μm thick n-type Cz substrate was 0.01 Ωcm with oxygen concentration exceeding 10^{18} cm^{-3}.

5.3.1 Effective doping concentration after irradiation

The epi-Si diodes were irradiated up to $\Phi_{eq}=10^{16}$ cm^{-2} and show (Fig. 5-11) no space charge sign inversion after proton and also neutron irradiations when N_{eff} is measured after 8 to 30 min (annealing at 80°C) resp. 200-400 h (annealing at 20°C). In contrast to the FZ detectors this point in time doesn't correspond to the minimum, but to the maximum of full depletion voltage evolution with annealing time. Nevertheless full depletion voltage of neutron-irradiated samples doesn't exceed the initial value.
To understand annealing of N_{eff} studies were started in Hamburg and Ljubljana on a large set of epi-Si detectors. Annealing of the diodes at different temperatures: 20°C, 40°C, 60°C and 80°C was performed and is still underway for lower temperatures where time constants are much longer. Typical annealing curves at 80°C are shown in Fig. 5-12. The annealing curves were fit with the Hamburg model to extract the damage parameters. The annealing curves were fit with the Hamburg model to extract the damage parameters.

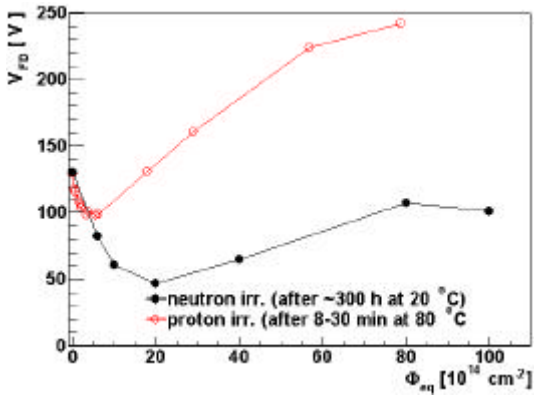

Fig. 5-11.: Dependence of full depletion voltage on fluence as measured for 50 μm thick neutron and 24 GeV/c proton irradiated diodes.

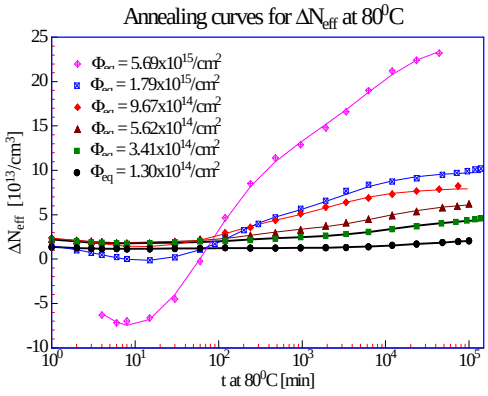

Fig. 5-12.: Annealing of ΔN_{eff} for 50 μm thick diodes irradiated with protons.

5.3.2 Reverse Annealing

In standard FZ detectors charged acceptors generated during the reverse annealing (also called late stage annealing) add to the effective acceptor concentration representing the stable damage. This leads to significant increase of the effective doping concentration if detectors are not kept at low temperatures. On the other hand the reverse annealing is beneficial for epi-Si detectors as the effective acceptors compensate the stable positive space charge. The difference between FZ and epi-Si detectors irradiated to similar fluences can be seen in Fig. 5-13.

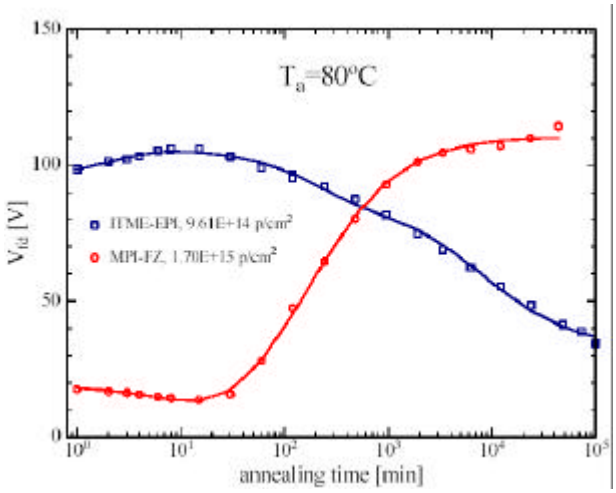

Fig. 5-13.: Difference in evolution of full depletion voltage between 50 μm thick high resistivity FZ and Epi-detectors.

Although the high resistivity FZ detector has much lower full depletion voltage after irradiation it increases with time and after few hundred minutes at 80°C reaches that of the epi-Si detector.

The concentration of defects responsible for first component of the reverse annealing was found to linearly increase with fluence (Fig. 5-14) with g_{Y1}=2.6?10^{-2} cm^{-1}. Except for the lowest fluences, where the time constant of the reaction could not be reliably determined, the time constant of the reaction was found not to depend on fluence (see Fig. 5-15) thus confirming the 1st order kinetics. The difference of reaction time constants obtained from 60°C and 80°C annealing indicates that the process is governed by the same activation energy as in FZ detectors (E_a=1.32 eV) an assumption confirmed also by similar time constant, t_{y1}~1000 min at 60°C.

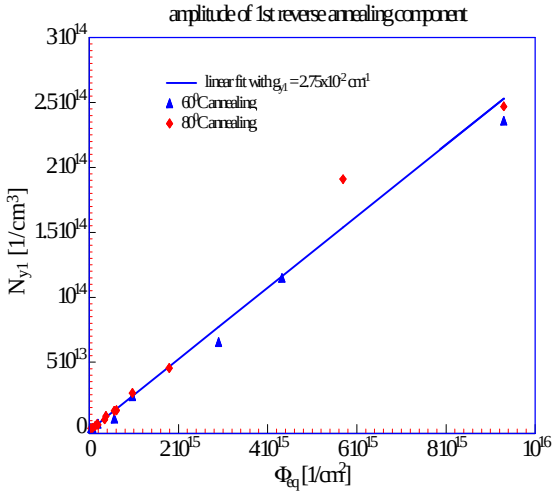

Fig. 5-14.: Introduction rate for defects responsible for initial component of reverse annealing.

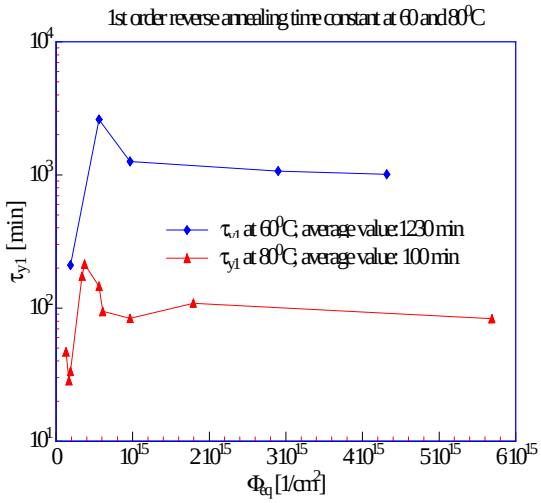

Fig. 5-15.: Dependence of time constant for initial component of reverse annealing on fluence.

The prolonged component of the reverse annealing contributes significantly to the effective doping concentration at time scales of around 10 years at 20°C. It exhibits, decrease of the generation rate g_{y2} with fluence as can be seen in Fig. 5-16. The time constant depends linearly on the inverse of defect concentration (Fig. 5-17) as expected for 2nd order process. Preliminary results derived from annealing at 60°C and 80°C show that the activation energy is comparable to the one of the first component.

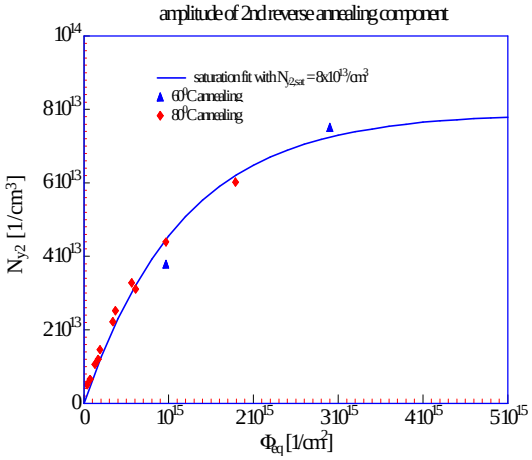

Fig. 5-16.: Introduction rate of defects responsible for second component of reverse annealing.

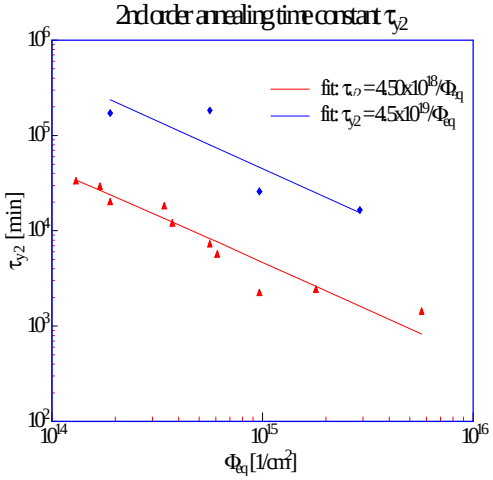

Fig. 5-17.: Dependence of time constant of second component of reverse annealing on fluence.

5.3.3 Charge collection efficiency measurements and simulations

Charge collection efficiency measurements in the epi-Si detectors have been performed with minimum ionizing electrons from collimated ^{90}Sr source. The measurement setup employs a charge sensitive preamplifier and LHC speed (25 ns) shaping amplifier. The small scintillator underneath the diode triggered the read-out. The purity of the trigger was almost 100%, which enabled reliable determination of the signal also when signal could not be clearly separated from the noise.

The setup was calibrated by 60 keV photons from ^{241}Am source so the absolute charge could be determined for each measurement. The recorded spectra were fitted with convolution of Landau and Gauss function from which the values for average and most probable energy loss were obtained. The most probable and mean deposited energy of 79 and 99 e-h pairs/μm were measured.

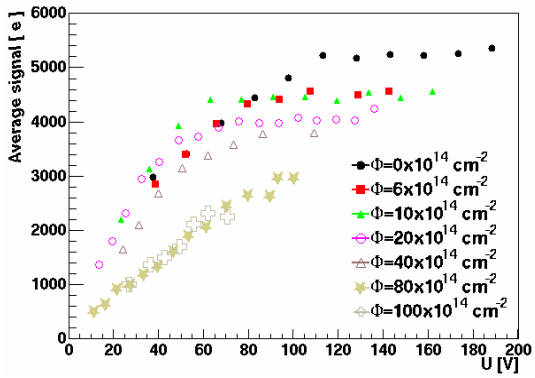

Fig. 5-18.: Dependence of mean charge on bias voltage for epi-Si samples irradiated with neutrons to different fluences.

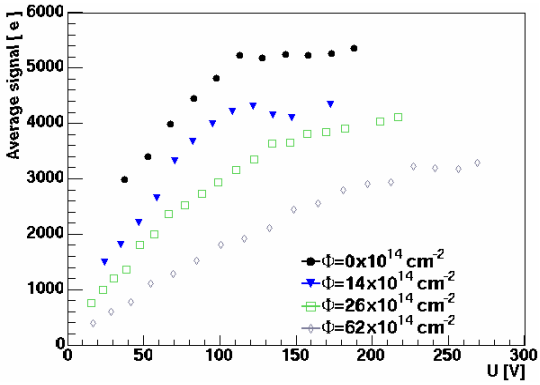

Fig. 5-19.: Dependence of mean charge on bias voltage for epi-Si samples irradiated with 24 GeV/c protons to different fluences.

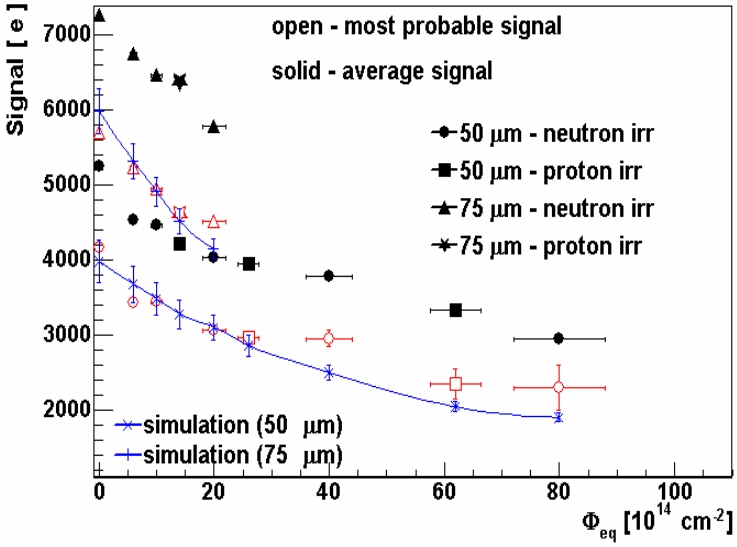

Fig. 5-20.: Figure 14: Collected charge for different epi-Si samples and the comparison with simulation (lines).

The charge collection measurements were performed on several samples irradiated with protons and neutrons up to $\Phi_{eq}=10^{16}$ cm^{-2}. The dependence of mean collected charge on voltage at T=-10^{o}C is shown in Fig. 5-18 and Fig. 5-19. It was found that full depletion voltage determined from C/V agrees with the one determined from the Q/V and that over-depleting the detectors doesn't improve much the signal. Average of the collected charge above the full depletion voltage as the function of fluence is shown in Fig. 5-20. To evaluate the effect of trapping the measured points were compared with simulation. Below F_{eq}=2?10^{15} cm^{-2} the simulation agrees nicely with measurements for both 50 and 75 μm diodes while at larger fluences underestimates the collected charge. Charge collection at F_{eq}>2?10^{15}cm^{-2} is strongly dependent on effective trapping times of electrons and holes and much less on electric field distribution. This leads to conclusion that effective trapping probability at very high fluences could be lower than extrapolated from measurements found in [8,9,10].

Collected charge was found independent on operation temperature in the range from -20°C to 10°C, which is in agreement with expectations. The decrease of mobility with temperature is compensated by the decrease of effective trapping probabilities.

5.3.4 Summary on Epi-Si detectors

Superior radiation hardness of Epi-Si in terms of N_{eff} has so far been demonstrated for both neutron and proton irradiated samples. Good reproducibility of results and similar damage parameters extracted from samples of different thicknesses are very encouraging. The main difference between n-type epi-Si and FZ materials is generation of positive space charge in epi-Si, which doesn't anneal out (stable damage). As the introduction rate of negative space charge, which appears during the late annealing stages, surpasses the introduction rate positive space charge it is possible to find an operation scenario where effective acceptors compensate donors. Effective doping concentration can thus be controlled in such a way that detectors could be fully depleted over entire period of SLHC. Measurements performed so far show that it will be possible to keep detectors at RT during the beam off period. Charge collection measurements using minimum ionizing electrons from ^{90}Sr source have been performed at equivalent fluences of ~10^{16} cm^{-2} and compared to simulations. Very good agreement was found for F_{eq}<2?10^{15} cm^{-2} while at larger fluencies more charge is measured than expected. Keeping detectors with n^{+} read-out at room temperature could have additional advantage, because effective trapping probability for electrons anneals roughly by 40% [8, 11].

In the near future p-type epi-Si detectors will be produced on p-type Cz substrate to investigate the radiation hardness of n^{+}-p epi-Si detectors, where major contribution to the signal comes from drift of electrons.

5.4 TCT Studies in FZ, DOFZ and MCz Silicon

The materials used in this study are n-type FZ (f2), DOFZ (d1), MCz (n320) processed by the Helsinki Institute of Physics, and high resistivity n-type 15 kΩcm oxygenated FZ (W317) processed by the ST Microelectronics. The samples are all 300 μm thick, 0.25 cm^2 area with an aluminum grid on the rear ohmic contact and an opening in the front aluminum for laser studies. The irradiations were performed at the CERN PS with 24 GeV/c protons. Before the measurements all of the diodes were annealed for 4 minutes at 80°C.

5.4.1 Leakage Current

The Fig. 5-21shows the normalized leakage current as a function of 1 MeV neutron equivalent fluence.

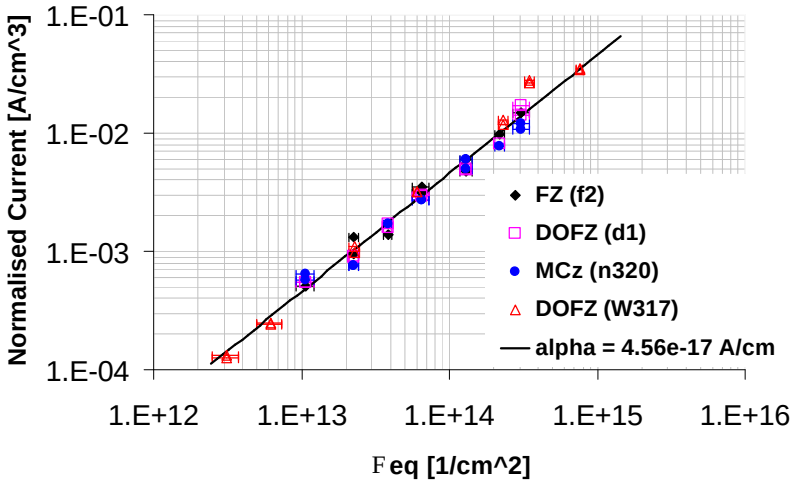

Fig. 5-21.: Normalized leakage current as a function of 1 MeV neutron equivalent fluence.

The α parameter values determined from fits to the above data for the materials under study are:

$\alpha(f2) = 4.96 \times 10^{-17}$ A/cm
$\alpha(d1) = 4.85 \times 10^{-17}$ A/cm
$\alpha(n320) = 4.73 \times 10^{-17}$ A/cm
$\alpha(W317) = 4.75 \times 10^{-17}$ A/cm

and agree well with the data given in [12] which are represented by the solid line in Fig. 5-21.

5.4.2 Full Depletion Voltage

The following plots show the evolution of the full depletion voltage of the detectors as a function of radiation. The solid lines are used for the depletion voltage determined using capacitance-voltage measurements at 10 kHz in parallel mode and the dashed lines are from current-voltage measurements.

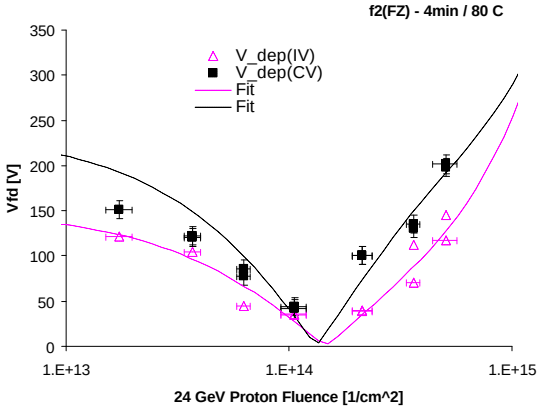

Fig. 5-22.: Evolution of the full depletion voltage of FZ(f2) pad detectors as function of proton fluence.

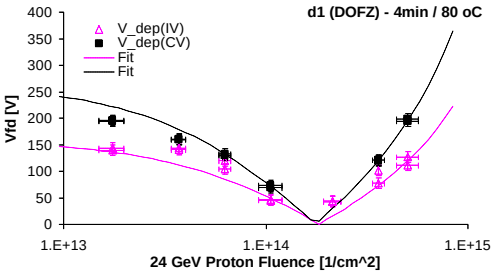

Fig. 5-23.: Evolution of the full depletion voltage of DOFZ(d2) pad detectors as function of proton fluence.

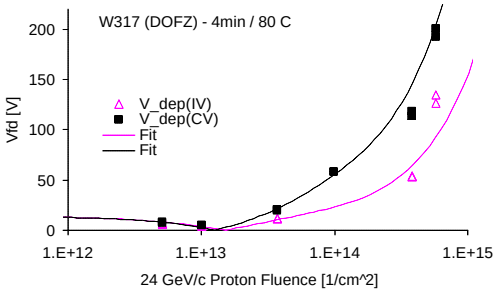

Fig. 5-24.: Evolution of the full depletion voltage of DOFZ(W317) pad detectors as function of proton fluence.

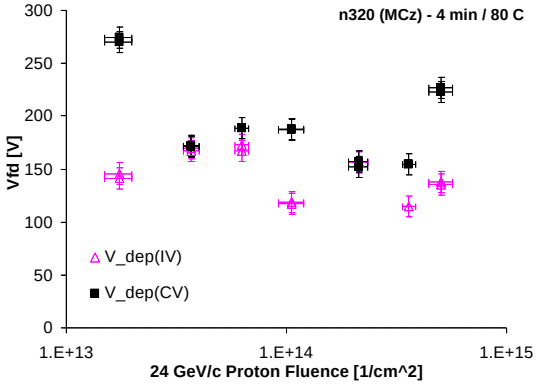

Fig. 5-25.: Evolution of the full depletion voltage of MCz(n320) pad detectors as function of proton fluence.

All materials processed at the Helsinki Institute of physics had approximately the same initial resistivity. However the FZ and DOFZ materials type inverted at a fluence a factor 2.5 times lower than the

maximum fluence of the MCz. The measurements of the MCz material are consistent with previous measurements [13]. These measurements alone are inconsistent and can not prove whether MCz type inverts. The SCSI in different materials was further studied by Transient Current Technique (TCT) measurements.

5.4.3 DOFZ type inversion

Fig. 5-26 shows the current signal resulting form hole injection into DOFZ silicon irradiated to 2 x 10^{13} p/cm^2. This shows the holes are moving towards the high electric field region. Hence the front implant still has the high electric field, indicating the bulk material is still n-type and the DOFZ has not undergone type inversion yet.

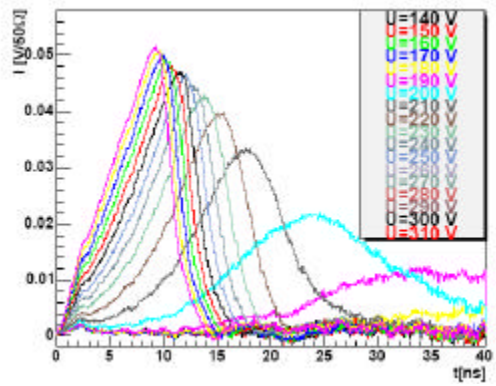

Fig. 5-26.: Hole injection into DOFZ silicon detector irradiated with 2 x 10^{13} p/cm^2.

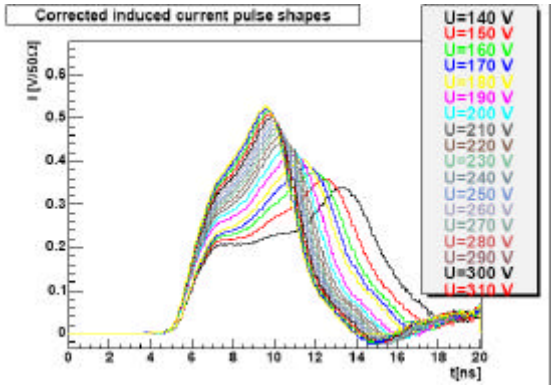

Fig. 5-27.: Electron injection into DOFZ silicon detector irradiated with 5 x 10^{14} p/cm^2.

Fig. 5-27 shows electron injection into DOFZ silicon which has been irradiated to 5 x 10^{14} p/cm^2. The current signal shows that the electrons are traveling towards the region of the high electric field, the back n^+ implant. Hence the DOFZ material has undergone type inversion.

5.4.4 Magnetic Czochralski Silicon

A MCz diode was irradiated to 5 x 10^{14} p/cm^2. The silicon had the same initial resistivity as FZ and DOFZ diodes, which type inverted at a fluence of 2 x 10^{14} p/cm^2. Hole injection was performed and Fig. 5-28 shows the resultant signal for various applied bias voltages. The holes are moving toward the region of high electric field, the front p^+ implant.

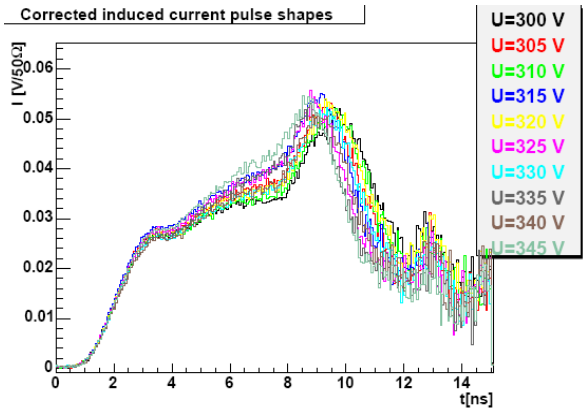

Fig. 5-28.: Hole injection into MCZ silicon detector irradiated with 5 x 10^{14} p/cm^2.

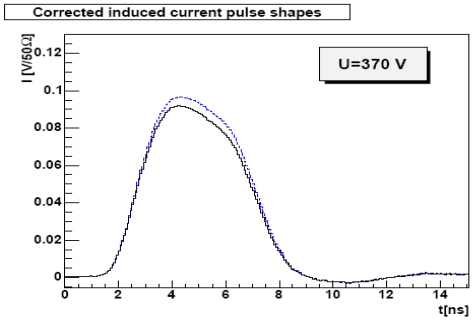

Fig. 5-29.: Electron injection into MCZ silicon detector irradiated with 5 x 10^{14} p/cm^2.

Electron injection was also performed on the same MCZ sample. Fig. 5-29 shows the resultant current signal before (black solid line) and after (blue dashed line) correcting for the trapped charge. The electron injection confirms the silicon still has not type inverted, since the electrons are traveling towards the region of low electric field, the back n^+ implant. Hence even at this high fluence, MCz silicon still has not type inverted at 5 x 10^{14} p/cm^2 fluence.

5.4.5 Effective trapping times

The effective trapping time for each carrier type, $\tau_{eff,e,h}$, depends linearly on the radiation.

$$\frac{1}{t_{eff_{e,h}}} = b_{e,h}\Phi_{eq}$$

Φ_{eq} is the fluence expressed in terms of 1 MeV neutron equivalence. We have measured the proportionality constant, β, for both carrier types in all 4 materials. In Table 5-3 the values we have found are compared with previous results. The trapping rate is material independent. β_h is approximately 30 % larger than β_e.

	b_e [10^{-16} cm^2/ns]	b_h [10^{-16} cm^2/ns]	T [^{o}C]
Dortmund [14]	5.16 $\pm$ 0.16	5.04 $\pm$ 0.16	0
Lancaster/Hamburg [15]	5.4 $\pm$ 0.3	7.0 $\pm$ 0.3	0
Ljubljana [16]	5.6 $\pm$ 0.2	7.7 $\pm$ 0.2	-10
Hamburg [13]	4.85 $\pm$ 0.15	5.72 $\pm$0.5	+20
f2 (FZ)	5.59 $\pm$ 0.29	7.16 $\pm$ 0.32	+5
d1 (DOFZ)	5.73 $\pm$ 0.29	6.88 $\pm$ 0.34	+5
n320 (MCz)	5.81 $\pm$ 0.32	7.78 $\pm$ 0.39	+5
W317 (DOFZ)	5.48 $\pm$ 0.22	6.02 $\pm$ 0.29	+5

Table 5-3: Trapping parameters β_h and β_e taken from the indicated references and as measured for 4 different materials in this work. The measurement temperature is indicated in the last column.

5.5 References for Chapter 5

[1] E. Verbitskaya at al., “Results on Technotest subproject: correlation between material properties, processing and characteristics of Si detectors irradiated by neutrons”, pres. 5th RD50 Collaboration Workshop, CERN, Geneva, Oct. 14-16, 2004, www.cern.ch/rd50

[2] C. T. Sah and C. T. Wang, J. Appl. Phys. 46 (1975) 1767

[3] E. Verbitskaya et al., Sov. Phys. Semicond. 26 (1992) 1101

[4] J. Härkönen et al., “Particle Detectors made of High-Resistivity Czochralski Silicon”, Physica Scripta T114 (2004) 88-90.

[5] D. Menichelli, M. Bruzzi, Z. Li, V. Eremin, “Modelling of observed double-junction effect”, Nucl. Instr. and Meth. A426 (1999) 135-139.

[6] V. Eremin. E. Verbitskaya, Z. Li. “The Origin of Double Peak Electric Field Distribution in Heavily Irradiated Silicon Detectors”. Nucl. Instr. and Meth. A 476 (2002) 556-564.

[7] E. Verbitskaya et al., “Operation of Si detectors irradiated at very high fluence in non-depletion mode”, pres. 5 RESMDD, Oct 1-13, 2004, Firenze, Italy.

[8] G. Kramberger et al., Nucl. Instr. and Meth. A 481 (2002) 297.

[9] E. Fretwurst et al., ``Survey Of Recent Radiation Damage Studies at Hamburg", presented at 3rd RD50 Workshop, CERN, 2003.

[10] O. Krasel et al., ``Measurement of Trapping Time Constants in Proton-Irradiated Silicon Pad Detectors", presented at 3rd RD-50 Workshop, CERN, 2003.

[11] T. Lari et al., Nucl. Instr. and Meth. A 518 (2004) 349.

[12] M. Moll, Radiation Damage in Silicon Particle Detectors, DESY-THESIS-1999-040.

[13] E. Fretwurst et al., Survey of Recent Radiation Damage Studies at Hamburg, 3rd RD50 Collaboration Workshop, 4th Novemebr 2003.

[14] O. Krasel et al., Measurement of the Trapping Time Constants in Silicon with the Transient Current Technique, 2nd RD50 Collaboration Workshop, 18th May 2003.

[15] T. J. Brodbeck et al., A New method of carrier Trapping Time Measurement, Nuc. Instrum. and Methods A 455 (2000) 645-655.

[16] G. Kramberger et al., Effective Trapping Time of Electrons and Holes in Different Silicon Materials Irradiated with Neutrons, Protons and Pions, Nuc. Instr. and Meth. A 481 (2002) 297-305.

6 New Structures

6.1 3D detectors

The interest in 3D detectors is continuously growing because of their intrinsic capability to control the depletion mechanism by acting on the layout of the electrodes rather than via material engineering. By properly designing the electrodes width and pitch, one can obtain a depletion voltage, (V_{depl}), two orders of magnitude lower and a collection time one order of magnitude lower than those of standard planar detectors, while maintaining the same active detector thickness. The standard designs of 3D detectors, as, for instance, those proposed by Parker et al. [1], present columnar electrodes of both doping types arranged in adjacent cells. The path of the electric field lines begins at one electrode type and ends at the closest electrode of the opposite type perpendicular with the detector surface. Changing the bias voltage one can modulate the strength of the electric field inside the device. Two main drawbacks characterize these devices: (i) columnar electrodes are dead-regions [2]; (ii) the regions located in the middle between electrodes of the same type present a null field, therefore delaying the collection of carriers generated in such zones that slowly move by diffusion until they reach a region with a sufficient electric field. Over biasing of the structures negates these effects by the removal of the low field zone.

6.1.1 Fabrication of 3D detectors

The fabrication process of 3D detectors is rather long and requires several steps that are not commonly used in standard detector technology [3]. This makes future mass production of 3D devices very critical as far as the fabrication yield and the costs are concerned.

One of the groups involved in 3D detectors ITC-irst, Trento, Italy, in conjunction with CNM Barcelona, Spain, has developed, for their first production run, a new 3D detector architecture [4] with the aim to simplify the manufacturing process. In particular, the proposed device features electrodes of one doping type only, e.g., n+ columns in a p-type substrate. The main advantage is that the column etching and doping are performed only once, a fact that provides a considerable process simplification. The columns may extend deep into the bulk or all the way through it. The first option leads to a further process simplification, indeed, the initial wafer bonding and the final mechanical lapping of the support wafer, (as reported in [3]), are not required.

The electric field configuration of these detectors forces the electrons generated in the substrate to move laterally to the closest n+ electrode, whereas the holes gather in the mid region between the electrodes and then slowly move to the backside, rather than to a p+ electrode.

The main drawback of the proposed structure is that it is not possible to control the electric field strength with the applied voltage when full depletion is reached. The only way to control it is by selecting the appropriate substrate doping concentration. As a result, the low-field regions may have a larger extension with respect to the original 3D detector design.

As already mentioned, the fabrication process of these devices includes steps that are not standard for planar detector technology and need to be carefully developed before using them for a real device fabrication. For the most critical steps, some dedicated process tests have been performed on samples featuring circular columns (200 μm deep and 10 μm in diameter) that were previously etched at CNM in Barcelona by means of a DRIE machine.

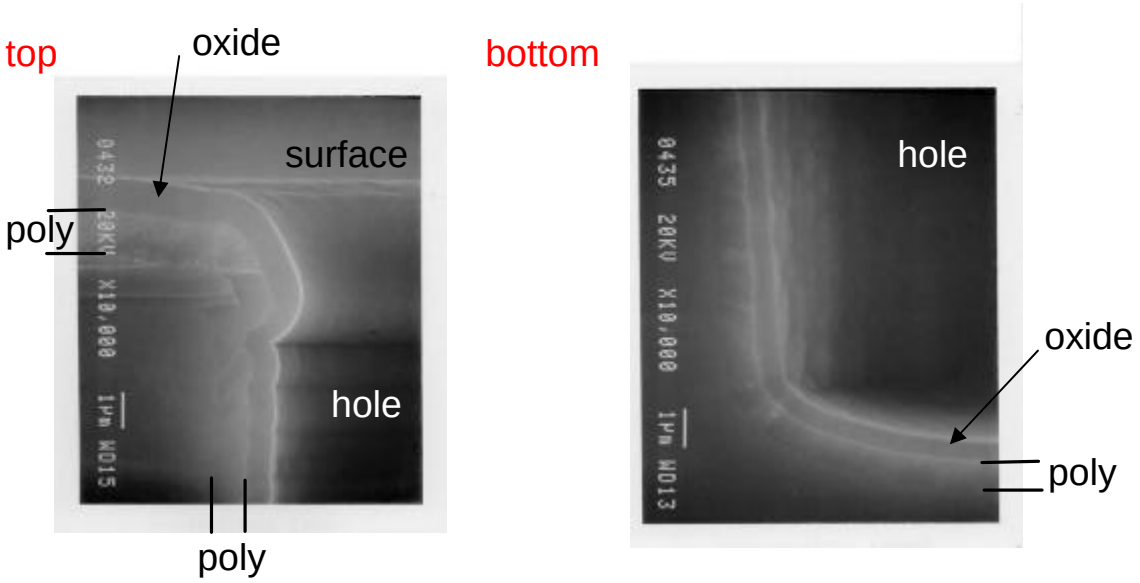

Fig. 6-1. An SEM photograph of a 3D hole with a poly deposition and filled with Silicon oxide.

As an example, figure 1 shows SEM photographs of a hole in which a layer of polysilicon and a layer of oxide have been deposited. It is visible that both materials can be deposited down to the bottom of the hole. Similar tests have been performed for other process steps giving positive results.

A layout, containing various detectors based on vertical electrodes, has been designed. The fabrication of a first batch is starting, and it is expected to be completed in the beginning of 2005.
The Glasgow group has pursued the fabrication of the full 3D detector device.

6.1.2 Pore formation

The pores for the 3D detectors were etched using one of two methods. Deep reactive ions etching has been investigated in conjunction with DRIE machine manufacture STS. To date the best aspect ratio obtained is 18:1 with holes of 10 µm in diameter. This result was only possible after modification to both the etch process and the etching equipment itself.

The second method of pore formation is electrical chemical etching with hole catalyzed HF acid etch of the silicon. This produced very parallel pores with the best aspect ratio of 30:1 with 10 µm hole diameter's. This process takes up to 24 hours. At present only one wafer can be etched at a given time. However, the apparatus is cheap and easy to assemble. Figures 2 and 3 illustrated pores fabricated by the two methods.

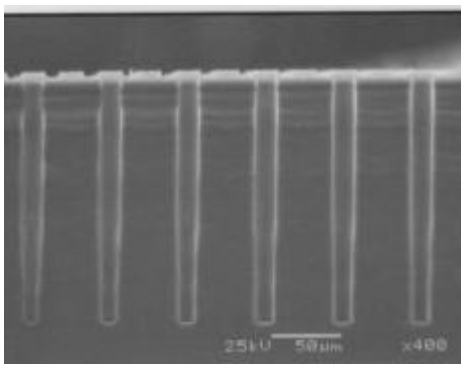

Fig. 6-2. SEM images of the structures formed by DRIE

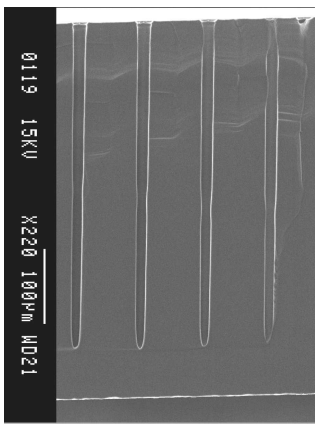

Fig. 6-3. SEM images of the structures formed by EE

6.1.3 Contact formation/Pore filling

Boron diffusion has been performed in order to form p-n junctions in n-type silicon pore walls. Several techniques were used to analyse the doping distribution in the pore walls: Scanning Electron Microscopy (SEM), Scanning Spreading Resistance Microscopy (SSRM) and Secondary Ion Mass Spectrometry (SIMS). SEM and SSRM were used to confirm that boron diffused into the holes and formed a conductive layer at the pore surface. Finally, SIMS was used to obtain the doping profiles through the pore wall at different positions along the pore depth. This analysis revealed that boron diffusion is a suitable technique to dope deep pores and to form p-n junctions in the walls
The use of an oxide mask (the initial oxide layer used for the lithographic step) over the surface of the wafer was used as a barrier during the diffusion process to prevent boron diffusion into the top side of the wafer. If this had occurred all the pores would be connected together. These devices were tested electrically to prove that they were in fact electrically disconnected. A second set of holes is then etched into the wafer after the formation of the p-n junction. Due to the fact that phosphorous could not be used at Glasgow the second set of holes was filled with metal to form a metal-semiconductor contact. A slightly rectifying forward bias IV characteristic results from this diode construction due to the fact that when the p-n junction is forward biased the metal-semiconductor junction is reversed biased.

6.1.4 Test device fabrication and testing

The good rectifying nature of the p-n junction has been proved, as illustrated in figure 4. The p-n junction was shown to respond to illumination, line b on figure 4. Figure 4 also shows the IV curve obtained when a short RIE cycle was used to disconnect the p-n doped pores rather than the oxide diffusion mask. A high current was observed and therefore this method was not favored.

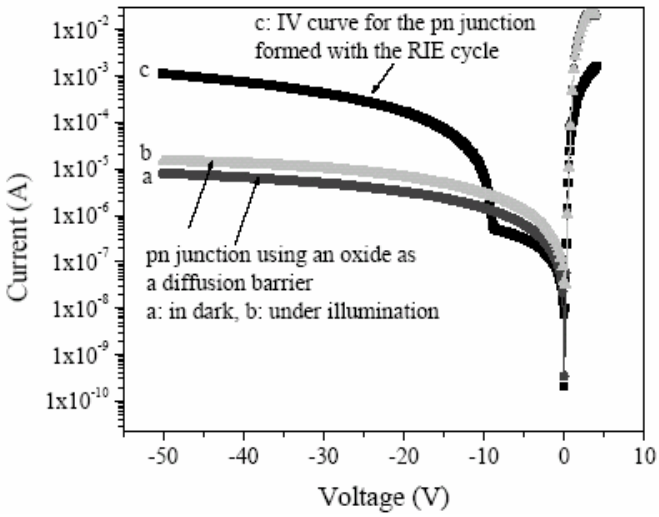

Fig. 6-4. IV characteristics of p-n junctions formed by boron diffusion in to thin pores; a: with oxide boron diffusion mask; b: as a under illumination; c no oxide mask used instead an RIE cycle was used to remove the top layer of wafer to isolate the pores.

6.1.5 Large scale 3D detectors

Pixel and strip detector masked have been designed. A first Pixel mask compatible with the Medipix-1 chip has been designed and fabricated. The layout of the pores is shown in figure 5, and a photograph of the fabricated device is shown in figure 6. The pore diameter is 10 µm. A square unit cell has been fabricated with a cell pitch of 57 µm repeated three times to give a unit cell of 170 µm which is consistent with the 170 µm Medipix-1 pixel size. The p-pores were fabricated from boron

diffusion into the pore. The p-pores were fabricated with metal deposition into the pores using atomic layer deposition at Metorex.

The IV and CV characteristics of a unit cell of the Medipix-1 device have been made. The CV curve shows full depletion at 1.5V with a capacitance for a given Medipix-1 pixel of 500 fF. This is 50 times higher than one would obtain for a standard planar device. The IV curve, shown in figure 7, shows a leakage current of a few pAs per pixel. The IV curve shows a good rectifying nature in reverse bias as expected from the p-n junction. In forward bias the leakage current is rectified to an extent by the metal-silicon junction in the n-pores.

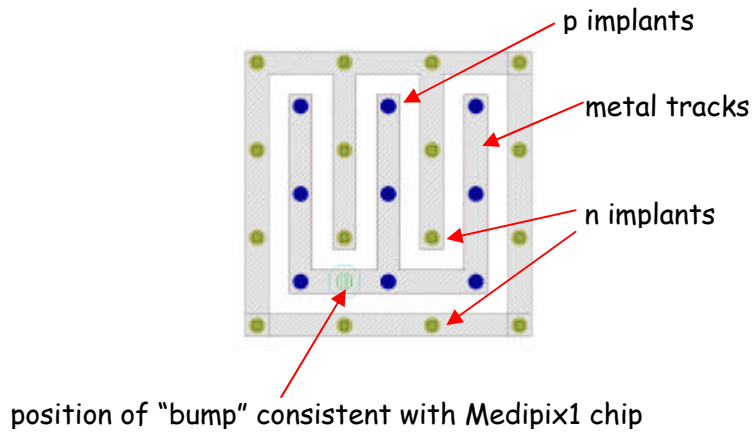

Fig. 6-5. Layout of a cell of a 3D Medipix-1 pixel detector

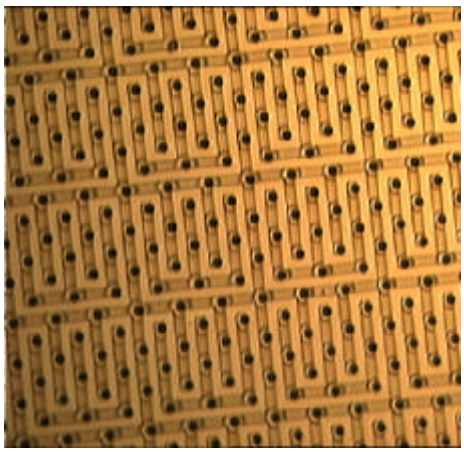

Fig. 6-6. Photograph of a 3D Medipix-1 pixel detector

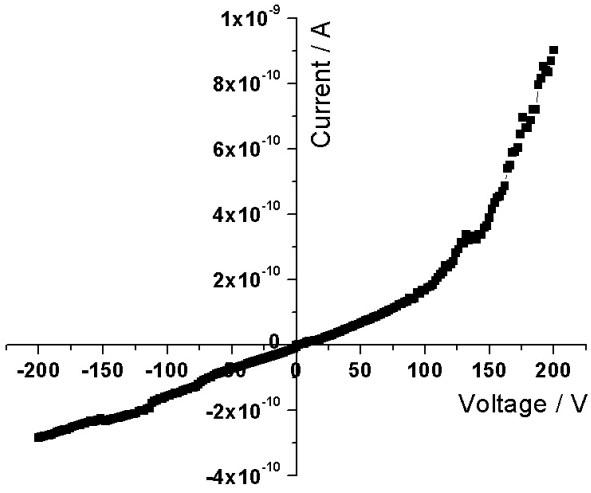

Fig. 6-7. IV curve of a cell of a 3D Medipix-1 pixel detector

A mask set has been designed that allows the same pore geometry to be used for the Medipix-1 pixel detector and a 80 µm pitch strip detector. The pores are 2 or 5 µm in diameter with an n-to-n pitch of 42.5 µm and an n-to-p pitch of 30 µm. The top wafer surface metallization defines weather a Medipix-1 or strip device is realized. Figure 8 shows the Medipix-1 layout and figure 9 shows details of the strip device. These devices have not been fabricated to date.

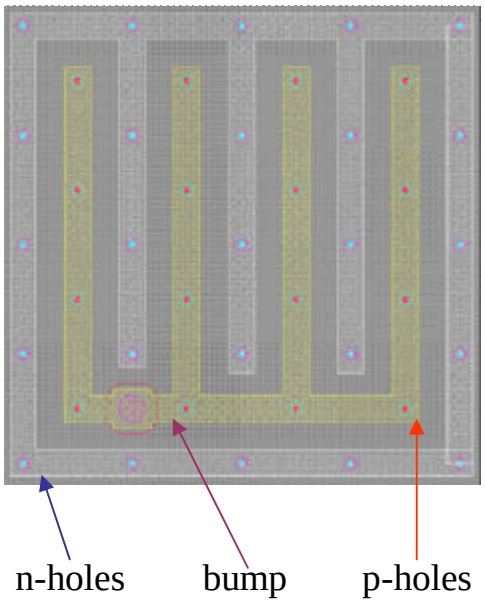

Fig. 6-8. Layout of a cell of a 3D Medipix-1 pixel detector

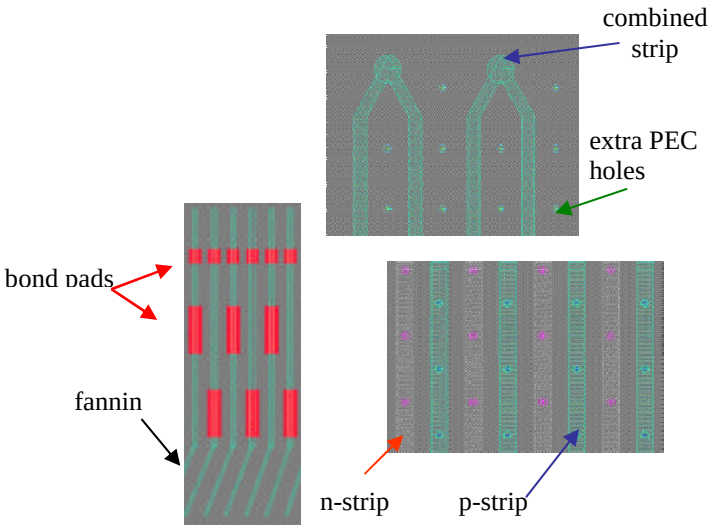

Fig. 6-9. Layout of a strip detector

A mask set for the VELO shaped strip detector has also been design and fabricated. The layout of the pores follows the strips on the R-measuring detector (a micro-strip detector) and thus the 3D-VELO detector may be bonded to previously used readout chips such as the VA2 chip. Production of these devices has been finished and they are in the process of being tested. The pores in this design are 10 µm in diameter with a pitch of 55 µm for the inner radius strips increasing linearly to a 90 µm pitch for the outer radius. Figures 6-10 and 6-11 show the mask of the 3D VELO sensor.

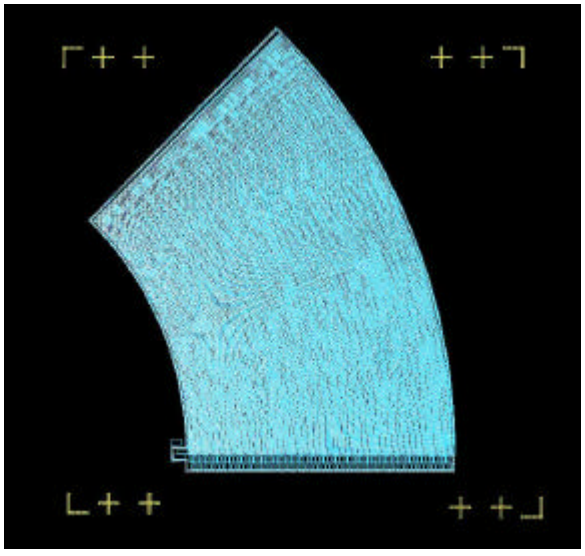

Fig. 6-10. Mask of the 3D VELO strip detector

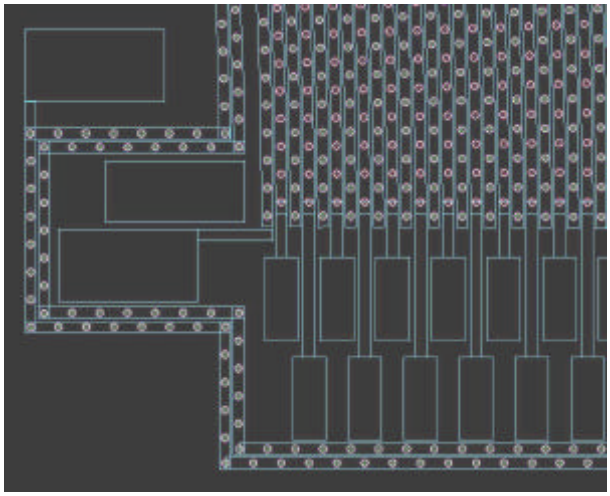

Fig. 6-11. Detail of the bond pads and guard ring of the 3D VELO strip detector

6.2 Development of semi 3-D detectors

A semi-3D detector has both p+ and n+ strips implanted on the top side of an n-type substrate while the backside has a uniform n+ implant. In this novel structure, all n+ strips are connected to a positive bias or left floating while each p+ strip is connected to an electronics channel for signal

readout. Before space charge sign inversion, (SCSI), the depletion develops both vertically from the p+ strips to the back n+ plane and laterally from the p+ strips to the neighbouring n+ strips.

During the past year BNL, Syracuse and Purdue simulated the performance of these detectors with ISE-TCAD. The simulation shows that the full depletion voltage will be about 20% higher than a conventional single-sided p+/n/n+ strip detector before irradiation. After the sensors are irradiated beyond type inversion the depletion develops both from the n+ strips in the front side, and the n+ back plane towards the p+ readout electrodes and a reduction in the full depletion voltage of about a factor of 2 is expected compared to standard planar strip detectors.

A few wafers containing semi-3D detectors and standard pad diodes were fabricated by BNL in 2004. The Purdue group measured several devices before and after irradiation. Samples were irradiated at CERN with a 24 GeV/c proton beam to two fluences of 5×10^{14} n_{eq}/cm^2 and 1×10^{15} n_{eq}/cm^2. Several diodes were also irradiated at IUCF with a 200 MeV proton beam to a total fluence of 5×10^{14} n_{eq}/cm^2. To date, only the samples irradiated to 5×10^{14} n_{eq}/cm^2 have been measured. The expected depletion voltage of a standard planar diode exposed to this fluence is about 370 V. The depletion voltages of the semi-3D detectors were measured to be 125 V and 150 V for the samples irradiated at CERN and at IUCF respectively. These first measurements after irradiation confirm that semi-3D detectors deplete at about half the expected voltage of standard silicon, as expected from simulation. More investigation is required to understand; the shape of CV measurements, the dependency of the measured depletion voltage on frequency and on the voltage applied to the n+ strips. A study of the detectors charge collection efficiency, measured by connecting the sensors to the SVX4 readout chip, is planned.

6.3 Thin Silicon

The enhanced radiation hardness of thin silicon detectors is attractive for pixel and strip sensors operating at the LHC and future high-energy hadron colliders.

The Purdue group has received several 150, 200 and 300 μm thick silicon strip detectors manufactured by Micron Semiconductor. The DC properties of the sensors have been measured on a probe station. The measurements confirm that the coupling capacitance, inter-strip capacitance and the bias resistance do not change with the sensors thickness. Confirmation of the expected changes in depletion voltage is observed. The depletion voltage decreases from ~100 V for the 300 μm device to ~15 V for the 150 μm thick sensors. The SVX4 chip developed for Run IIb of the Tevatron will be used for S/N studies of the thin strip detectors.

Purdue has also received thin pixel wafers manufactured by Micron but these have not so far been measured. After the measurement of their DC characteristics the Purdue group plans to conduct studies of the detectors coupled to the CMS .25 μm readout chip S/N performance using the laser system that has been set up for the CMS pixels.

The research activities of the Trento, Padova and Firenze groups in 2004 has been concerned with the characterization of devices fabricated at IRST in 2003 [5] from the viewpoint of radiation hardness and charge collection efficiency.

Radiation damage tests have been performed with 58 MeV Li ions at the SIRAD Irradiation Facility of the INFN National Laboratory of Legnaro, Italy. Diodes fabricated on 50 μm and 100 μm thick high resistivity, (>1 kΩcm), Si membranes along with 300 μm thick reference diodes have been irradiated in a vacuum chamber ($< 8 \times 10^{-6}$ mbar) and at room temperature in single steps, i.e., different devices were considered for each fluence. The delivered fluences ranged from 2.11×10^{12} Li/cm^2 to 1×10^{14} Li/cm^2. After irradiation devices were electrically characterized by 10 kHz capacitance-voltage (C-V) and current voltage (I-V) measurements. It should be noted that all the considered Li fluences are high enough to cause substrate type inversion.

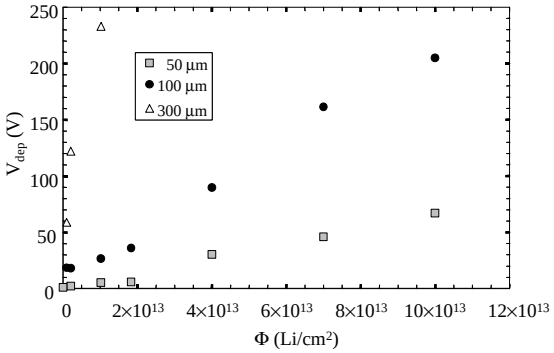

Fig. 6-12. Depletion voltage (V_{dep}) as a function of the Li ion fluence (Φ) for diodes of different thickness: 50 µm (dashed squares), 100 µm (close circles) and 300 µm (open triangles).

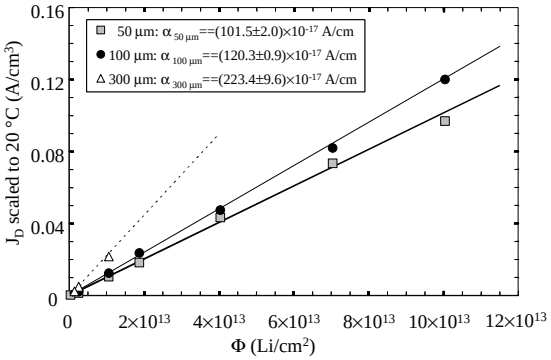

Fig. 6-13. Leakage current volume density (J_D) as a function of the Li ion fluence for diodes of different thickness: 50 µm (dashed squares), 100 µm (close circles) and 300 µm (open triangles). The values of the damage constant α, i.e., the slope of linear fit for the J_D data, are reported in the inset.

Figure 12 shows the depletion voltage, (V_{dep}), as a function of the 58 MeV Li fluence, as obtained by the C-V measurements, for diodes of different thickness. As can be seen, devices made from thinned substrates exhibit a very low depletion voltage even after the maximum fluence. In particular, V_{dep} does not exceed 60 V for the 50 µm thick detectors even at the highest fluence, confirming the expected higher radiation hardness with respect to 300 µm thick sensors, for which V_{dep} = 230 V at only 1 × 10^{13} Li/cm^2. As expected, the leakage current volume density, (J_D), linearly increases with the Li fluence (see figure 13). Moreover, it should be stressed that the damage constant, (α), increases with increasing detector thickness. This effect, already discussed in [6], is due to the fact that, although the range of the 58-MeV Li ions is 400 µm, the damage produced in 300 µm thick diodes increases with increasing the depth in the Si bulk. Nevertheless, we remark that the α values shown in figure 13 are in agreement with the results reported in [6,7], suggesting that the considerations reported therein for the Li ion induced damage in thick and thin silicon detectors are independent of the diode manufacturer, at least for what concerns the α parameter.

Charge collection efficiency, (CCE), tests with a ^{90}Sr β-particle source, (0.1 mCi), have been carried out at INFN-Firenze on both non-irradiated and irradiated samples. The experimental setup, optimized for single-channel detectors and suitable for measurements in the range from -20 to 20°C, is shown in figure 14. The β-particles are collimated onto the device under test that can be biased at different voltages. The resulting current signals are fed to a low-noise charge amplifier and shaper circuit, with a shaping time of 2.4 µs, and an ENC lower than 300 e$^-$ rms. A NaI scintillator coupled to a photomultiplier tube is used for triggering the sampling and ADC circuits.

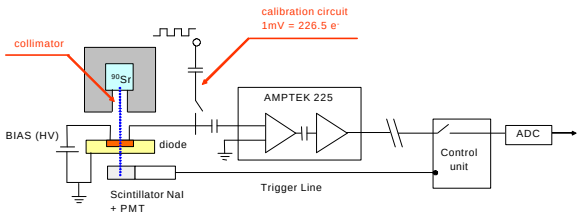

Fig. 6-14. The experimental setup for the charge collection efficiency measurements.

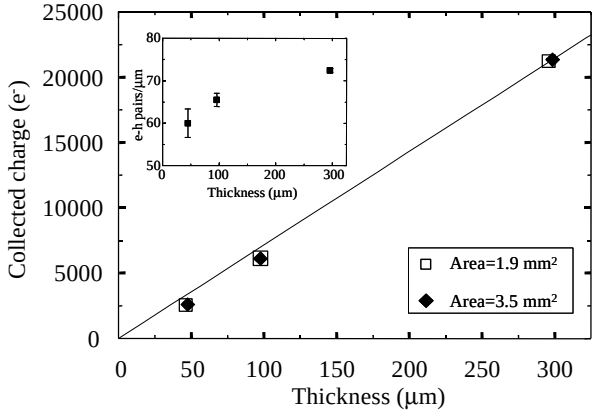

Fig. 6-15. Collected charge before irradiation for the 50 µm, 100 µm and 300 µm thick devices for two different areas. The number of electron-hole (e-h) pairs generated per unit thickness is also reported in the inset.

The collected charge for the 50 µm, 100 µm and 300 µm thick devices before irradiation is shown in Figure 15. The collected charge as a function of device thickness is approximately linear with no dependence on the device surface area. Nonetheless, the number of electron-hole, (e-h), pairs generated per unit thickness and calculated from the collected charge values is not constant, but decreases in thinner diodes, as evidenced in the inset: this effect, presently under study, is in agreement with the model in [8] accounting for straggling in thin silicon detectors.

The CCE measurements have been performed on the 1.9 mm^2 area diodes irradiated at 10^{13} Li/cm^2 and 1.8 × 10^{13} Li/cm^2. The percentage CCE values, estimated with respect to the data before irradiation of the collected charge, are shown in figure 16 as a function of the bias voltage (V_{bias}) for the 50 µm thick diodes. The data refers to measurements performed at -20 °C because device cooling was necessary to reduce the shot noise arising from the high leakage current after irradiation. The CCE increases by increasing the bias voltage and 100% CCE can be recovered for both the considered irradiation fluences. As expected, a higher bias voltage is required for the device irradiated to the higher fluence. The CCE recovery is achieved at the expense of a high bias voltage, largely exceeding the depletion voltage values extracted from the C-V measurements. A similar behaviour is observed for the 100 µm thick devices, (see figure 17). In this case the CCE increase, as a function of the bias voltage, is slower than for the 50 µm thick devices, but a 100% CCE can be still recovered at $V_{bias} \approx$ 300V. Before reaching the CCE recovery, i.e. for 120 V < V_{bias} < 250 V, the CCE is, as expected, higher for the device irradiated to the lower fluence.

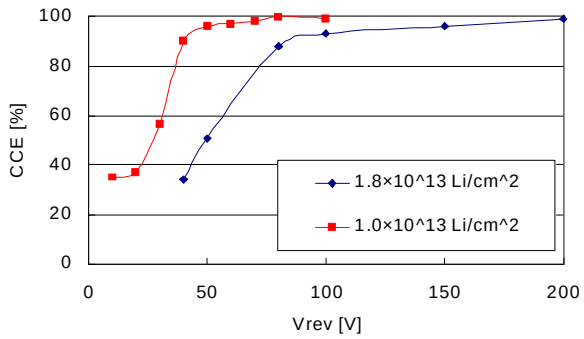

Fig. 6-16. Charge collection efficiency (CCE) as a function of the reverse bias voltage for 50 µm thick, 1.9-mm^2 area diodes irradiated at the two highest fluences. Data refer to measurements performed at -20°C.

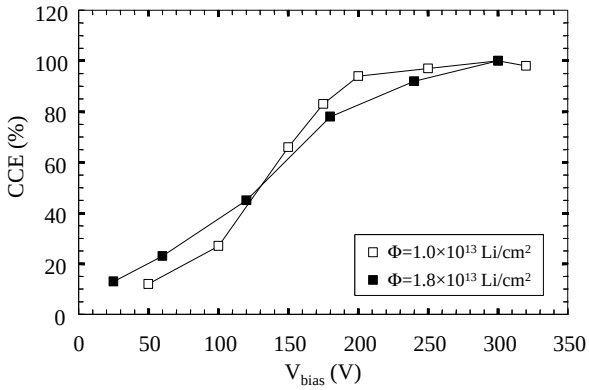

Fig. 6-17. Charge collection efficiency (CCE) as a function of the reverse bias voltage for 100 µm thick, 1.9-mm^2 area diodes irradiated at the two highest fluences. Data refer to measurements performed at -20°C.

The depletion voltage values extracted from CCE measurements before and after irradiation are summarized in Table 6-1. In non-irradiated devices, the depletion voltage values extracted from the CCE measurements are close to those extracted from C-V measurements. In the table, the depletion voltage values after irradiation are extracted from CCE measurements at ≈90% of the maximum CCE.

TABLE 6-1
Summary of the depletion voltage values extracted from CCE measurements on diodes of different thickness before irradiation and after irradiation at 10^{13} Li/cm^2 and 1.8×10^{13} Li/cm^2. Data could not be extracted for the irradiated 300 µm thick diodes.

Thickness (µm)	Before irradiation	After Φ = 10^{13} Li/cm^2	After Φ =1.8×10^{13} Li/cm^2
50	0.8±0.1 V	40±5 V	75±10 V
100	1.4±0.5 V	175-200 V	230-300 V
300	16.7±1 V	/	/

After irradiation, it was not possible to measure the CCE for the 300 μm thick diodes within the range of reverse bias voltages that could be applied with the available instrumentation, (up to 400V), due the high leakage current present even at -20°C.

6.4 References for Chapter 6

[1] S.I. Parker, C.J. Kenney, J. Segal, "3D - A proposed new architecture for solid-state radiation detectors", *Nucl. Instr. Meth. Phys. Res.* A395 (1997) 328-343.
[2] J. Morse et al., C.J. Kenney, E.M.~Westbrook, I.~Naday, S.I.~Parker, "The spatial and energy response of a 3d architecture silicon detector measured with a Synchrotron X-ray microbeam", *Nucl. Instr. Meth. Phys. Res.* A524 (2004) 236-244.
[3] C. Kenney et al., "Silicon Detectors with 3-D electrode arrays: fabrication and initial test results.", *IEEE Trans. on Nucl. Sci.*, vol. 46, no. 4, august 1999.
[4] C. Piemonte et al., “Development of 3D detectors featuring columnar electrodes of the same doping type.’’, presented at the V International Symposium on the Development and Application of Semiconductor Tracking Detectors, Hiroshima, June 14-17, 2004.
[5] S. Ronchin et al., "Fabrication of PIN diode detectors on thinned silicon wafers", *Nucl. Instr. Meth*, vol. A530, pp. 134-138, 2004.
[6] A. Candelori et al., "Lithium ion irradiation on standard and oxygenated silicon diodes", *IEEE Trans. Nucl. Sci.*, vol. 51(5), pp. 2865-2871, 2004.
[7] A. Candelori et al., "Lithium ion irradiation effects on epitaxial silicon detectors", *IEEE Trans. Nucl. Sci.*, vol. 51(4), pp. 1766-1772, 2004.
[8] H. Bichsel, "Straggling in thin silicon detectors", *Reviews of Modern Physics*, vol. 60(3), pp. 663-699, 1988.

7 New Materials

7.1 Research activity on silicon carbide

7.1.1 Growth of epitaxial 4H-SiC layers

Two new layers have been grown by the Institute for Crystal Growth of Berlin (IKZ), using 2" n-type *4H*-SiC. Ioffe group and Linköping University (Sweden) have grown *4H*-SiC epilayers 30µm thick with net acceptor concentration of 3-5×10^{15} cm^{-3} by sublimation epitaxy. *4H*-SiC epitaxial layers with thicknesses of 26-50 µm (net donor doping 6×10^{14} to 8×10^{15} cm^{-3}) were grown by CVD on commercial *4H*-SiC wafers, by Ioffe group with AMDS AB Sweden and CREE USA.

7.1.2 Processing tests structures

7.1.2.1 p^+n junction structures.

Perugia processed p^+n junctions on the new epilayers grown by IKZ institute (masks shown in Fig. 7-1). Perugia also processed p^+n diodes realized in collaboration with INSA-Cegely (Lyon, France) and CNR-IMM (Bologna, Italy). The diode structure is based on a 0.45µm deep N_A = 4×$10^{19}$$cm^{-3}$ doped p^+ emitter, ion implanted in an n-type epilayer with thickness equal to 40µm and nominal doping N_D = 1.1×10^{15} cm^{-3}.p^+-n-n^+ structures have been processed by IOFFE PTI with AMDS AB Sweden and CREE USA on of 26 µm thick and doping (6-8)×10^{15} cm^{-3} by implantation of Al^+ ions with an energy of 150 keV at a dose of 5x10^{16} cm^{-2} and a subsequent rapid high temperature annealing during 15 s in Ar ambient. Al and Cr/Al ohmic contacts to p^+- and n^+ - layers, respectively were made by thermal vacuum evaporation.

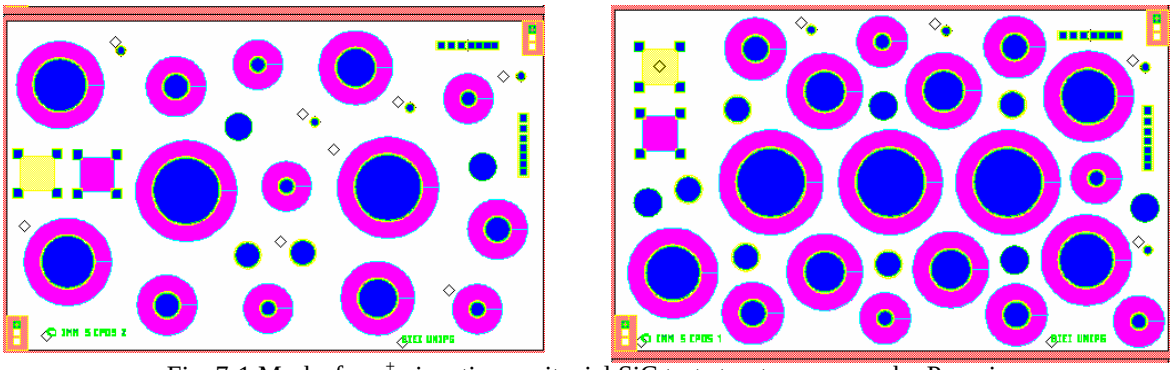

Fig. 7-1 Masks for p^+n junctions epitaxial SiC test structures grown by Perugia.

7.1.2.2 Schottky diodes

These have been processed at Glasgow University (Ni contacts) on IKZ epilayers grown in 2003 (thickness = 35 µm and net donor doping 5x10^{14} cm^{-3} , 1x10^{15} cm^{-3}). Ioffe and Linkoping University processed Schottky (∅ ~ 800 µm) and ohmic contacts by magnetron deposition of Ni. Ioffe also processed with AMDS AB Sweden Cr Schottky barriers with metal thickness of 0.1 µm and areas 1×10^{-2} cm^2 as well as Cr/Al ohmic contacts on 4*H*-SiC epitaxial layers (26µm-thick, doping 1×10^{15} cm^{-3}) and (50µm thick doping 6×10^{14} cm^{-3}). Schottky diodes have been processed already last year by Alenia Marconi Systems, Rome on *4H*-SiC epitaxial layers grown onto CREE substrates, by CREE and IKZ, the study of radiation hardness on these diodes, carried out by University of Modena and Florence continued this year.

7.1.3 Detection properties and radiation hardness of SiC Schottky diodes

7.1.3.1 IOFFE PTI and Linkoping University [1-5]

Diodes have been irradiated with protons up to $5x10^{14}$ cm^{-2} in an MGTs-20 cyclotron. Capacitance-voltage, current-voltage and DLTS spectra were measured before and after irradiation diodes. Already after irradiation up to $2x10^{14}$ cm^{-2} samples sheet resistance strongly increased and the irradiated material became semi-insulating. This result has been explained considering that in the p-type 4H-Si? epilayer the concentration of radiation-induced donor-like defects became comparable to the acceptor-like levels. A comparison between Si and SiC radiation hardness was carried out by these two groups in the following way. Samples were cut from a Si ingot doped with phosphorus in concentrations of about $6 \cdot 10^{15}$ cm^{-3}. 4H- and 6H-SiC layers of n-type with charge carrier concentrations of 10^{16} cm^{-3} were grown by sublimation epitaxy technique on SiC substrates. Samples ave been irradiated with 900keV fast electrons. Electrical measurements on initial and irradiated samples were conducted by means of the Van-der-Pauw and capacitance–voltage techniques. Under the same irradiation conditions the charge carrier removal rates in n-Si and n-SiC differ by a factor of about ten. The averaged removal rates of charge carriers in both 4H- and 6H-n-SiC do not exceed 0.015 cm^{-1}. The dose dependence of the effective space charge concentrations $N_{eff}= N_d - N_a$ in irradiated n-SiC at room temperature is shown in Fig. 7-2. This concentration in irradiated SiC starts to fall at a dose above 10^{17} cm^{-2}.

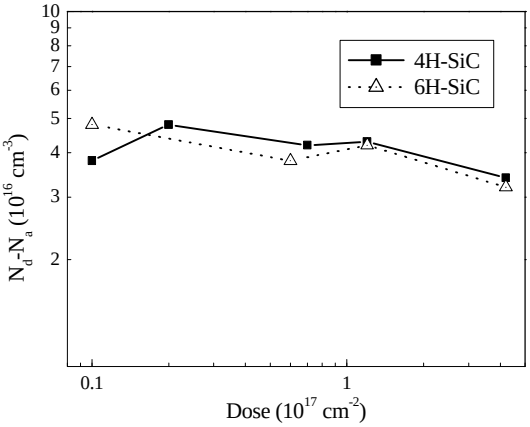

Fig. 7-2: N_{eff} dose dependence in n-type 4H-SiC irradiated by fast electrons with the energy of 900 keV.

7.1.3.2 Ioffe with AMDS AB Sweden and CREE <USA) [6-9]

Cr Schottky barriers were irradiated by 1 MeV neutrons, 245 MeV Kr^+ and 710 MeV Bi^+ up to fluences (1.2-6.2)$x10^{14}$ cm^{-2}, (1-5)$x10^{10}$ cm^{-2} and (0.1-5)$x10^{10}$ cm^{-2}, respectively and studied by photoluminescence (PL) capacitance-voltage and current-voltage characteristics and DLTS. The neutrons and high energy ions introduced very similar defect centers in 4*H*-SiC. N_{eff} decreased with increasing fluences, mass and energy for different kind of irradiations. Maximum fluences resulted in capacitance values independent of reverse bias. These "saturated" capacitance values correspond to an "effective" dielectric layers of 20-30 μm thick, which were comparable with the thickness of the CVD epitaxial layer. Cr Schottky barriers were also irradiated by 4.8-7.7 MeV α-particles using radioactive isotopes ^{226}Ra, ^{239}Pu, ^{240}Pu, ^{241}Am and ^{238}Pu. Amplitude spectra was analysed for total channels number of 4000. The lines of ^{226}Ra decay and high precision Si detector (worked out in the

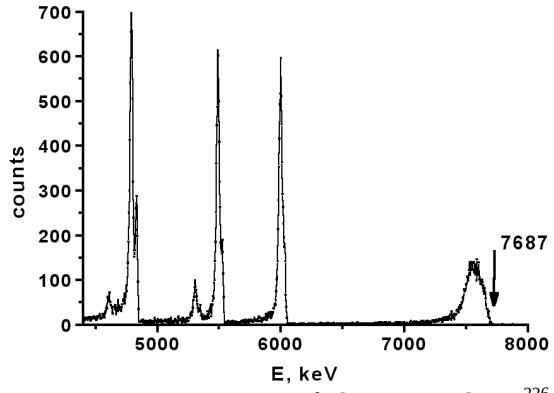

Fig. 7-3 Energy spectrum of the α-particles ^{226}Ra measured under U_{rev} = 400 V.

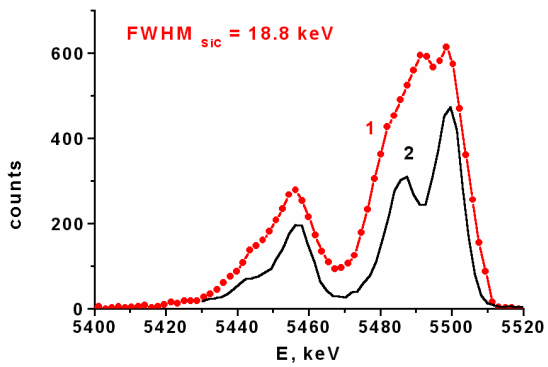

Fig. 7-4 Energy spectrum of the α - particles ^{241}Am + ^{238}Pu for 4*H* - SiC (1) and high-precision Si (2) detectors.

Ioffe institute) were used to calibrate the channel value. Charge collection efficiency (CCE), energy resolution (FWHM), value for the average electron - hole pair creation energy (ε_{SiC}) and character of the noise in the 4H-SiC detectors were determined. The energy spectrum of the α-particles presented in Fig. 7-3 allowed to estimate of the maximum energy of α-particles which could be detected by Schottky barrier diode structures. This value was closed to 7.7 MeV for V_{rev} = 400 V, when the width of the space-charge region in diode structures and the α-particles ranges were equal to 27 μm and 31 μm, respectively for two different CVD layers. An energy resolution of 0.35 % was achieved for 4H-SiC based detectors for the first time, which allowed to reveal visually the fine structure peaks of α-particles spectrum with lines separated by about 20 keV (Fig. 7-4).
Close to 100% charge collection efficiency at 150 V for CVD layers with N_d-N_a=1×10^{15} cm^{-3} was measured. The high quality of detector reflects a relatively high value of the minority carrier diffusion length (10-12μm), a small reverse currents (less than 1 nA up to 500 V). As a consequence the noise of the dark or photo-current was "shot" without any surplus noise up to 500V. Average electron-hole pair creation energy in 4H - SiC was determined to be 7.7eV. The spectrometry properties of 4*H*-SiC based detector was thus revealed to be commensurable with precision Si-detectors for the first time.

7.1.3.3 Universities of Modena and Florence [10,11]

Schottky diodes with epilayer thickness 20μm and effective doping 5.3×10^{14} cm^{-3} was studied in past by RD50 and proved to have 100% CCE (1100e) at 400 V (1100 e-) [10]. This year it has been irradiated with 24GeV/c protons up to 1.4 ×10^{16} /cm^2 at PS (CERN). After irradiation the capacitance was independent of the applied voltage, reaching the geometric value of the order of 10pF for test signal frequencies in the range 100kHz-1MHz. The charge collection efficiency was studied at room temperature with mips from a ^{90}Sr source and a low noise electronic read-out with 2μs shaping time, series noise of 280e+10e/pF. A charge collection efficiency of the order of 30% was found at 800V, the collected charge is very close to electronic noise values. Various samples with thickness 40-50μm have been irradiated with neutrons up to 7×10^{15}/cm^2 in Ljubljana: the charge collection efficiency was studied with α-particles at room temperatures before and after irradiation at the University of Modena. Results are shown in Fig. 6. If up to 1x10^{14}n/cm^2 a 90% charge collection was measured, at 7x10^{15} n/cm^2 only a 20% was attained (at 700V) [11]. These results, showing a limited radiation hardness of epitaxial 4H-SiC to fast hadrons, must be confirmed by a more systematic work on the same material, which is presently under way.

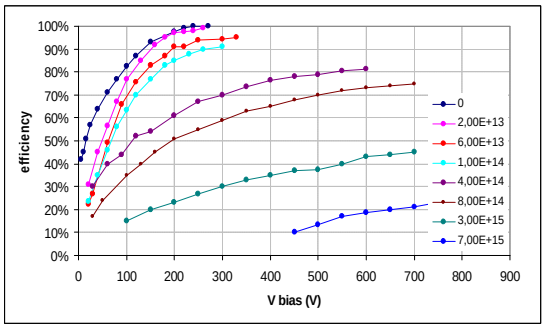

Fig. 7-5 Charge collection measured with α particles at University of Modena on neutron irradiated samples

7.1.4 Detection properties and radiation hardness of SiC p$^+$n junction diodes

7.1.4.1 Ioffe with AMDS AB Sweden and CREE USA [6-7,12]

p $^+$-*n*-*n*$^+$ ion implanted diode structures were irradiated by 1 MeV neutrons, 245 MeV Kr$^+$ and 710 MeV Bi$^+$ respectively up to the fluences (1.2-6.2)x10^{14} cm^{-2}, (1-5)x10^{10} cm^{-2} and (0.1-5)x10^{10} cm^{-2}, respectively. Irradiation with neutrons and Bi$^+$ ions resulted in elimination of the diode structures rectifying properties. Devices degraded after irradiation with fast neutrons and high-energy Kr and Bi ions recovered their properties if they were measured at high temperatures (up to 500^{o}C) (Fig. 7-6). The temperature dependences of the resistance of 4*H*-SiC CVD epitaxial layers irradiated with different particles and fluences are shown in Fig. 7-7. Activation energy 0.5 eV after neutrons and Bi$^+$ ions irradiation, a more complex behavior is observed for the Kr$^+$ irradiation. Differences are supposed to be mainly due to the formation of vacancy clusters, which size, concentration, and temperature stability depend on irradiation kind and fluence of irradiation, as well as on the purity of

the initial material. Also, the behavior of SiC diode structures with shallow ion implanted p^+-n-n^+ junctions was studied under 22ns ionization pulse X-ray radiation in the dose-rate range up to $3x10^{10}$ rd(SiC)/s. A linear dependence of the ionizing current vs dose-rate was observed, with a diode recovery time of about 25ns. Transient radiation response demonstrated sufficient benefit as compared to Si devices, even if the reduction of ionizing current was in the range from 5-7 times under the same dose rate, related to a lower carrier generation and excess carriers lifetime in SiC as compared with Si.

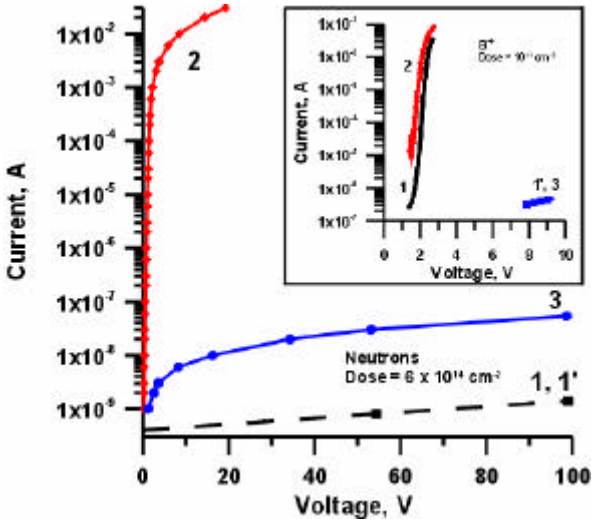

Fig. 7-6 : Forward (1, 2) and reverse (1', 3) I-V characteristics of the SiC p^+-n-n^+ structure irradiated with neutrons and Bi+ ions (inset) .Curve 1,1' - measurement at room temperature; Curves 2, 3 - measurements at 650 K or 428K (inset).

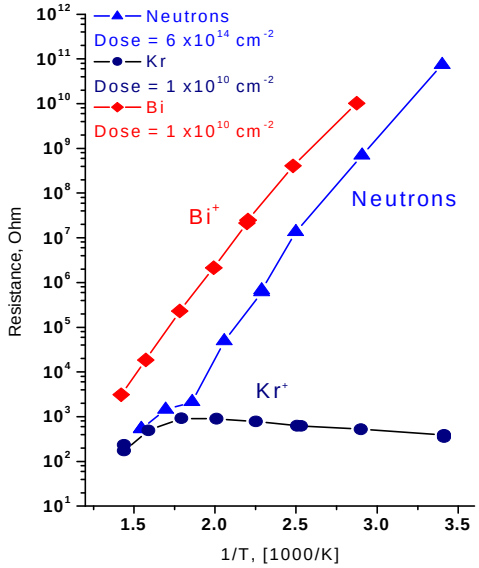

Fig. 7-7: Temperature dependence of the resistance of 4H-SiC CVD epitaxial layers irradiated with different particles.

7.1.4.2 Perugia University [12-15]

Here are presented the studies carried out on p^+n diodes produced in collaboration with INSA-Cegely (Lyon, France) and CNR-IMM (Bologna, Italy). The room temperature C-V profile is shown in Fig. 7-8. I-V measurements have also been performed. The ideality factor calculated at low voltages is between 2.0-2.2 and then decreases at 1.5-1.6, but it never reaches 1 before the series resistance dominates the forward characteristic. The breakdown voltage of these diodes varied with the measurement ambient (up to 1.3kV in air and up to 4.8kV in Galden or SF6 for the diodes featuring an emitter diameter of 0.3mm). For the diodes featuring 1mm emitter diameter, analyzed in the present study, the breakdown voltage in air is in the range 700-900V. The full depletion voltage is close to 1600V. It should be underlined that the CCE and DLTS measurements could only be performed on large area diodes, which unfortunately feature the worst breakdown voltages.

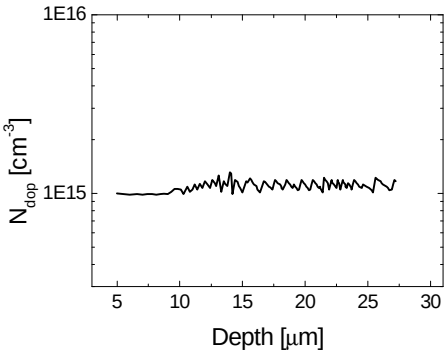

Fig. 7-8 Doping profile extracted with C-V measurements on p^+/n junctions

The charge collection efficiency to minimum ionizing particles has been investigated by a ^{90}Sr β source. The measurements have been carried out in collaboration with the University of Florence. The series noise of the instruments is linearly proportional to the capacitance. The pulse height spectrum giving the charge response yielded by the SiC detectors when exposed to ^{90}Sr β source was measured as a function of the reverse voltage in the range 0-880V. The distribution signal mean value

and the electronic noise contribution to this signal were evaluated independently. At each bias point the signal was stable and reproducible, showing the absence of polarization effects. At 880 V the collected charge was 1720 e^-. Assuming that the source produced 55 e-h pairs/μm and no recombination took place, the collection length is: $L = \frac{\langle Q \rangle_{collected}}{55\ e/\mu m}$. Fig. 9 shows the comparison between the collection length and the calculated depleted region length. As these two lengths are very similar we can consider that the CCE for these SiC diodes is 100%, in spite of the fact the signal given by the Landau distribution convoluted with the electronic gaussian noise merges with the pedestal signal due to the gaussian noise itself. A SiC epitaxial layer with lower doping and higher thickness would have made possible the separation between these signals and would have confirmed that the fabrication of particle detector in silicon carbide can be done also using p^+-n junction diodes. Such a demonstration has recently been published for SiC Schottky diodes. Simulations have been carried out using the ISE-TCAD DESSIS device simulator. In fact DESSIS makes available both a 6H-SiC model and a Heavy Ion Crossing stimulus. Moreover, with DESSIS we can introduce deep levels related to defects. Radiation damage introduces many defects, which reduce the CCE. Introducing these defects in DESSIS simulations, we are able to analyze which defects are important to decrease the CCE. The simulation tool solves the fundamental semiconductor equations in a spatial and time discretization. The first simulated structure is a Schottky diode manufactured on a typical low resistivity n-type substrate (with donor concentration of the order of 10^{18} atoms/cm^3) and a 38 μm thick *n* epilayer featuring sensibly lower donor concentration ($N_D = 4\times10^{13}$ cm^{-3}). We consider a 100μm thick two-dimensional test structure comprising a 50μm wide single diode. The second simulated structure is a 50μm wide p^+n diode featuring the same substrate and epilayer concentration and epilayer thickness. In this case the p^+ doping concentration is $N_A = 4\times10^{19}$ cm^{-3} and we consider a 300μm thick two-dimensional test structure. The parameters in the DESSIS Heavy Ion crossing model have been varied in order to obtain a generation of 55 e/h pairs per micron. Using this simulation model, it was possible to reproduce the experimental CCE as a function of the applied voltage for the p+/n junction and the Schottky diodes as it is illustrated in Fig. 7-9 and Fig. 7-10, respectively. This is an important result because using this model the design of radiation particle detectors can be optimized in a fast and inexpensive way. Moreover introducing in DESSIS simulation the deep levels related to defects, produced by radiation damage, we will be able to analyze which defects are important when the CCE is decreased.

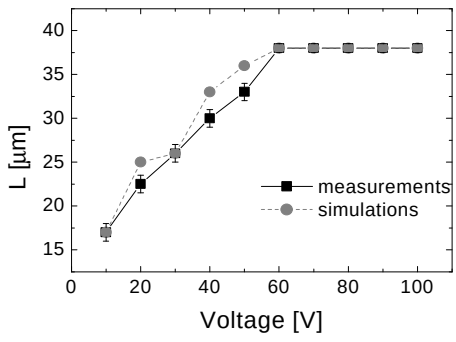

Fig. 7-9. Comparison among the collection length, the calculated depleted region length and simulated collection length as a function of the reverse voltage measured with a ^{90}Sr source on p^+/n junctions.

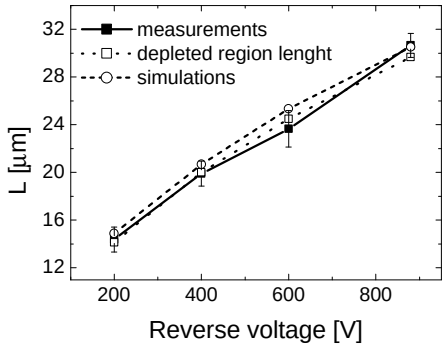

Fig. 7-10. Comparison between the ISE-TCAD simulated and the experimental collection length for the Schottky diode reported in Ref.[13]

5.2. Semi-Insulating SiC

The performance of irradiated planar detector diodes made from 100μm-thick semi-insulating SiC was studied by Glasgow and Vilniusm, continuing an activity astarted in 2003. Ohmic/Schottky diodes were produced and characterised using Schottky barrier measurements and charge collection efficiency (CCE) measurements were made for 5:48 MeV 241Am alpha particles. A 60% CCE was measured before irradiation, due to the presence of deep traps limiting the carrier lifetime. Irradiation

took place at Paul Scherrer Institute (PSI) to fluences of 10^{12}; 10^{13}; and $5x10^{14}$ cm^{-2}; with 300 MeV/c π, the charge collection was found in the same order of the one measured before irradiation [17-19]. Incomplete collection should be due to the presence of vanadium. Semi-insulating material without vanadium is still under study by the Glasgow group.

References

[1] N.B.Strokan, A.M.Ivanov, N.S.Savkina, A.A.Lebedev, V.V.Kozlovskii, M.Syvajarvi, R.Yakimova. Semiconductors, 38, 807-811 (2004).

[2] A.A. Lebedev, A.M. Ivanov, N.B. Strokan. Semiconductors, 38, 125-147 (2004).

[3] N.B. Strokan, A.M. Ivanov, A.A. Lebedev. "SiC Nuclear-Radiation Detectors" in "SiC Power Materials" Zhe Chuan Feng (Ed.), p. 411-445, Springer 2004.

[4] A.A. Lebedev, A.M. Ivanov, V.V. Kozlovski, D.S. Rumiannntsev, M.Syväjärvi, R.Yakimova. Accepted for publication for Proceedings ECSCRM-2004, August 31 – September 04, 2004 Bologna, Italy.

[5] V.V. Kozlovski, E.V. Bogdanova, V.V. Emtsev, K.V. Emtsev, A.A. Lebedev, V.N. Lomasov. Accepted for publication for Proceedings ECSCRM-2004, August 31 – September 04, 2004 Bologna, Italy.

[6] E.V. Kalinina, G.F. Kholujanov, G.A. Onushkin, D.V. Davydov, A.M. Strel'chuk, A. Hallén, A.O. Konstantinov, A.Yu. Nikiforov, V.A. Skuratov, and K. Havancsak. Semiconductors, Vol. 38 (10), 1 (2004).

[7] E. Kalinina, G. Kholuyanov, G. Onushkin, D. Davydov, A. Strel'chuk, A. Konstantinov, A. Hallén, V. Skuratov, A. Kuznetsov. Accepted for Proceedings ECSCRM 2004, 31 August-04 September, 2004, Bologna, Italy.

[8] A. Ivanov, E. Kalinina, G. Kholuyanov, G. Onushkin, N. Strokan, A. Konstantinov, A. Hallén. Technical Physics Letters 30 (14), 1 (2004).

[9] A. Ivanov, E. Kalinina, G. Kholuyanov, G. Onushkin N. Strokan, A. Konstantinov, A. Hallen, A. Kuznetsov. Accepted for publication in Proceedings ECSCRM-2004, August 31–September04, 2004, Bologna, Italy.

[10] M. Bruzzi et al., Diamond Relat. Mater. 12 (2003) 1205–1208

[11] S. Sciortino et al., presented at the Int. Conf. on Radiation Effects on Semiconductor Materials, detectors and Devices, Oct. 10-13, 2004, Florence, Italy.

[12] A.Y. Nikiforov, P.K. Skorobogatov, D.V. Boychenko, V.S. Figurov, V.V. Luchinin, E.V. Kalinina. Proceedings RADECS 2003, Noordwijk, The Netherlands, 15-19 September 2003, (2004).

[13] C. Raynaud et al., Mater. Scien. Forum (2003) Vol. 457-460: 1033-1036

[14] Bertuccio et al., IEEE Trans. Nucl. Sci., vol. 50, pp.175-185, 2003

[15] F. Nava, et al., IEEE Transactions on Nuclear Science, Vol. 51, No. 1 (February, 2004).

[16] F. Nava et. al., Nuclear Instruments and Methods in Physics Research A, 510 (2003) 273-280

[17] W. Cunningham, J. Melone, M. Horn, V. Kažukauskas, P. Roy, F. Doherty, M. Glaser, J. Vaitkus, M. Rahman Performance of irradiated bulk SiC detectors Nucl Instr. Meth A 2003, 509, p. 127-131.

[18] Cunningham W, Cooke M, Melone J, Horn M, Kazukauskas V, Roy P, Doherty F, Glaser M, Vaitkus J, Rahman M. Bulk SiC devices for high radiation environments. SILICON CARBIDE AND RELATED MATERIALS 2003, PRTS 1 AND 2. Editors: Madar R, Camassel J. MATERIALS SCIENCE FORUM, 457-460, Part 1&2 (2004) pp.1093-1096.

[19] Quinn T, Bates R, Bruzzi M, Cunningham W, Mathieson K, Moll M, Nelson T, Nilsson HE, Pintillie I, Reynolds L, Sciortino S, Sellin P, Strachan H, Svensson BG, Vaitkus J, Rahman M. Comparison of bulk and epitaxial 4H-SiC detectors for radiation hard particle tracking. 2003 IEEE NUCLEAR SCIENCE SYMPOSIUM, CONFERENCE RECORD, VOLS 1-5, Editors: Metzler SD., (2004) pp.1028-1033.

7.2 Research activity on gallium nitride

This research is carried out mainly by Glasgow, Surrey and Vilnius groups. The irradiation facilities of Ljubljana and Imperial College were also involved The material (epitaxial and GaN bulk crystals) was supplied by Tokushima University&Nitride Ltd. (Japan) and Lumilog, Ltd. (France). Samples presently available to RD50 are: one 2" wafer 12μm thick (Lumilog); 3 wafers 2μm thick (Tokushima University & Nitride Ltd.). According to preliminary agreements with Lumilog, Ltd. one 50μm-thick epilayer wafer (substrate: sapphire) and one 50μm-thick semi-insulating GaN epilayer grown on a highly conductive substrate should be available in near future. Pad detectors were fabricated at Glasgow university, wafers have been characterized by optical and microwave spectroscopy before detector fabrication and irradiation. Measurements of I-V and CCE with α-particles are described below before and after irradiation.

7.2.1 Radiation hardness of already existing epitaxial GaN films

Material is semi-insulating GaN, grown using Metal Organic Chemical Vapour Deposition (MOVCD) techniques onto an Al_2O_3 (0001) substrate by Tokushima University. The material was 2.5 microns thick, (ρ ~$10^8\Omega$cm), grown on a buffer layer of 2 microns n^+ GaN. Au Schottky pad contacts were produced by the manufacturers. Due to the thickness of the epilayer, the contact potential was able to deplete the diode fully at 0V bias. As-grown GaN showed a constant leakage current of ~2pA up to 15V. A maximum CCE of 97%, measured with α-particles, was obtained at 15V. The CCE increased linearly with the applied bias. Neutron irradiation was performed at the TRIGA reactor at the Jozef-Stefan Institute in Ljubljana, Slovenia. Diodes were irradiated with fluences of $5x10^{14}$, $1x10^{15}$ and $1x10^{16}$ n/cm^2. The neutron irradiated samples showed a decrease in CCE with fluence (Fig. 7-11), while the leakage current showed a non-linear increase with fluence. One possible explanation accounts for the introduction of deep level acceptor states in the material. Leakage current after irradiation up to the highest fluence not exceeded 50pA in this voltage range. One GaN diode was also irradiated up to $1x10^{16}$ cm-^{2} 24GeV/c protons at CERN. Leakage current up to 20pA was measured at 15V, CCE is shown in Fig. 7-12. X-ray irradiation was performed at the Imperial College Reactor Centre. A GaN diode was irradiated with 6 MGy of 10keV X-rays. A large increase in leakage current was observed after irradiation, while an almost 100% CCE was reached at 30V (Fig. 7-13 and Fig. 7-14). This combination of effects may be attributed to surface damage, which would contribute significantly to the leakage current but have no effect on the space charge region, and hence CCE values. A summary of the properties of irradiated GaN 2µm-thick epilayers as obtained from measurements in the frame of RD50 is given in Table 7-1.

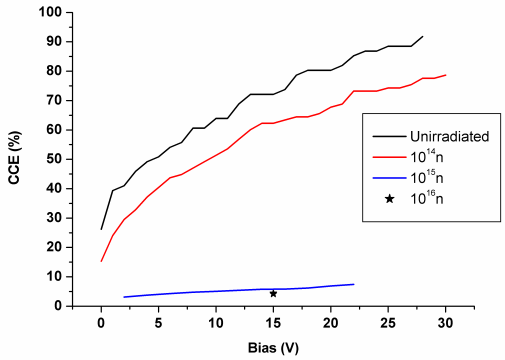

Fig. 7-11. CCE for neutron irradiated (Ljubljana) thin GaN.

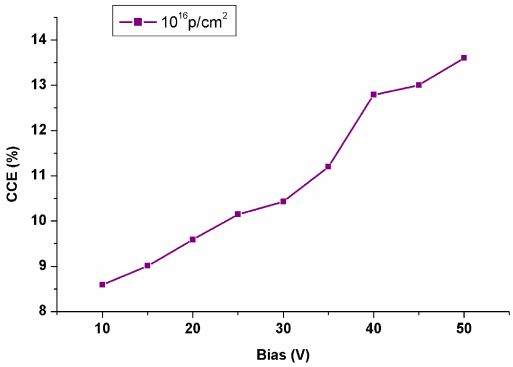

Fig. 7-12. CCE for proton irradiated (CERN) thin GaN

Sample irradiation /fluence	CCE,% /@ bias, V	I_{10V}, nA cm^{-2} /character	t_{fast}, µs
Non-irradiated	95 / 30	0.06 /barrier	0.1-0.5
X-rays (10 KeV) / 600 MRad	100 / 26	5.50 /barrier	0.08
Neutrons / 5 10^{14} cm^{-2},	77 / 28	0.35 /resist.	0.015
(reactor, 100 KeV) 10^{15} cm-^{2},	10 / 30	0.65 /barrier	0.02
10^{16} cm-^{2}.	5 / 16	0.23 /resist.	<0.01
Protons, 24 GeV/ 10^{16} cm^{-2}.	13.6 / 30	0.40 /barrier	0.034

Table 7-1. Summary of properties of GaN 2µm-thick epilayers before and after irradiation.

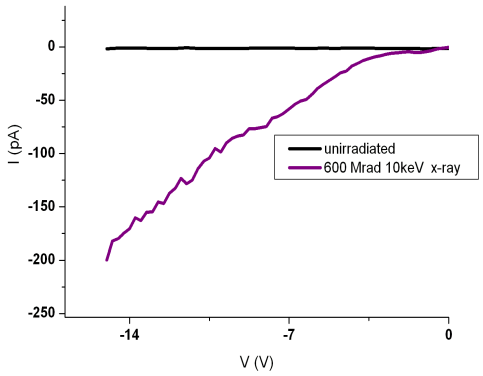

Fig. 7-13. I-V_{rev} for X-rays irradiated thin GaN

.

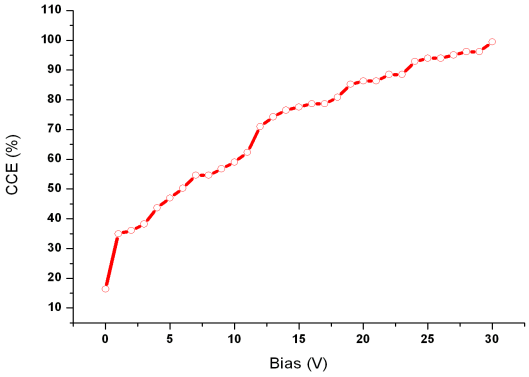

Fig. 7-14. CCE for X-rays irradiated thin GaN

7.2.2 Preliminary characterization of new GaN epitaxial layers

Fig. 7-15. Pd/Au Schottky contacts on GaN

Materials recently produced are: one GaN epitaxial layer grown at Lumilog, Ltd., one new thin GaN epi-material grown by Tokushima, one bulk (350µm-thick) sample. Standard photo-lithographic techniques were used for fabrication of samples. Before applying metals, samples were cleaned in 1:1 HCl:H_20, for removal of oxide layer on the surface of the material. Contacts were manufactured via evaporation of Pd(80nm)/Au (200nm) Schottky contacts. Contacts (Fig. 7-15) were in the shape of pad/guard ring structures, (0.75mm diameter pad, with 0.5 mm guard ring, separated by 50 micron gap) and diced into pairs using a diamond saw. The maximum CCE values for the Toshikima samples were between 85-95% (Fig. 7-16). These values are in line with the previous CCE measurement using Toshikima samples shown above. The 12µm GaN film produced by Lumilog has a maximum CCE of 50% (Fig. 7-17), the reasons of this incomplete charge collection is still a matter of study. Results from P. Sellin et al. presented in the previous status report of RD50 (2003) , showed by IBIC measurements that charge generated from incident MeV α's could only be collected from directly below the contact areas. Therefore, it is possible that the measured CCE is geometrically limited and a more optimised diode design could enhance the measured CCE of the device.

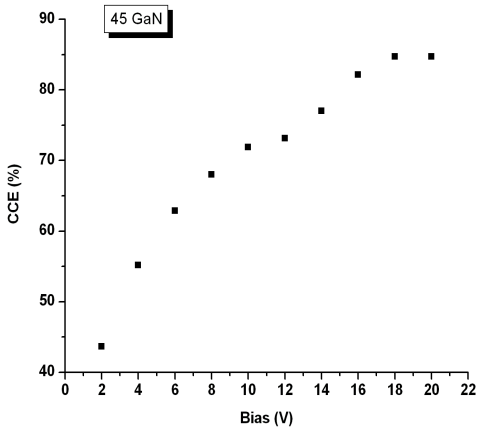

Fig. 7-16. Fig. 16 CCE measure 12µm GaN films

.

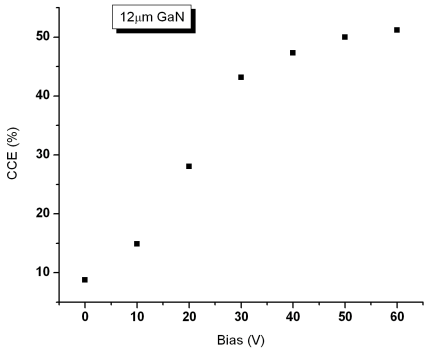

Fig. 7-17. Fig. 17 CCE measured with α-particles with a 12µm GaN film

Bulk GaN has so far been difficult to fabricate. Pipes which run through the material – and can be attributed to dislocations caused by the twisting of the hexagonally shaped growth columns - reduce the area of the surface available for Schottky contacts. In addition, the material has been found to be extremely brittle, probably due to the tensile and compressive strains resulting from the high density

of dislocations. This material thus often splitted during successive stages of the fabrication process. However, a device was successfully fabricated (including a back contact as well) and yielded the I-V characteristics shown in Fig. 7-18.

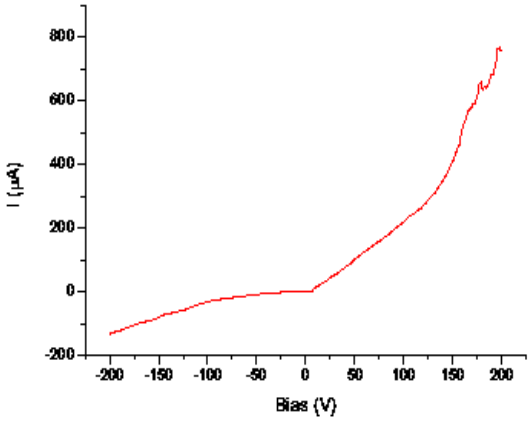

Fig. 7-18. I-V characteristic for unirradiated Bulk GaN

References

1. Vaitkus J, Gaubas E, Kazukauskas V, Lacroix Y, Sakai S, Smith K, Storasta J, Wang T. Space charge effects and carrier capture transient behaviour in semi-insulating GaAs and GaN Proc. 12TH INTERNATIONAL CONFERENCE ON SEMICONDUCTING & INSULATING MATERIALS. Editors: Breza J, Dubecky F, ZatKo B. pp.185-189, 2002
2. R. Aleksiejunas, M. Sudžius T. Malinauskas, J. Vaitkus, K. Jarašiunas, S. Sakai. Determination of free carrier bipolar diffusion coefficient and surface recombination velocity of undoped GaN Applied physics letters, 2003, vol. 83, no. 6, p. 1157-1159
3. J. V. Vaitkus, E. Gaubas, S. Sakai, Y. Lacroix, T. Wang, K. M. Smith, M. Rahman, W. Cunningham Role of potential barriers in epitaxial layers of semi-insulating GaN layers. Solid state phenomena. 2003, vol. 93, p. 301-306
4. J. Vaitkus, W. Cunningham, E. Gaubas, M. Rahman, S. Sakai, K.M. Smith, T. Wang. Semi-insulating GaN and its evaluation for alpha particle detection / Nuclear instruments & methods in physics research. Section A - Accelerators, spectrometers, detectors and associated equipment. 2003, vol. 509, no. 1-3, p. 60-64.
5. J. Vaitkus, E. Gaubas, T. Shirahama, S. Sakai, T. Wang, K. M. Smith and W. Cunningham. Space charge effects, carrier capture transient behaviour and particle detection in semi-insulating GaN. Nuclear Instruments and Methods in Physics Research Section A: Accelerators, Spectrometers, Detectors and Associated Equipment, Volume 514, Issues 1-3 , 2003, Pages 141-145
6. Rahman M, Bates R, Blue A, Cunningham W, Gaubas E, Gouldwell A, Horn M, Kazukauskas V, Parkes C, Quinn T, Roy P, O'Shea V, Smith KM, Vaitkus J, Wright V Super-radiation hard particle tracking at the CERN SLHC. IEEE TRANSACTIONS ON NUCLEAR SCIENCE50 (6): 1797-1804 Part 1 DEC 2003.
7. J.V.Vaitkus, W.Cunningham, M.Rahman, K.M.Smith, S.Sakai. Semi-insulating GaN and its first tests for radiation hardness as ionizing radiation detector / in UV Solid-State Light Emitters and Detectors, ed. by M.S. Shur and A. Zukauskas (Kluwer Academic Publishers, Dordrecht, 2004), pp. 279-286.
8. Gaubas E, Kazlauskas K, Tomasiunas R, Vaitkus J, Zukauskas A Radiation-defect-dependent photoconductivity transients and photoluminescence in semi-insulating GaN, APPLIED PHYSICS LETTERS 84 (25): 5258-5260 (2004)
9. P.J. Sellin, D. Hoxley, A. Lohstroh, A. Simon, W. Cunningham, M. Rahman, J. Vaitkus, E. Gaubas. Ion beam induced charge imaging of epitaxial GaN detectors. Nuclear Instruments and Methods in Physics Research A 531 (2004) 82–86.
10. E. Gaubas, S. Juršenas, S. Miasojedovas, J. Vaitkus, and A. Žukauskas Carrier and defect dynamics in photoexcited semi-insulating epitaxial GaN layers. J. Appl. Phys., 96, No. 8 (2004), pp.4326-4333.
11. J.Vaikus, W.Cunningham, K.Smith, E.Gaubas. "New radiation hard semiconductor - semi-insulating GaN: the photoelectric properties" Proc. 27th International Conference on the Physics of Semiconductors. To be published in AIP. (Paper number 10835)

7.2.3 Radiation hardness of already existing epitaxial GaN films

PC, MWA, PL and TSC measurements are currently being carried out on all materials. This will allow full comparison of the 4 types of material pre and post irradiation with varying fluence of neutrons and protons.Room temperature photoluminescence (PL) measurements were carried out under excitation by a continuous wave (cw) He-Cd laser operating at 325 nm wavelength and by a pulsed yttrium-aluminum-garnet (YAG:Nd^{3+}) laser (266-nm wavelength). The PL signal was dispersed by a double monochromator and detected using an UV-enhanced photomultiplier. Also, time resolved photoluminescence (TRPL) measurements were performed to display initial carrier decay processes [1]. Investigations of the long-time scale carrier decays were performed using non-invasive microwave absorption (MWA) technique and contact photoconductivity (CPC). The MWA method is based on pump-probe technique with optical excitation and microwave absorption by the free-carriers [2]. The CPC technique relies on measuring photocurrent decays. Pulsed excitation of the excess carriers was performed by a focused beam of the 3rd harmonic (355 nm) of YAG:Nd^{3+} lasers with either 10-ns or 30-ps pulses. In the MWA and CPC experiments, the excess-carrier density decays were examined over a wide time scale ranging from 1 ns to 400 ms. The measured PL spectra in n-type highly resistive GaN consist of three bands [1,3], as it also was observed in [4]. An ultraviolet (UV) band peaked at 3.42 eV is attributed to band-to-band recombination. The UV band is accompanied by a blue (B) band peaked at about 2.85 eV and a yellow one (Y) peaked at 2.18 eV. The latter two B and Y bands probably represent deep center related luminescence. The structure of the PL spectrum featuring a B band is inherent for GaN containing a high density of dislocations [4]. The Y band, probably, can be ascribed to point defects, e.g. complexes of Ga vacancy [1-5]. Concentration of the centers ascribed to the Y-band was evaluated [1,5] to be < 10^{15} cm^{-3} in the 2.5 μm thick MOCVD grown samples, characterized by PL spectrum 1 in Fig. 7-19. The density of B-band attributed centers was estimated to be of the order of 10^{18} cm^{-3} [1,5]. Y- and B- centers concentrations in the 12 μm-thick MOCVD and in the HVPE free-standing samples are lower than those in 2.5 μm thick MOCVD grown layers. However, in the HVPE grown free-standing samples, additional defects appeared to be PL active.

The PL spectra obtained in MOCVD as-grown highly resistive GaN 2.5 μm thick layers, after irradiation by x-rays and neutrons with fluence of 5×10^{14} cm^{-2}, exhibited a decrease in intensity for all bands. This can be attributed to a transform of deep centre distribution and type. It is known that X-rays introduce point defects while neutrons induce point defects and clusters. Thus, decreasing band-to-band luminescence intensity can be explained by carrier density reduction due to fast non-radiative recombination through radiation defects. In samples heavily irradiated by neutrons and protons (up to 10^{16} cm^{-2}), the intra-crystallite bulk recombination is estimated to be very fast due to the high density of radiation defects, while trapping process is weakened (in the proton irradiated sample) or suppressed (for neutron irradiation). Summarising, different concentrations of shallow and deep donor-acceptor pairs manifest in MOCVD and HVPE grown highly resistive GaN layers. Irradiation of the semi-insulating GaN epitaxial layers by X-rays of 600 Mrad and neutrons of fluences 5×10^{14} and 10^{16} cm^{-2} , and of protons of fluence 10^{16} cm^{-2} induces an increase of the non-radiative trap density within crystallites and at their boundaries, which results in quenching all three PL bands (UV, B and Y).

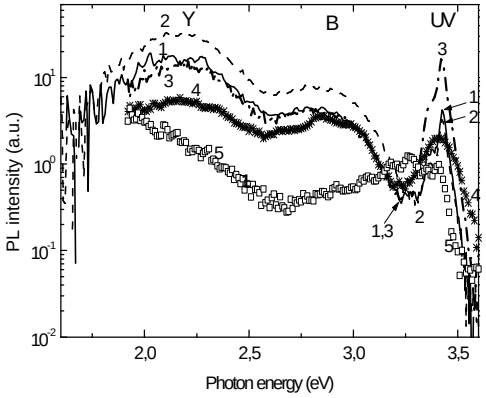

Fig. 7-19. Fig. 1. PL spectra under cw excitation of the same intensity in the intrinsic n-type MOCVD and HVPE (4) grown GaN layers of 2.5 μm thickness (1, 2), and of 12 μm thickness (3) compared with the Mg doped p-type GaN (5).

References

1. E.Gaubas, S. Juršenas, S.Miasojedovas, J.Vaitkus, and A.Žukauskas, *J. Appl. Phys*. **96** (2004) 4326.
2. E. Gaubas, *Lith. J. Phys.* **43** (2003) 145.
3. E.Gaubas, K.Kazlauskas, R.Tomašiunas, J.Vaitkus, and A.Žukauskas, *Appl. Phys. Lett.* **84**, (2004) 5258.
4. M. Albrecht, H. P. Strunk, J. L. Weyher, I. Grzegory, S. Porowski and T. Wosinski, *J. Appl. Phys*. **92** (2002) 2000.
5. C.G.Van der Walle, and J.Neugebauer, *J. Appl. Phys*. **95** (2004) 3851.

7.3 Radiation studies with a-Si(H)

In the RD50 proposal it was paid attention to amorphous Si as a potentially radiation hard material. Recently, 10-50μm-thick a-SiC(H) samples have been made available to RD50 (from Neuchatel group: [H] 8%). Samples (13μm thick) have been tested by Glasgow and Vilnius groups before and after 10^{15}cm^{-2} to 10^{16}cm^{-2} neutron fluence irradiation in Ljubljana. After irradiation 10^{15}cm^{-2} the α-particle charge collection efficiency decreased to few percents of the vakue before irradiation. No charge collection was observed in the sample irradiated to 10^{16} cm^{-2}. A 13μm thick a-Si:H p-i-n sandwich-type structure deposited on the glass substrate was investigated. Resistivity before irradiation was higher than 10^{10} Ωcm and mt for electrons was estimated of the order of $1.3\cdot10^{-7}$cm^2/V. After irradiation to 10^{15}cm^{-2} the bulk resistivity decreased to $1.2\cdot10^{9}$ Ωcm while mt reduced to $1.7\cdot10^{-8}$ cm^2/V. These preliminary results seem to indicate a low radiation hardness for a-Si(8%H) in view of a possible application for super-LHC.

8 Full Detector Systems (FDS)

The FDS research line of RD50 aims to test the properties of segmented detectors after heavy irradiation. The final goal is to test quantities like signal over noise (S/N) ratio and occupancy versus purity with simple but realistic systems (one detector coupled to one LHC-speed ASIC) in order to give indications on the performances of the devices after heavy irradiations. The activity of the FDS research line is here presented divided by sub-groups: miniature microstrip detectors (mini-strips), pixel detectors, electronics (newly created group).

8.1 Status of the investigation of p-type substrates

The benefits of reading out silicon detectors from the segmented n-side are now well understood and widely accepted [1, 2]. A large improvement in the charge collection efficiency at lower voltages has been demonstrated. The improvement is due to the relatively fast collection of electrons (more mobile than holes) obtained by keeping the read-out segmented electrode on the side of the high electric field after irradiation.

This solution is now already used for the silicon detectors closer to the interaction point in the LHC experiments (LHCb VELO, ATLAS and CMS pixels). All these devices use n-side read-out on standard n-type substrates (n^+-in-n diode structure).

However, this solution requires photolithographic processing of both sides of the wafer, resulting in roughly 50% greater expense than single-sided processing. Another inconvenience of n^+-in-n devices is the necessity to operate over-biased prior to the radiation induced inversion of the bulk to p-type, after which the junction becomes located on the n-side of the detector. Both issues are avoided by using an initially p-type substrate. The feasibility of this approach has been successfully demonstrated using large area devices irradiated to the level expected for the LHC tracker (e.g. ATLAS SCT) [3].

It is also well accepted that the degradation of the electrical properties of n-type silicon after charged hadron irradiation is reduced by the introduction of interstitial oxygen in the silicon crystal by high temperature diffusion from a SiO_2 surface layer. A similar improvement might be expected with p-type substrates. To investigate the effects of high temperature diffusion in the case of p-type substrates, we used this technique to enhance the oxygen content of p-type FZ wafers with initial resistivity of about 2.5-3 kΩ cm.

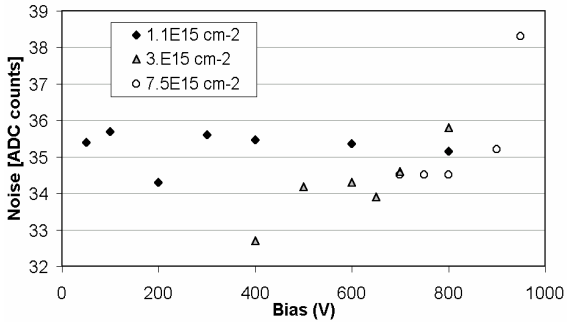

Fig. 8-1 Noise as a function of the applied voltage for the three different irradiation doses. The pre-irradiation value is about 35 ADC counts, similar to the value found after irradiation [4].

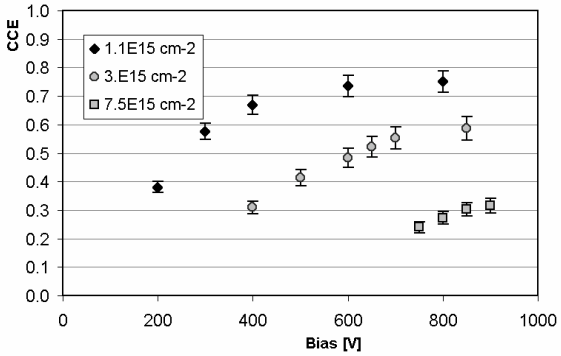

Fig. 8-2 Charge collection efficiency vs applied bias voltage, normalised to the pre-irradiation value, of n-in-p detectors after 1.1, 3 and 7.5 10^{15} p cm^{-2}. The detector irradiated to 3. 10^{15} cm^{-2} is standard p-type substrate, while the other devices are oxygen-enriched [4].

Standard p-type substrates (identical substrates that were not diffused at high temperature) were used in order to compare the results. Oxygen enriched and standard wafers were than used to produce large area

(6x6 cm^2) and a few miniature (1x1 cm^2) n-in-p capacitively coupled, polysilicon biased microstrip detectors, with strip pitch of 80µm. These devices have been produced by CNM-Barcelona using a mask-set designed by the University of Liverpool. The initial full depletion voltage (V_{fd}) was about 350 V. Some oxygen enriched and standard miniature devices have been studied in terms of CCE(V) after very high proton irradiation [4].

A few oxygenated and standard detectors have been irradiated to 1.1, 3 and 7.5 10^{15}p·cm^{-2} in the CERN-PS IRRAD facility at room temperature and unbiased. The detector irradiated to 3. 10^{15} cm^{-2} was standard p-type substrate, while the other devices were oxygen-enriched. After irradiation they were kept at low temperature (<-10^{o}C).

The irradiated devices have been measured using a 1060 nm laser and fast electrons from a ^{106}Ru source (with an energy deposition comparable to minimum ionising, m.i.p., particles). The source measurements allowed the evaluation of the absolute CCE(V) (relative to the pre-irradiation value of identical detectors) and the laser measurements allowed the study of the relative CCE(V) at low biases. The detectors were read-out with a SCT128A LHC speed (40MHz) chip [5]. The noise of the detector as a function of the applied bias has been measured for different irradiation fluences and the results are shown in Fig. 8-1. The CCE(V) and the noise measurements have been performed at –20/25 ^{o}C. The noise does not show a clear dependence on the bias or on the irradiation level, though a substantial increase of the reverse current is measured after the different radiation doses. This is expected because the noise, with LHC speed electronics, is dominated by the input capacitance, with reduced dependence on the shot noise induced by the increased reverse current. The low dependence of the noise on the applied bias also indicates that the measured devices are remarkably robust against noise associated with microdischarge even up to the highest bias voltages applied after irradiation (950V). Fig. 8-2 shows the CCE(V) characteristic of the detectors at the different radiation doses up to 7.5 10^{15} p·cm^{-2}. The charge collection efficiency is strongly dependent on the irradiation dose, being further reduced with fluence as a result of charge trapping.

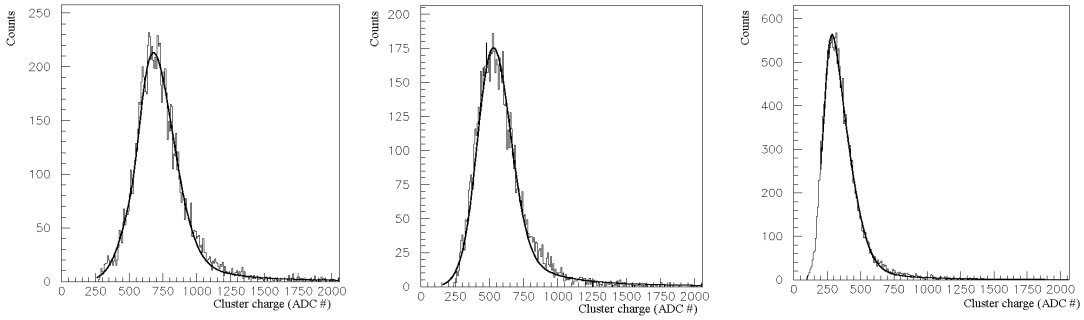

a) b) c)

Fig. 8-3 Energy loss distribution of miniature n-in-p detectors after different irradiation doses and applied bias voltages: a) 1.1 10^{15}pcm^{-2}, 800V b) 3.0 10^{15}pcm^{-2}, 800V c) 7.5 10^{15}pcm^{-2}, 900V

Fig. 8-3 shows the energy distribution of the m.i.p. signal collected at the highest applied bias voltages after the three different irradiation doses. Fig. 8-4shows the maximum collected charge as a function of the received fluence. Even after the highest dose, the charge collected at the maximum applied bias (900 V) by these n-in-p mini-strip detectors is > 6500 electrons. This corresponds to a signal over noise value of ~7.5, which is still sufficient for efficient tracking. This is presently the only measurements made with segmented detector at such a high fluence and it is use to inform the extrapolation of collected charge for the highest doses expected in the innermost layers of sLHC (see below the pixel section).

The collected charge at the highest dose corresponds to the signal deposited in ~90µm thick non-irradiated silicon detector. In the presence of charge trapping the collected charge is only a fraction of the charge produced by the passage of an ionising particle. This indicates that the collected charge was deposited in a much thicker depth of silicon. With this geometry (n-side read-out), even after high doses

of hadron irradiation it appears to be advantageous to operate relatively thick (200-300µm) detectors in terms of the total collected charge. It should also be noted that the charge collection is still not saturated at 900V, as shown by the measurements made with the 1060 nm laser (Fig. 8-5).

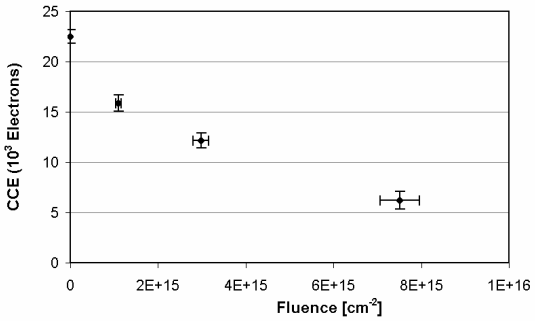

Fig. 8-4 Degradation of the collected charge as a function of the irradiation fluence for n-in-p microstrip detectors. The applied voltages are 800, 800 and 900 volts for the three different irradiation fluences, respectively [4].

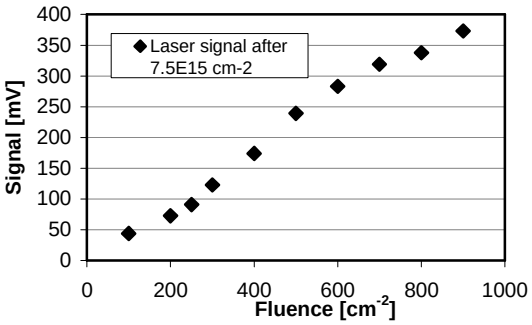

Fig. 8-5 Signal induced by 1060 nm pulsed laser illumination on a n-in-p detector after 7.5 10^{15} p cm^{-2} [4].

These results already show that with the choice of the appropriate geometry (cell size) and with low noise electronics, silicon detectors able to survive the doses anticipated for the SLHC trackers can be fabricated. There are still open questions about the p-type material, and namely: systematic investigation of the role of oxygen in this material (high temperature enriched silicon vs standard silicon), use of p-type MCZ, influence of the processing on the electrical performances of the devices, accurate modelling of charge trapping versus fluence (refinement of the variation of the trapping time constant with fluence), definition of the optimal thickness of the devices (optimisation of the electric field distribution in order to keep the optimal efficiency vs purity ratio as a function of irradiation), annealing studies. In view of these studies, a dedicated RD50 mask with 20 pad diodes, 12 pixel devices and 26 miniature strip detectors has been designed and fabricated. It is envisaged to use this mask with two manufacturers (two different processing) and perform systematic irradiation studies to compare performances of the various geometries (diodes, ministrips and pixels) made with the various materials.

8.2 Pixel Activities (Europe)

8.2.1 View on the Pixel Detectors in upgraded LHC-Experiments

Any increase of the LHC luminosity will lead to an extension of the pixel detectors to higher radii in the upgraded experiments. For CMS a 8-9 layer pixel system covering the volume up to a radius of ~50cm has been proposed [6] and for ATLAS similar studies are under way. The intensity of the radiation in the innermost parts of the tracker varies almost with the second power of the radius. In the following a subdivision of regions is performed according to their radiation levels.

8.2.1.1 Innermost Layer (radius between 4 and 7cm)

In this region the modules (detectors plus hybrid electronics) have to survive an expected particle fluence of 1. 10^{16} cm^{-2}. In planar silicon devices the maximum expected signal charge is about 2500 electrons for perpendicular tracks (Fig. 8-6) [7]. This value is determined by the signal trapping which leads to a mean

free path of about 25-30 µm, even with high applied voltage. In order to find a suitable detector to equip this region the following open points have to be investigated:

- Is it possible to built readout electronics that can work with such small signals (in such a hostile environment) ? In this case planar devices with the opportune cell size can still be used.
- It is possible to provide devices that deliver a higher signal charge ?

The RD50 research program is investigating these points: the first by the newly formed *electronics group* within the FDS research line and the second by the New Devices research line.

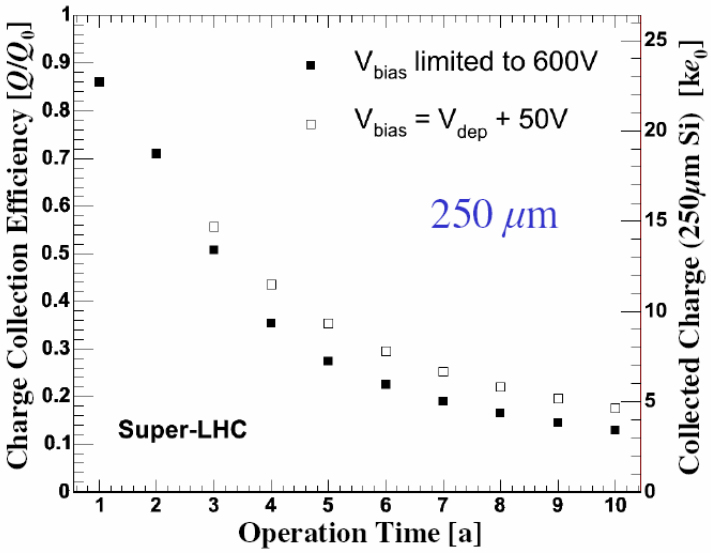

Fig. 8-6 Average signal charge expected for a planar silicon device after irradiation 7.8 10^{14} n_{eq}/y cm^{-2} [8].

8.2.1.2 Remaining Volume of the present Pixel Detectors (radius between 8 and 14cm)

The region between 8 and 14cm is roughly the volume of the present pixel detectors and will have to sustain a total fluence of 2-3 10^{15} Neq/cm^2. According to [4] and [7] a signal of ~8000-10000 electrons can be expected (Fig. 8-4). So it might be possible to use pixel detectors similar to the ones presently used in ATLAS and CMS. Moderate changes in the readout electronics (more data buffers) to account for the higher occupancy will, however, be necessary.
In order to confirm the predicted signal levels, silicon sensors with the CMS-barrel pixel sensor design have been irradiated at the CERN PS to fluences up to 2-4 10^{15} Neq/cm^2. The bump bonding of these devices is very challenging and is currently under way. It is planned to test such a device in a test beam at the CERN SPS in November 2004.

8.2.1.3 Radii between 18 an 22cm

The radiation hardness required at radii between 18 and 22 cm is in the order of 1 10^{15} Neq/cm^2. This dose is about equal to the radiation level anticipated for the present pixel detectors of ATLAS and CMS. Therefore the present design could, in principle, be used to instrument these layers. However, such an approach will be too costly. As the most cost driving component of a present pixel module is the double sided processed n-in-n sensor, a replacement by a single sided device should lead to substantial savings.

A promising candidate is the n-in-p concept which (potentially) offers the same radiation hardness without requiring backside processing.
To investigate the potential of the n-in-p approach a few (12) pixel detectors (described later) have been included in the RD50 mask set. They will be used for a more detailed study of the fluences and bias dependence of the signals as well as for system tests with a generic pixel readout electronic. In a pixel system using single sided sensors the possibility of destructive sparks between the sensor edge (being at a potential of several hundred volts) and the closely spaced readout chip is a concern and dedicated counter-measures have to be tested.

8.2.1.4 8.2.1.4 Radii between 30 and 50 cm

The radiation hardness is not a major concern in this region. However, due to the high density of tracks "conventional" strip detectors cannot be used here. Large pixels or short strips will be required. The driving issue for the choice of geometry is a trade between the granularity needed for physics and the cost for instrumenting this large volume. This problem is outside the scope of the RD50 activity.

8.2.2 Description of Pixel Sensors on the RD50-Mask Set

The pixel section of the FDS-RD50 mask contains 3x4 pixel sensors with two different pixel designs. These are made to match a generic readout chip currently under design by the CMS pixel collaboration.
The mask set was mainly dedicated to strip detectors and the pixel sensor design was forced to fit the strip detector design, with the following implications:

- Wafer will not have the passivation layer to restricts the bump bonding to lift off processes (in most cases Indium). This makes bump-bonding much more difficult and expensive.
- The poly-silicon layer (used for the bias resistors in the strip detectors) has to be used for the contact *vias* between implant and aluminium. In the pixel devices the poly was used to implement field plates at the edges of the n-implant.
- A completely single sided process (suitable for n-in-p devices) is simulated. In particular the absence of guard rings on the back side (with the possible problems due to the presence of high electric field on the edges) is investigated.
- The area for the pixel devices is very limited (the "reticule" size of 12.5 * 12.5 mm^2 was given to the pixel project). For this reason it is unlikely that the bump deposition can be performed on wafer level. This limits the choice of possible bump vendors.

In the given reticule a set of four small "single chips sensors" with 22 * 40 pixels of 150*100 μm^2 could be placed as shown in Fig. 8-7. They fit the readout chip dedicated to sensor characterization currently being designed by the CMS pixel collaboration. The sensors are placed in a way that they can be bump bonded to 4 chips without being separated. Each sensor contains all features of a full detector module, like the elongated edge pixels (see Fig. 8-8). A simple guard ring structure of 10 rings with increasing distance was used. They contain field plates realized in poly silicon as well as aluminium (also visible in Fig. 8-8).

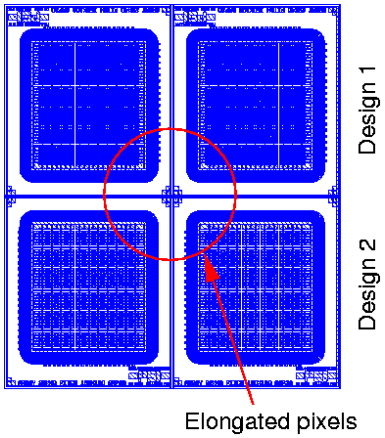

Fig. 8-7: Reticule containing four small pixel sensors.

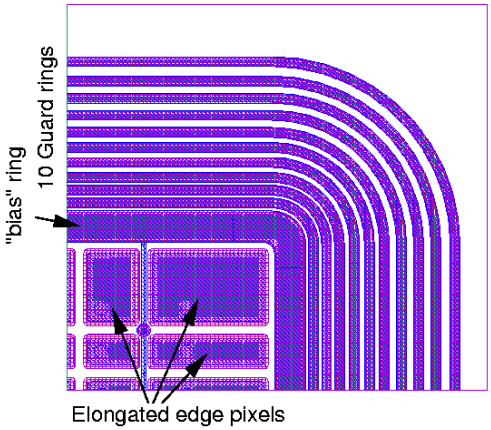

Fig. 8-8 Edge of a pixel sensor with elongated edge pixels and multi guard ring structure.

Two different pixel designs were made. One was optimised for best possible yield while the other was laid out to mimic the designs of the ATLAS and CMS collaboration.

Pixel Design 1

This design, shown in Fig. 8-9, was optimised to achieve the best possible yield, with a coarse feature size. The bias grid necessary for taking IV curves prior to bump bonding is implemented in a simple way. The punch through dots are placed between four pixels and are connected via a metal line. This metal line never crosses any non-connected poly line or n-implant, to reduce the quality requirements to the thermal oxide covering the implant and the low temperature oxide encapsulating the poly. The poly is used to implement the field plates covering the lateral pn-junctions of the pixels (see Fig. 8-9).

As there is no passivation layer, the bump bond pads have to be optically marked by other means. As indicated in the cross section in Fig. 8-10 the contact layer between the aluminium and the poly was closed in the region of the bump pad. This causes a topography which should be optically visible when placing the bumps, providing additional protection to the device when a high pressure is applied during the bump bonding procedure.

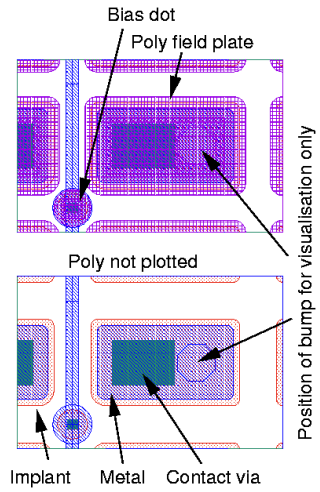

Fig. 8-9 : Layout of a single pixel in layout 1. For clarity the poly silicon layer was not plotted in the lower figure.

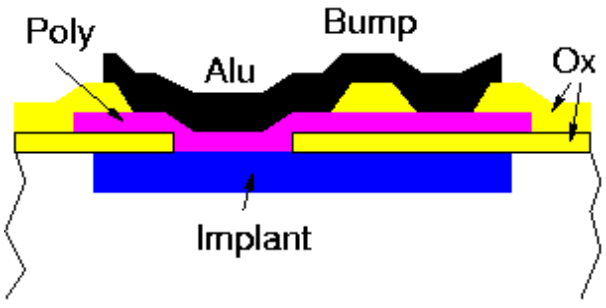

Fig. 8-10 Cross section through a pixel cell.

Pixel Design 2

This design, shown in Fig. 8-11, is as close as possible to the ATLAS and CMS pixels. The biasing structure is moved into the pixel implant (bias dot). This minimises the loss of signal caused by this structure but has metal line crossing the implant (and the poly layer) of the pixel. A pin hole in this region will cause a short to this pixel, reducing the yield. Also here the poly layer was used to implement field plates.

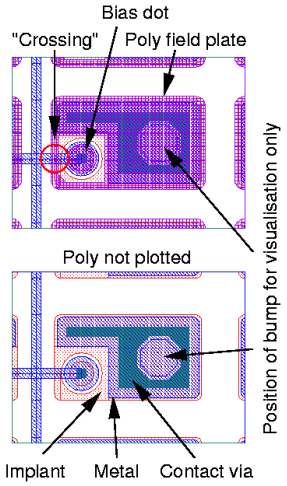

Fig. 8-11: Layout of a single pixel in layout 2. For clarity the poly silicon layer was not plotted in the lower figure.

8.3 System for evaluation of micro-strip detectors in Prague

A system to evaluate the response of silicon strip detector to laser illumination has been developed by the Prague groups together with IFIC Valencia .
The reason for developing such a system is to mimic the response to a minimum ionising particle with a laser, resulting in a much more ready to use system. Testing detector in test beam is expensive and requires a complicated set up, while laboratory sources (e.g. beta particle) cannot give information on position resolution. The laser system is a good alternative solution.
The ionisation characteristics of the laser light are different from a m.i.p., as described in Fig. 8-12 and Fig. 8-13. In particular:

1. The semiconductor laser beam has nonzero rise edge (nanoseconds), a finite size beam profile (sigma more 1 um) and a minimum pulse duration of 3ns
2. the light is reflected by metal layers and at the various interfaces (Si, SiO_2, poly etc.).
3. Interference effects can be originated by reflections

The results are very sensitive to the optimal focus distance, therefore a sophisticated focusing procedure was developed. The system can be cooled down to –20^{o}C in dry atmosphere in order to study the property of irradiated devices. The time resolution and the spatial resolution of the system are 1ns and 3µm, respectively. Further details are available at [9].

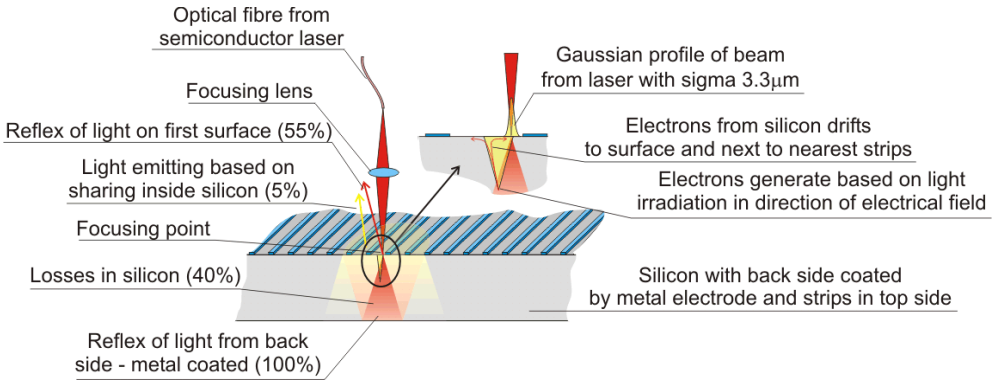

Fig. 8-12 Sketch of the charge deposition in laser tests.

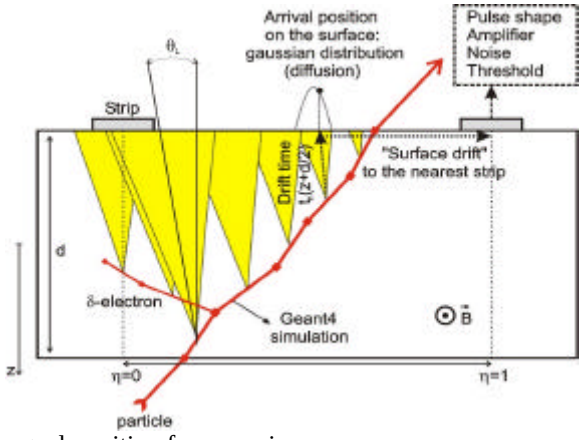

Fig. 8-13 Sketch of the charge deposition from a m.i.p

8.4 The TECHNOTEST subproject

The goal of the TECHNOTEST subproject is to study the influence of the initial resistivity and of the detector planar processing technology on the radiation hardness properties of silicon detectors. We concentrate on two aspects:

- the physics of formation of the deep levels in the energy band-gap and their influence on the charge carrier transport. This subject is within the “Pad Detector Characterization” scope in the RD50 research program;
- the segmented detector response according to the detector geometry which is a within the RD50 “Full Detector Systems” topic.

Here are presented the results of this second topic.

8.4.1 Detector response and related characteristics (comparative study)

It was shown in Chapter 5 (PDC) that the detector processing could affect the ration of the concentrations of deep donors and deep acceptors induced by the processing or by radiation. This ratio controls the electric field distribution in the detector sensitive region. In particular, in heavily irradiated Si

detectors the electric field is distributed quite non-uniformly with two asymmetric peaks at the contacts and the low field region *in-between*. This peculiarity plays a crucial role for detector operation because it determines the shape of the detector pulse response and the amount of collected charge. Firstly, the low field region leads to a delay in charge collection and to an increase of the detector collection time (t_c). Secondly, in heavily irradiated detectors this low field region "subdivides" the detector into two nearly independent regions with high electric field near the p^+ and n^+ contacts with the thickness of W_p and W_n, respectively. Since in the low field region the carrier drift velocity is rather small and the time for the carrier transfer is significant, the charge vanishes during the drift and only a small portion of the carriers can reach the region with high electric field at the opposite contact. This is well illustrated in Fig.5-9 (Chapter 5) where the responses of irradiated pad detectors processed at PTI and HIP from CZ n-Si are shown. The influence of the processing technology on the detector response is evident. For HIP detector the first peak of the double peak (DP) shape dominates at any bias voltage V whereas for PTI detector the second peak increases with voltage and becomes dominating from a given voltage (e.g. from 330 V for the detector shown in Fig.5-9). This difference is due to different concentrations of the charged mid-gap levels, which leads to a difference in the electric field gradient in the depleted regions.

We observed that in any irradiated detectors processed from different types of Si and using various technology, the maximum electric field (up to $2\text{-}3\cdot10^4$ V/cm) is located at the n^+ contact (see Fig.5-10 in Chapter 5). This difference in the electric field at the p+ and n+ contacts implies that an improved charge collection efficiency (CCE) in strip detectors made on n-type silicon, is achieved with n-on-n configuration, because the high weighting field correlates with the location of the high electric field. Qualitative consideration shows that n-on-n detectors irradiated beyond SCSI will operate with the effective thickness of W_n, which is the bigger part of the detector active volume, while irradiated p-on-n detectors are less effective due to lower electric field near the p^+ strip and smaller depth of W_p.

The influence of technology is demonstrated by the voltage dependence of the detector signal (collected charge Q). To follow the LHC/SLHC experimental conditions (we suppose shaping time of 20 ns and 10 ns), the collected charge was estimated in a first approximation by integrating the detector current response over the time equal to the shaping time of front-end electronics. The value of the Q depends on three factors:

- ballistic deficit
- charge loss due to carrier trapping,
- changes of electric field distribution with bias.

The Q vs V dependences at 20 and 10 ns shaping time are presented in Fig. 8-14 for two pairs of detectors processed at PTI and HIP from the same FZ n-Si and CZ n-Si. The corresponding current pulses are presented in Fig 5-9 (Chapter 5). In both detectors made by HIP (FZ-Si and CZ-Si) the first peak is dominating since the electric field in the W_p region is independent on the bias. Therefore the collected charge is practically constant for the 10 ns shaping time. The increase of the collected charge with voltage at 20 ns shaping time is due to the second peak.

For CZ-Si detector processed by PTI, the collected charge increases with bias due to the higher electric field in the W_p region that reduces significantly the total charge loss.

The current pulse response measurements show that in detectors irradiated $5\cdot10^{14}$ n cm^{-2} the bias corresponding to the pinch-off between the W_p and W_n regions is practically independent on the type of material and detector processing.

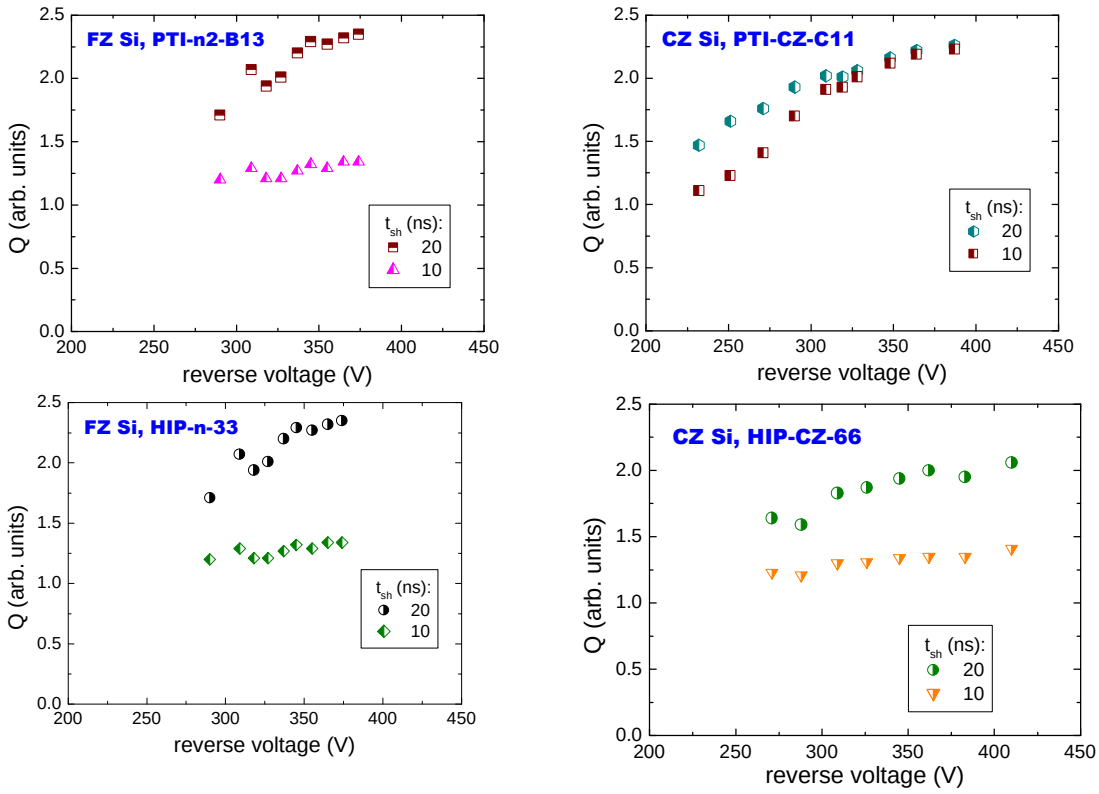

Fig. 8-14 Collected charge versus voltage of p-on-n pad detectors at 10 and 20 ns shaping time.

8.4.2 Summary

1. For all the tested Si materials and processing, the detectors irradiated to = $5 \cdot 10^{14}$ n cm^{-2}:
   - the electric field has double peak shape;
   - the electric field at the n^+ contact is at least 20 times higher than that at the p^+ contact.
   - the pinch-off voltage depends only on the irradiation fluence.
2. The electric field at the p^+ contact in irradiated detectors is sensitive to the type of Si and processing.
3. The n-on-n geometry allows better charge collection for segmented detectors in high radiation environment.
4. The TECHNOTEST subproject plans to study the MIP detection properties of detectors processed within this collaboration.

8.5 MCz Silicon Testbeam

The potential increase of radiation hardness obtained by using high resistivity magnetic Czochralski (MCz) silicon have driven the idea of using a full size MCz silicon strip detectors for a test beam in CERN. Although the FZ growth method can yield high purity and high resistivity silicon and is currently the base material used for all HEP silicon tracking detectors, the relatively high resistivity (1KOcm) MCz silicon can be used for detector applications. The possible advantages of this choice are related to the significantly increased oxygen concentration in MCz compared with the diffusion oxygenated float zone material that is currently the reference for radiation hardness [7].
The LHCb vertex locator (VELO) will operate in an extreme radiation environment (> 1.3×10^{14} 1 MeV neutron equiv. / cm^2) and hence is likely to be the first detector to be upgraded at the LHC. A number of

members of the LHCb VELO group are active in the RD50 collaboration and have conducted the first test-beams on a full scale (6cm by 4cm) RD50 MCz sensor equipped with LHC speed electronics. The full results of this testbeam are discussed in [10].

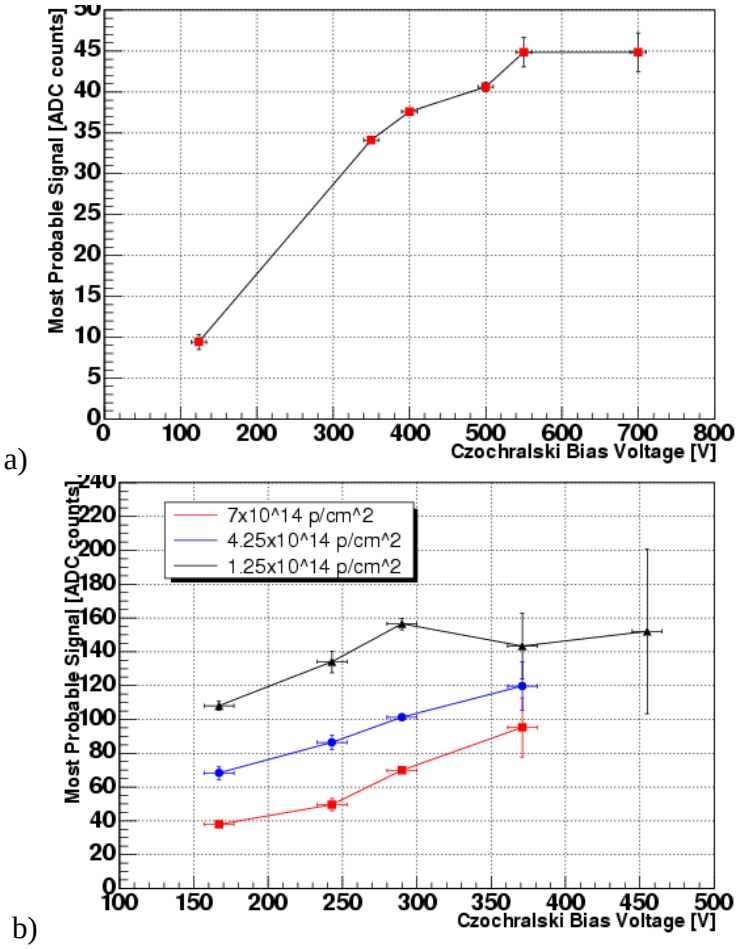

Fig. 8-15 CCE for the unirradiated (a) and irradiated (b) Czochralski silicon detector. The radiation levels are quoted for 24 GeV protons/cm^2. The ADC values in the unirradiated and irradiated test beam periods can not be directly compared.

The detector under study was a 50 μm pitch AC coupled microstrip sensor processed on 900Ocm MCz [11]. The initial depletion voltage was measured as 420 V prior to irradiation. The detector was read out with 40MHz clocking rate SCT128A analogue readout electronics. The detector was operated in a test-beam, then irradiated and re-tested in the test-beam. The irradiation was performed with 24GeV protons at the CERN PS and a maximum fluence of 7.8×10^{14} p/cm^2 was delivered. The sensor was annealed, taking advantage of the beneficial annealing process, to the minimum of its depletion voltage curve.

The Cz testbeam was performed at the CERN SPS 120 GeV pion and muon beam using an eight-plane silicon telescope of LHCb VELO prototype silicon sensors. The irradiated sensor was mounted in a nitrogen flushed silicon oil cooled box and operated at -10^0C. The data was processed applying pedestal and common mode noise algorithms to the recorded signals and track reconstruction was performed through the silicon telescope. Dead, noisy and unbonded channels were masked out from the analysis. The Cz silicon sensor was then aligned with respect to these reconstructed telescope tracks. The tracks

were then extrapolated to the Cz sensor and the charge summed from four strips around the track intersection point.
The Charge Collection Efficiency (CCE) was measured as a function of both irradiation and voltage and is shown in Fig. 8-15. Prior to irradiation (see Fig. 8-15a) the full charge collection voltage was estimated at 550V and the detector was successfully operated at up to 700V. The signal to equivalent one-strip noise ratio was measured at greater than 23:1. Limitations in the experimental cooling set-up prevented the detector from being fully depleted after irradiation for the highest fluences. However a significant charge collection efficiency (see Fig. 8-15b) was measured at 7x 10^{14} 24GeV protons/cm^2 at a relatively modest voltage.
In these tests a full scale irradiated sensor has been successfully operated with LHC speed electronics. These studies show that Czochralski silicon is a promising alternative base material for use in LHC experiments and will be studied further by the RD50 Collaboration and its LHCb VELO group partners.

8.6 INFN–RD50 collaboration on design of silicon micro-strip detectors

8.6.1 Wafer layout

The Italian institutes member of both the RD50 collaboration and INFN started a project focused on the study of micro-strip detectors made with non-standard silicon materials using a dedicated mask. The project encompasses mask design, wafer processing and detector characterization before and after irradiation. Wafer design has been optimized to be used with different bare silicon material as Cz, MCz, Fz and Epitaxial with different sensitive thickness.
Fig. 8-16 shows a picture of a full processed wafer. The layout consists of 10 silicon micro-strip detectors surrounded by a set of test structures. The micro-strip detectors have 4.5 cm implanted strips, AC-coupled and biased through poly-silicon resistors. Each sensor has different geometrical parameters, as summarized in Table 8-1, in order to compare the detector performances as a function of the strip width/pitch ratio and of the percentage of metal overhang.
The test structures included in the layout are: multi-guard diodes (designed for high bias voltage operations), MOS structures and Gate Controlled Diodes (to measure the oxide trapped charge and the interface states), poly-silicon resistors and Van der Paw structures (to verify the implant doping).
All test structures are used to qualify and investigate different process steps and to quantify the effect of radiation damage on basic parameters, such as leakage current, depletion voltage, oxide charge, which define the global radiation hardness of micro-strip detectors.

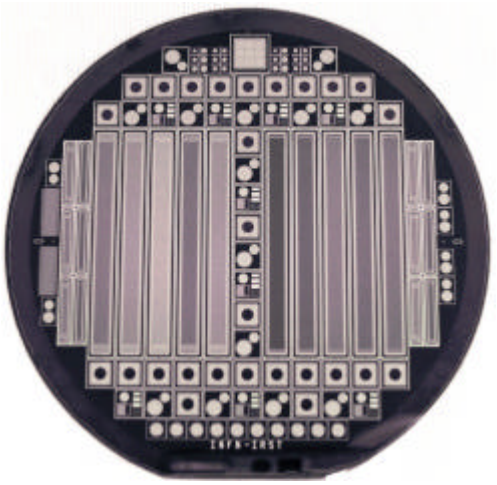

Fig. 8-16 Layout of a processed wafer

m-strip #	pitch (mm)	p+ width (mm)	Poly width (mm)	Metal width (mm)
S1	50	15	10	23
S2	50	20	15	28
S3	50	25	20	33
S4	50	15	10	19
S5	50	15	10	27
S6	100	15	10	23
S7	100	25	20	33
S8	100	35	30	43
S9	100	25	20	37
S10	100	25	20	41

Table 8-1 Geometrical parameters of micro-strip detectors

8.6.2 Materials and processing

The different types of Si wafers used for processing belong to the common RD50 wafer procurement. The processed wafers were mainly MCz, with both *n* and *p* type of doping. In addition, a few Epitaxial wafers with different thickness have been processed, as well as Cz and Standard Fz material, used for comparison.
The ITC-IRST institute (Trento, Italy) has processed *n* type and *p* type materials in two successive runs. For the second run (on p-type wafers) the p-spray technique has been used to increase n^+ implants isolation.
The first run has been fully qualified with on wafer and pre-irradiation characterisation and micro-strips devices and test structures are currently under irradiation. The wafers belonging to the second run are presently under qualification.
In both cases the process has been tuned to minimize undesired effects, such as Thermal Donor activation in Cz or MCz wafers. For this purpose, process steps like sintering at T<380 ^{o}C, Thermal Donor Killing Temperature schemes or avoiding the final passivation coverage have been used. The comparison wafers were processed according to standard techniques.

8.6.3 Characterization of detectors

The performances of micro-strip detectors and test structures have been studied in a clean-room under controlled environmental conditions (T=20 ^{o}C; RH 50%). A standard apparatus for semiconductor parameter analysis has been used where the probing zone can be kept at relative humidity as low as 20 %. Cohort statistics of IV and CV characteristics of micro-strip sensors have been performed according to the common procedure defined within the RD50 collaboration.
Fig. 8-17 shows IV characteristics of all 10 micro-strip detectors of a MCz wafer.

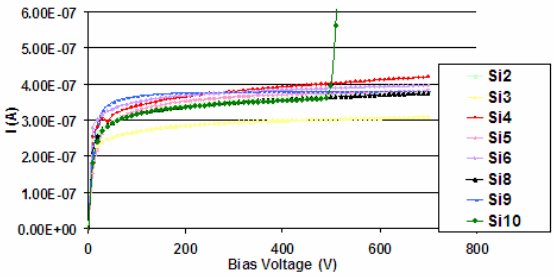

Fig. 8-17 IV Characteristic of MCz micro-strip sensors

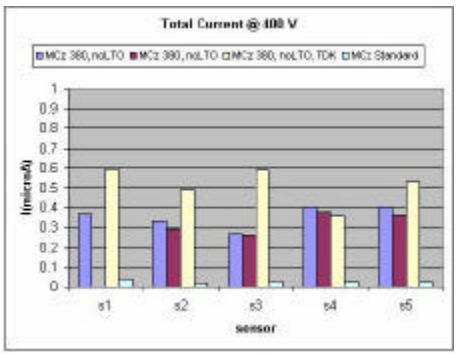

Fig. 8-18 Leakage current measured at 400 V for micro-strip sensors with 50 µm pitch processed with different techniques

A common feature is the low value of the current density (about 1.4 nA/mm^2 at 400 V) and the high value of the breakdown voltage. Fig. 8-18 shows a comparison of the total current measured at 400V on micro-strip sensors with 50 µm strip pitch made with different processes. These results show a dependence of the total current on the different temperature steps of the various processes.
The measurement of the bulk capacitance as a function of bias voltage is shown in Fig. 8-19. The resistivity values are compatible with the ones extracted from the same measurement on diodes, while the total capacitance is a function of the geometrical segmentation of the junction side.

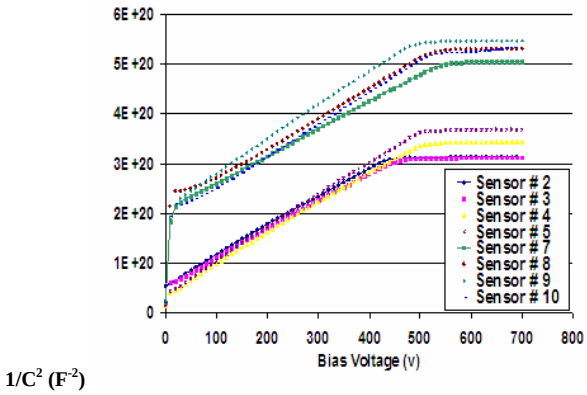

Fig. 8-19: $1/C^2$ vs. V Characteristic of MCz micro-strip sensors

The inter-strip capacitance has been measured on dedicated structures and on micro-strip sensors. Values compatibles with the expectations have been found: 0.8 pF /cm for the devices with 50 µm strip pitch and 0.6 pF/cm for the devices with 100 µm strip pitch.
Test structures have been measured to investigate wafer quality and process performance.
Diodes have been used to check the uniformity of the resistivity and of the leakage current density across the full wafer. A superimposition of the leakage current measured at 400 V is shown in Fig. 8-20 as an example. The measurements show a good uniformity of the leakage current density, with a well defined peak at low values and with a small tail uncorrelated to the process type or the bulk material.

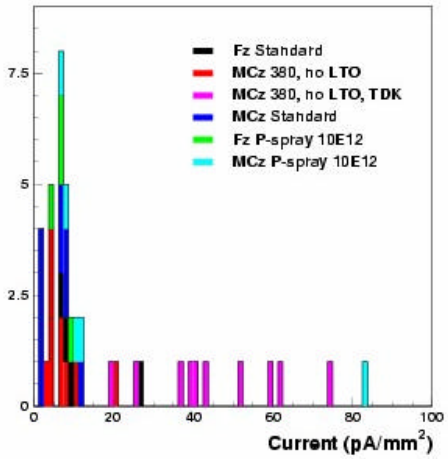

Fig. 8-20: distribution of leakage current density measured at 400 V on diodes

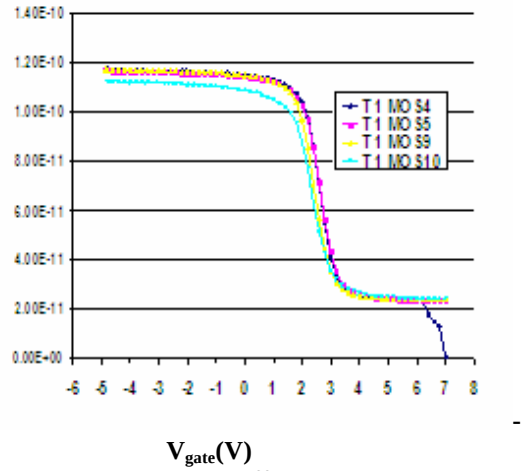

Fig. 8-21: CV Characteristic on different MOS structures

The quality of the oxide has been checked with measurements on the MOS and GCD structures. The CV curves on the MOS devices, shown in Fig. 8-21, demonstrates that the oxide thickness is uniform across the wafer, with typical values of the surface density of trapped charges about $6\text{-}7 \cdot 10^{10}$ cm $^{-2}$. From the IV curve on the GCD we can extract a surface recombination velocity in the order of 1 cm /s.
The pre irradiation study showed a good overall quality of the processed wafer. The devices behave as expected. The new materials, such as MCz 1KΩ cm, seem to be suitable for micro-strip processing. The radiation hardness of these devices is under investigation, with irradiations performed with a proton beam (24 GeV/c^2, CERN) up to very high fluences (10^{16} p/cm^2).

8.7 RD50 Electronics group

Within the FDS Research Line, an Electronics Group was formed, with the aim of

1. Providing a point of contact to the pixel and strip electronics communities of the LHC detector upgrade groups.
2. Supporting investigation of emerging technologies (e.g. SiGe, DSM CMOS) with irradiations and characterization.
3. Working on requirements of the detector-readout electronics interface: e.g. Signal-to-Noise, operating temperature, power, voltage levels, layout questions.
4. Providing a test bed for readout electronics.
5. Providing detector parameters to electronics groups in the detector upgrade collaboration.

The participating institutions are Barcelona (M. Ullan), UC Santa Cruz (H. Sadrozinski), Padova (A. Candelori), Tel Aviv (A. Ruzin).

UC Santa Cruz is investigating a biCMOS process with fast bipolar transistors fabricated in SiGe for the use in the frontend of the silicon readout. This would be appropriate for short strips and fast timing (12.5ns) or for longer strips, requiring a survival fluence of about 10^{15} n_{eq}/cm^2. To assess the radiation damage beyond the measured level of about 10^{14} n_{eq}/cm^2, we irradiated during the RD50 irradiation run in October 2004 a total of 6 test chips with a set of test structures of diverse geometries to fluences varying from 10^{13} n_{eq}/cm^2 to close to 10^{16} n_{eq}/cm^2. The pre-rad characterizations confirmed the expected very high values for the current gain β. Post-rad results will be available in early 2005 after cool down and retest.

8.8 RD50 Common Mask for segmented Si detectors

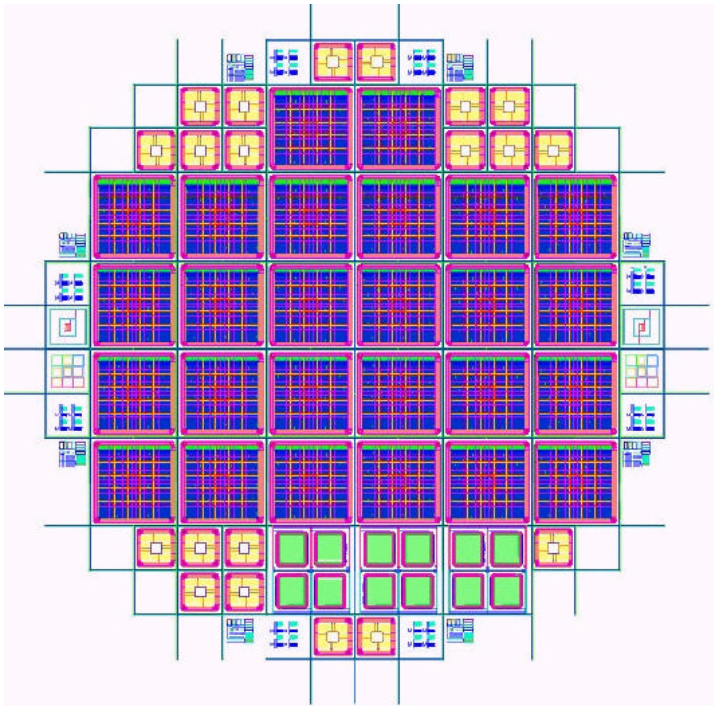

Fig. 8-22 RD50 mask for the FDS project

The RD50 mask for the FDS project include 20 pad diodes, 12 pixel detectors, 26 mini-strip detectors and 8 test structure sets. These test structure are implemented for quality control of the processing. The presence of pad, pixel and mini-strip detectors will allow direct comparison of the measured parameters (differences in CCE(V) between pad and segmented devices, correlation of CV and CCE(V) measurements etc.). The pixel devices have been described in details in a previous paragraph. The pad detectors are multiguard structures, approximately 5x5 mm^2, with an opening on the aluminium top metal contact to allow illumination with laser light. The mini-strip are approximately 1x1 cm^2 devices, with 100 strips, 80µm strip pitch, multiguard, capacitevely coupled and with high resistivity polysilicon biasing. The mask design allows for single side (p-in-n, n-in-p) and double side processing (n-in-n).

8.9 References for Chapter 8

[1] S. Marti i Gracia, P.P. Allport, G. Casse, A. Greenall, "A Model of Charge Collection for Irradiated P+N Detectors", *Nucl. Inst and Meth. A*, vol 473, pp. 128-135, 2001.

[2] P.P. Allport, T.J.V Bowcock, G. Casse, A. Greenall, J.N. Jackson, T.J. Jones et al, "Charge Collection Efficiency Studies with Irradiated Silicon Detectors", Nucl. Inst and Meth. A, vol 501, pp.146-152, 2003.

[3] G. Casse, P.P. Allport, T.J.V Bowcock, A. Greenall, M. Hanlon, J.N. Jackson, "First Results on the Charge Collection Properties of Segmented Detectors Made with P-type Bulk Silicon ", Nucl. Inst and Meth. A, vol 487, pp.465-470, 2002.

[4] G. Casse "Recent results with n in p miniature microstrip detectors after heavy proton irradiation" presented at the 4th RD50 workshop 5-7 May 2004, CERN-Geneva

[5] F. Anghinolfi , W Dabrowski, E. Delagnes, J. Kaplon, U. Kotz, P. Jarron et al, "SCT A: A rad Hard BiCMOS Analog Readout ASIC for the ATLAS Semiconductor Tracker" IEEE Trans. Nucl. Sci. vol 44, pp 298-303, 1997.

[6] R. Horisberger "Pixel Systems at SLHC" presented at VERTEX 04 13.-18. September in Como

[7] RD48 Collaboration, Radiation Hard Silicon Detectors – Developments by the RD48 (ROSE) Collaboration, Nucl. Instr. & Meth. A 466 (2001) 308-326

[8] O.Krasel, "The Development of the ATLAS Pixel Detector", presented at RESMDD04, Florence, Oct. 10.-13. 2004, to be published in NIMA.

[9] http://ific.uv.es/~kodys/LaserTest/LTSummary.pdf

[10] A.Bates et al.,Results from the first test beam of a large microstrip Czochralski silicon detector equipped with LHC speed electronics, CERN-LHCB-2004-052 (2004)

[11] J. Harkonen et al., Processing of microstrip detectors on Czochralski Grown high resistivity silicon substrates, Nucl. Instr. & Meth. A 514 (2003) 173-179

9. Workplan and milestones for the year 2005

9.1. Defect and Material Characterization

Workplan / Milestones

1. Investigation of the influence of the oxygen dimer on the radiation induced formation of "thermal" donors in silicon and silicon detectors.

2. Multivacancy-oxygen centers in irradiated silicon. The activities regarding assignment of the so-called X- and I-centers will be intensified. The outcome is very crucial in order to understand and properly model the defect evolution during irradiation (this has strong implications on both the defect engineering and the device modelling).

3. Characterization of irradiation-induced defect clusters in silicon. Correlation between PL- and DLTS-results on defect clusters will be made using "identical" samples (that is, the samples are prepared simultaneously and under exactly identical conditions).

4. Characterization of irradiated silicon carbide samples. Detailed point defect characterization of n-type 4H-SiC "detector structures" irradiated with 24 GeV protons to understand the strong decrease in charge collection efficiency after irradiation.

5. Further characterization of hydrogenated silicon detectors (see also DE line)

9.2. Defect Engineering

Workplan

1. Processing and systematic studies on specific process steps for controlled introduction or annealing of thermal donors and introduction of hydrogen will continue on:
   - Oxygen enriched FZ-silicon
   - High resistivity n- and p-type MCZ-silicon (Okmetic/Finland)
   - Epitaxial silicon layers (material: ITME)

2. Hydrogenation in hydrogen plasma will be performed by Minsk. The needed material and defect characterizations will be performed in close cooperation with the DMC-project.

3. For a further optimization of epitaxial detectors the growth of 50 µm thick p-type epi-layers at ITME and a processing at CiS is foreseen for the beginning of 2005. A production of epi-layers on oxygen lean low resistivity FZ-substrates is envisaged.

4. Defect engineering by oxygen-dimer enriched silicon: This work will be performed in close collaboration with the DMC-project line. The work plan for 2005 includes basic studies on a possible optimization of the oxygen dimerization process with respect to the temperature during electron irradiation and fluence in order to minimize the introduction of harmful defects by retaining at the same time a sufficiently high dimer concentration.

5. Defect engineering by pre-irradiation: The characterization of irradiated test detectors on pre-irradiated and untreated high resistivity FZ and MCz silicon will continue in 2005. Surface problems had lead to a new process run at ICT-IRST in Trento. In this run also p-type FZ silicon and NTD silicon supplied by Topsil will be included. Proposed is a beginning early 2005.

Milestones

1. Processing and characterization of detectors on defect engineered FZ-, n- and p-type MCz-silicon and pre-irradiated FZ-, MCz-silicon and NTD-silicon.

2. Growth, processing and characterization of 50 μm p-type epitaxial silicon layers on low resistivity p-type Cz-substrates.

3. Study of radiation hardness of all defect engineered FZ-, Cz- and epitaxial silicon and pre-irradiated silicon up to fluences of 10^{16} cm^{-2} (1 MeV neutron equivalent) with charged hadrons and neutrons.

4. Verification of hydrogenation of different silicon in a hydrogen plasma and basic microscopic studies in correlation with macroscopic measurements after irradiation with low energy electrons and/or gammas.

5. Oxygen dimerization at higher temperature (350°C) and lower electron fluence ($<10^{18}$ cm^{-2}) for optimizing the amount of dimers in comparison to the concentration of radiation induced defect centers.

9.3. Pad detector characterization

Due to the shut down of CERN accelerators, the availability of irradiation beam time for radiation hardness studies will strongly be reduced in 2005. Efforts to obtain beam time for RD50 activities from different laboratories around the world are currently in progress.

1. Processing and systematic studies on specific process steps for controlled introduction of thermal donors (TD) and introduction of hydrogen will continue on high resistivity p-type MCZ-silicon (Okmetic/Finland).

2. Production of $p^+/n^-/n^+$ detector structures, where bulk is p-type MCz-silicon that has been compensated electrically n-type by controlled introduction of TDs.

3. Transfer this technology to full-size strip detectors.

4. Improvement of processing technology for $n^+/p^-/p^+$ detector structures, where p-type bulk is p-type MCz-silicon.

5. Irradiation and CV/IV characterization of these devices.

6. Charge Collection Efficiency (CCE) study of heavily irradiated $p^+/n^-(TD)/n^+$ and $n^+/p^-/p^+$ detectors.

7. Improved modeling of TD generation in high resistivity p-type MCz-silicon. This requires accurate measurements of oxygen concentration and distribution is this material.

8. Annealing at elevated temperatures irradiated $p^+/n^-(TD)/n^+$ devices. Annealing behavior of high oxygen concentration (MCZ-silicon) silicon is opposite to the traditionally used Fz-Si devices. Annealing of Cz-Si creates TDs that compensate acceptor type radiation induced defects. Furthermore, annealing reduces greatly leakage current. Whether the annealing recovers the CCE of irradiated devices will be studied in 2005.

9. Influence of hydrogen on annealing rate irradiated $p^+/n^-(TD)/n^+$ devices. Introducing hydrogen can enhance the TD introduction rate. That may open a possibility to recover heavily irradiated detectors at relatively low temperatures (e.g. 100^0C).

9.4. New Structures

Workplan/Milestones

1. 3D detectors. (Glasgow, Barcelona, IRST, Florence) In IRST-Trento a 3D layout, containing various detectors based on vertical electrodes, has been designed. Testing of first devices will be done with MIPS in collaboration with Florence. The fabrication of a first batch is starting, and it is expected to be completed in the beginning of 2005. Aim is, like in 2004, to improve the fabrication method and realizing the junction doping technique. CNM Barcelona and IRST Trento will work with Glasgow in this.

2. Semi 3D detectors. (US groups) Semi-3D device has been completed. Intense testing will verify operation against simulations. Analysis of irradiations and characterization will be done. A study of the detectors charge collection efficiency, measured by connecting the sensors to the SVX4 readout chip, is planned in 2005.

3. Thin Detectors. (Trento, Purdue) Testing of thin detector structures after irradiation with 10^{16} cm^{-2} of 24GeV/c protons and reactor neutrons will be completed in 2005. Further thin detectors in the CMS tracker format will be completed and tested. The comparison between the performances of epitaxial Si detectors and thinned low resistivity and high resistivity Si detectors before and after irradiation will be carried out. A process of thin detectors made with epitaxial thicker layers (up to 100-150μm n-type and/or p-type) is also planned in 2005 in IRST_ITC Trento with materials provided by ITME.

9.5. New Materials

Workplan/Milestones

1. Study before and after irradiation up to fast hadron fluences of $10^{16}cm^{-2}$ of detectors made with epitaxial 4H-SiC of IKZ, Berlin and CREE. In 2005 a systematic campaign to verify the preliminary results obtained in 2004 will be carried out.

2. Continue the study of the charge collection properties and perform preliminary radiation hardness studies on thick high resistivity GaN Schottky barrier detectors.

9.6. Full Detector Systems

Workplan/Milestones

1. Continuing the studies of the charge collection efficiency on microstrip and pixel detectors produced in the common process of RD50 (p-type and n-type, standard epitaxial, MCZ Si) after fast hadron irradiation up to $10^{16}cm^{-2}$.

2. Determination of the *survival scenario* of microstrip detectors when coupled to the available LHC speed electronics (study of the signal to noise ratio for devices with different thickness and capacitive load as a function of fluence). Evaluation of charge collection efficiency in case of a reduced collection time to 10ns.

10. Resources

All participating institutes organize their own resources required for the research activities in their home laboratories. Integration in a CERN approved R&D project allows them to apply for national funding in terms of financial and manpower resources. The collaboration comprises several institutes, which have access to irradiation sources (reactors and accelerators), as well as clean room and sensor processing facilities. A very wide range of highly specialized equipment for characterization of sensors and materials is also available (see [1]) .

10.1. Common Fund

RD50 has a Common Fund to which each institute contributes every year a certain amount. The Common Fund is used for project related investments, like processing of common test structures or purchasing of special material and equipment. Furthermore it is used to cover the organization of collaboration workshops, common irradiation runs, or other specific activities of common interest.

10.2. Lab space at CERN

The RD50 collaboration was temporarily using existing infrastructure and equipment at CERN in 2004 and requests to continue to do so in 2005. As a member of the collaboration, the section PH-DT2/SD can provide access to available lab space in building 14 (characterization of irradiated detectors), in building 28 (lab space for general work) and in the Silicon Facility (hall 186, clean space). The collaboration would like to keep the RD50 visitor office in barrack 591 and use the CERN infrastructure to organize one workshop at CERN in 2005.

10.3. Technical support at CERN

A low level of support from PH-DT2/SD (wire bonding and sensor mounting) may be profitable. The expected work volume for 2005 is estimated to be very limited.

10.4. References in Chapter 10

[1] R&D Proposal - DEVELOPMENT OF RADIATION HARD SEMICONDUCTORDEVICES FOR VERY HIGH LUMINOSITY COLLIDERS, LHCC 2002-003 / P6, 15.2.2002.